Conservative time integration on beams under contact constrains using B-Spline interpolation

Alberto Pedro Sibileau

Thesis submitted for the Master of Science degree

Departament de Matemàtica Aplicada III

Universitat Politècnica de Catalunya

June 2011

Abstract

The present work describes the dynamics of beams undergoing sliding contact conditions. The physics of such systems lead to non-linearities in the resulting model of equations. When aiming to approximate numerically a solution, within the context of the finite element method, three topics are considered the most challenging: the kinematic description of the beams, the time-integration schemes and the treatment of the sliding contact. Each of them are relevant enough to be studied as separate subjects. However, when these subjects are brought together to attempt the system solution, their behavior is no longer independent. Two particular examples of the previous can be: the interpolation chosen for the beam kinematics will affect the contact performance, or an approach for the contact description will have consequences on the time-integration conserving properties.

The beam model presented further on is 2D and based on the geometrically exact (also known as Reissner-Simo) theory. This is particularly suitable to describe the presence of large displacements and rotations [1]. It is worth to notice here that the 2D context allows the beam rotational field to be interpolated in the same way as displacements for the variational formulation. Nevertheless, when conservative time-integration is developed, incremental rotations are interpolated instead and special treatment has to be done. Regarding contact formulation, non constraint equations are added to the equations of motion as the master-slave approach is used to model the sliding conditions. This is an important advantage, together with the fact that non additional degrees of freedom are added to the system equations.

It is intended to show in the present work, an important contribution to the discrete solution of sliding contact in beams. The discretization of the slideline is proof to play a key role in the convergence of the method. Following this direction, B-Spline is introduced to interpolate the beam variables. This allows a smooth transition between finite beam elements and improves performance in the numerical simulation compare to the most popular interpolation used, the standard Lagrangian polynomials. In this context, the master-slave method is extended to model flexible beam mechanisms whereas the conserving properties of the underlying time-integration schemes are mantained. It is consider as well that the work presented here can be extended to 3D geometrically exact beam formulations without any theoretical difficulty.

[1] Let remark the term *rotations* in a 2D context is used to refer to the finite beam discretization

Acknowledgements

I would like to express first my trully recognition to José Muñoz, who gave me the opportunity to work under his supervision. I have really appreciated during this time of research his enthusiasm for the field and generous advices.

This work has not been possibly as well without the financial support of the European Commission through the Erasmus Mundus programme. My sincere grace is acknowlegde for the opportunity of studying abroad, which has been a very fruitful personal and proffesional time.

Furthermore, I am deeply indebted to my working group at ITBA in Argentina. I would like particulary to name Sebastián D'hers, Pablo Bucello, Martín Arregui and Nicolás Pontelli. They have tought me the first steps and above all, how to work very professionally and without loosing the fellow felling and sense of humor.

During the two years stay in Europe, I shared my studying life in Swansea and Barcelona with many people I really enjoyed to have met. Without naming them all, my Master's classmates and seniors, particularly Anuj Sharma, Shabeer Khan, Pavan Kumar, Faraz Khatami, Héctor Espinoza and Thomas Wilson. I will never forget as well the *locals* in Barcelona, Carles Estruch and Santiago Albo, who have shown me and the other internationals the very best of this marvellous city.

Last but not least, I am sincere grateful unto Pepi for she has been the kindest support all over the Master and we have shared one year of life in Barcelona, which has been an immensely funny and nice experience. My school friends of Buenos Aires, for the great moments spent together, and because they have always been present despite the distance. And to my family, my most kindly praise for their endless generosity and love.

Contents

List of Figures

Chapter 1

Introduction

1.1 Motivation

The modelling of flexible mechanisms have interesting Engineering applications in a broad fields such as Aerospace, Automotive and Robotics. Recently, potential applications in the field of Bio-mechanics have appear at reserach stage [CPF07]. The most natural choice for the structural analysis of the system in hand is to model beam elements. Moreover, in the analysis also contact mechanics and inertial forces has to be taken into account, as the mechanism joints and dynamics play an important role. In this work, the intention is focused on modelling beams under 2D sliding contact conditions together with conservative strategies for time-integration.

The master-slave method has been developed in the recent past years, and research has been done so as to model numerically with this approach more general contact conditions without the use of *constraint* equations, such as it is need when Lagrange multipliers or Penalty methods are used. The advantages of the previous are that as well as keeping the minimum set of degrees of freedom, the resulting system do not couple differential with *algebraic* equations, which avoids the complexities associated with the solution in the last case. However, when sliding conditions are intend to model with the master-slave method, the chosen beam interpolation particularly affects the computation of contact loads at element transitions. In this work the stability of the numerical model is improved by the introduction of B-Splines for the beam spatial discretization.

With respect to the system dynamics, let state that energy and momentum conserving algorithms (in non dissipative problems and in absence of external loads respectively) has been developed for geometrically exact beams during the last decade. However, the desired conserving properties are not carried over straightforward to constrained systems such as the ones in question. In the present work, it is shown the development and implementation of an algorithm that conserves energy and momenta.

1.2 Thesis Scope

As stated before, in the present attempt three different key topics are identified: the beam formulation, the chosen scheme to integrate dynamic equations in time and the way that sliding contact is treated. Let remark again that these topics do not behave independly but are studied separately to get a better understanding in each of them.

1.2.1 Beam formulation

In order to achieve a reallistic description of sliding joints, the beam kinematics must consider finite deformations [Muñ04]. The theory chosen for that purpose is knonw as *geometrically exact* (or Reissner-Simo beam theory [Rei81, Sim85]). The formulation describes not only large displacements but also rotations [SVQ86a, SVQ88]. For the present work, the study is focused in a 2D context, which simplify the complexity of dealing with large 3D rotations [SVQ86b]. Nevertheless, it is beleived that the contributions achieved can be extended to a 3D model without any other theoretical restriction.

For the spatial discretization of the beam's displacements and rotations, B-Splines are proposed as an alternative to the standard procedure, done through Lagrangian polynomials [ZT00]. In the context of isogeometric analysis and contact mechanics, this approach has already been tested with succesful results [HCB05, Muñ08, TWH11]. However, let remark that to the author's knowledge, this has not been explored in the literature of structural elements such as beams.

1.2.2 Time-integration

For the integration in time of the dynamic equations, two different group of algorithms shall be distinguished. Some of them are specially designed to preserve the conservative properties in mechanics, the energy and momenta. On the other hand, the non-conservative schemes do not deal strictly with that matter. Conservative schemes are derived from an incremental form of the equilibrium equations, whereas the latter are followed straighforward from the variational form.

The well known Newmark method [New59] is the non-conservative method implemented and it's performance is compared against an energy-momentum conserving scheme. The latter is developed using an incremental form of the equilibrium equations which ends up solving a modified mid point gradient. This technique is shown to be energy conserving [SS96], and in addition, interpolation of tangent scaled rotations is included to conserve the angular momenta. Indeed, the same energy-momentum method was originally presented in [STD95] for 3D geometrically exact beams.

The extension of the conserving properties of the described time-integration scheme is not straightforward in systems with contact constrains. Nevertheless, it will be described further on that special care has been taken in order to model sliding contact without spoiling the conservative time-integration features.

1.2.3 The sliding contact approach

Contact constrains can be either imposed through the use of Lagrange multipliers, a Penalty method or the master-slave formulation (also called the minimum set method). The latter approach will be the one described in the present work, and the idea behind is to relate the kinematics of a *slave* node through the displacements of a *master* element. This method has been presented in previous work in the context of general elastodynamics, and 3D geometrically exact beams with joints (see [MJ04, MJ06]). The main advantage of the master-slave method compare with the other two techniques named before is that in the former case non algebraic equations are added to the system of ODE. In consequence, the solution is done using the same methods developed for displacement based finite element formulations.

For the model of sliding contact using the master-slave method, first the beam equilibrium equations are obtained for the complete system considering no kinematic constrains. In the finite element implementation this means that each of the beam's equations are obtained by independent assembling. The second step is done by modifying the resulting equations in such a way that the work associated to the released displacements is taken into account in the Virtual Work Principle.

With the chosen method to model sliding contact, the resulting equilibrium equations can be integrated in time using the schemes described in the previous sub-section. In order to retain the conserving properties, an incremental form of the master-slave can be derived [MJ06]. Moreover, in this thesis there is a contribution to the method's performance at the contact transition between the set of aligned elements. It is also a novelty that energy and momentum conservation has been achieved for the constrained system with a relaxed sliding condition [SM11].

1.3 Outline of this Work

The thesis will be organized from now on in four chapters and a set of Appendices derived from the former ones. There will be one different chapter to deal with each of the topics presented in the previous sub-section and a final one that recopilates a series of numerical examples.

In Chapter 2, the beam 2D theory is fully presented, as well as a complete description of the finite element implementation. The beam equilibrium equations are first derived for the static case. For that purpose, the simplest constitutive model is chosen, which assumes a linear relation between strain and stresses. Finally, the equations are discretized using finite element interpolation. In addition, the last part of the chapter will introduce B-Spline interpolation and describe how is it implemented in the beam discretization.

Chapter 3 will introduce the beam dynamics and different approaches to perform time-integration of the equations of motion. The Newmark method is described first and will be the non-conservative scheme used in numerical examples. Although the purpose of the present work is to perform conservative

time-integration, the Newmark method will be used to compare and demostrate the robustness of the former schemes. The conservative scheme will then be introduced, together with a discussion about the link between the choice of the rotational interpolated variables and the algorithm properties.

Chapter 4 presents a complete description of the master-slave method implemented for 2D sliding contact in beams. First, a variational formulation is developed, which will usefull together with the Newmark method. On the other hand, an incremental form of the method has to be described in order to be used with the conservative time-integration scheme. Three different strategies are finally presented in the family of conserving algorithms. This arises from the compromise that exists between the fullfilment of the sliding conditions and the requirements of the angular momemtum conservation. In this way, a conservative algorithm that preserves the sliding condition and conserve energy is the first case studied. Furthermore, an angular momentum conserving algorithm with a relaxed sliding condition which fails to conserve energy is the second strategy. Last but not least, an energy and momentum conservative scheme with a relaxed contact condition is the novel approach presented.

The last chapter will present in detail different numerical examples, starting with a simple static case of beam modelling and finally including a set of dynamic problems with sliding contact. Some of the examples are taken from literature, and are specially chosen to show the algorithms' features and performance comparisson. All of them have been coded in *MATLAB* as well as the post-processing of results that is shown.

Chapter 2

The beam theory and implementation

The first attempt to describe large displacements and shear deformations in beams was done by Reissner, who obtained the strain measures for the planar [Rei72] and the three-dimensional case [Rei73]. After that, much work was developed by Simo and others in order to obtain a proper definition of the discretized equations of motion in time and space in the 3D case [Sim85, SVQ86a, SVQ88]. The complexity in the 3D case is given by the fact that large rotations belong to a special orthogonal group *SO(3)*, space which is a non-linear differential manifold [SVQ86a]. The beam theory is usually known as the geometrically exact or Reissner-Simo beam theory. The description in the present chapter is restricted to the planar beam case without accounting any inertial terms (equations in statics).

The kinematics of the planar beam is stated in Section 2.1. This is the basis of the definition of the strain measures, which are described in Section 2.2. Providing this knowledge, the variational form of the equilibrium equations is obtained in Section 2.3 through the application of the Virtual Work Principle and a standard finite element interpolation. For this purpose, a linear stress-strain relationship is assumed as the constitutive model. The remaining ingredient needed for the numerical implementation of the beam theory is the linearization of the variational form. This is also included in Section 2.3 and a detailed description is presented in Appendix B.

The last section of the present chapter introduces the B-Spline interpolation, (see Section 2.4). A general description of this technique and the application for the interpolation of the beam variables is also covered. The latter includes some modifications compared to standard finite element procedures such as element assembly and Gaussian numerical integration.

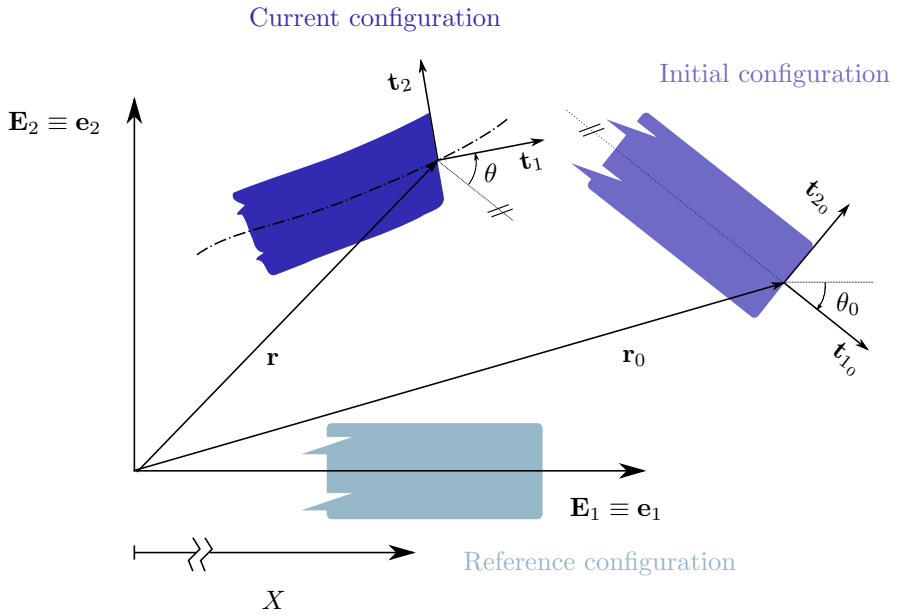

Figure 2.1: Finite motion of a planar beam

2.1 The beam kinematics

The kinematics of the geometrically exact beam is based on the idea that all the admissible deformed configurations can be described through a position vector $\mathbf{r}$ and a moving frame $\mathbf{t}_i$ attached to a typical beam cross-section [SVQ86a] (with vector $\mathbf{t}_1$ always normal to it, see Figure 2.1). The vector $\mathbf{r}$ maps the beam's line of centroids to its current position. The orientation of the moving frame $\mathbf{t}_i$ it is defined by a matrix $\mathbf{\Lambda} \in SO(3)$. In fact, by stating that the beam is fully defined by the position and orientation of the cross-sections, the theory assumes implicitly that these planes remain undeformed (Bernoulli hypothesis). Since $\mathbf{t}_1$ (see Figure 2.1) is not limited to take the orientation tangent to the beam's line of centroids, the formulation does account for shear deformations.

Let us assume the planar beam configuration depicted in Figure 2.1. There is a fixed *material* basis denoted by $\{\mathbf{E}_I\}_{I=1,2}$ and a fixed *spatial* basis $\{\mathbf{e}_i\}_{i=1,2}$, which are assumed to be coincident. Material quantities are referred to the former, while spatial quantities are referred to the latter.

The reference beam configuration is a straight line [1] of length L with perpendicular cross-sections and it longitudinal axis aligned with $\mathbf{E}_1$ (see Figure 2.1). The beam initial position and orientation is defined by $\mathbf{r}_0$ and $\mathbf{\Lambda}_0$ respectively. Let define then a parametrization:

$$\mathbf{r}(X,t) = \Re \rightarrow \Re^2\,,$$

where $X \in [0, L] \subset \Re$ is the beam's arc length parameter and t a time parameter. Furthermore, the orthogonal transformation $\mathbf{\Lambda}$ is such that:

[1] Initially non-straight beams theory can be found in [Sim85, Ibr95].

$$\mathbf{t}_I(X,t) = \left(\mathbf{\Lambda}(X,t)\,\mathbf{\Lambda}_0(X)\right)^{\mathrm{T}}\,\mathbf{E}_I\,,\; I=1,2\,, \tag{2.1}$$

where $\mathbf{t}_I$ and $\mathbf{E}_I$ are considered $\forall\ I$ vectors in column shape. This convection will be used for vectors through all this thesis.

Usually the beam kinematics is described separately for what displacements and rotations account. For practical reasons, and due to the simplicity of the rotation field in 2D the following will be used in the present section:

$$\mathbf{r} = \left\{\begin{array}{c} r_1 \\ r_2 \\ r_3 \end{array}\right\} = \mathbf{r}_0(X) + \mathbf{u}(X,t) = \underbrace{\mathbf{\Lambda}_0 \left\{\begin{array}{c} X \\ 0 \\ 0 \end{array}\right\} + \left\{\begin{array}{c} u_0 \\ v_0 \\ \theta_0 \end{array}\right\}}_{\mathbf{r}_0} + \left\{\begin{array}{c} u \\ v \\ \theta \end{array}\right\}\,, \tag{2.2}$$

where the beam rotation $\theta(X,t)$ has been included as the third component of the displacement vector $\mathbf{u}$. Accordingly, the following definition will also be used in this section:

$$\mathbf{\Lambda}_0 = \begin{bmatrix} \cos\theta_0 & -\sin\theta_0 & 0 \\ \sin\theta_0 & \cos\theta_0 & 0 \\ 0 & 0 & 1 \end{bmatrix}\;;\;\; \mathbf{\Lambda} = \begin{bmatrix} \cos\theta & -\sin\theta & 0 \\ \sin\theta & \cos\theta & 0 \\ 0 & 0 & 1 \end{bmatrix}\,. \tag{2.3}$$

2.2 Definition of the strain measure

The actual distinction between *material* and *spatial* quantities in the *reference* and *current* configurations respectively, together with the equivalence of the stress power, are the base in the derivation of the strain measures for the 3D beam theory (see for instance [SVQ86a]).

We will first resort to the strain density function of an elastic body, defined in terms of conjugate magnitudes of force and strain, which result for the planar beam as follows:

$$\Psi = \frac{1}{2}\int_{\mathrm{L}} \mathbf{N}\cdot\mathbf{\Gamma}\,\mathrm{d}X\,, \tag{2.4}$$

where $\mathbf{N} = \left\{\begin{array}{c} \mathrm{F}_u \\ \mathrm{F}_v \\ \mathrm{M} \end{array}\right\}$ and $\mathbf{\Gamma} = \left\{\begin{array}{c} \Gamma_u \\ \Gamma_v \\ \Gamma_\theta \end{array}\right\}$. Let remark that $\mathbf{N}$ holds the *material* stress and couple resultant (at a cross section of the beam), which therefore refers to the *reference* configuration. On the other hand, $\mathbf{n}$ will hold the *spatial* stress and couple resultant [2], and can be obtained transforming $\mathbf{N}$ to the *current* configuration (*push-forward*):

[2] For the plane case, it is trivial to make a distinction between *material* and *spatial* stress couple but here it is done for notation completeness.

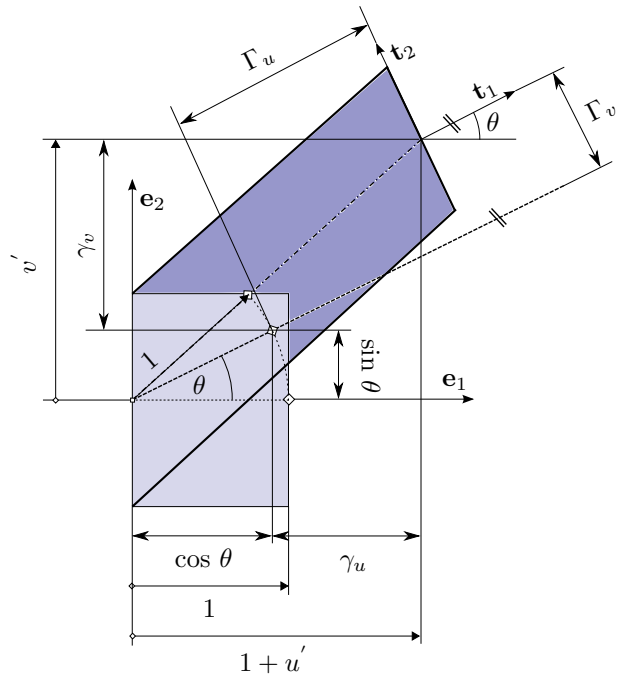

Figure 2.2: Geometrical interpretation of $\mathbf{\Gamma}$

$$\mathbf{n} = \left\{ \begin{array}{c} \mathrm{f}_u \\ \mathrm{f}_v \\ \mathrm{m} \end{array} \right\} = \mathbf{\Lambda}\,\mathbf{\Lambda}_0\,\mathbf{N}\,. \tag{2.5}$$

Note that due to equations (2.5) and (2.1), the components of $\mathbf{n}$ in the moving frame $\mathbf{t}_I$ are identical to the components in the basis $\mathbf{E}_I$ of $\mathbf{N}$, which contains the axial force, the shear force, and the bending moment at a cross-section of the beam. This is important to remark because will make clear later that $\mathbf{\Gamma}$ is energetic conjugate to $\mathbf{N}$ in (2.4), where the potential energy is defined relative to the moving frame $\mathbf{t}_I$.

Let us define the strain field in the following way:

$$\mathbf{\Gamma} = \left(\mathbf{\Lambda}\,\mathbf{\Lambda}_0\right)^{\mathrm{T}}\,\mathbf{r}^{'} - \mathbf{E}_1\,. \tag{2.6}$$

where here and all through the rest of the work, the dash symbol ($'$) denotes derivative with respect to X.

The geometric interpretation of $\mathbf{\Gamma}$ is depicted in Figure 2.2, where neither translation nor rotation in the beam initial configuration is assumed for simplicity ($\left\{u_0 \quad v_0 \quad \theta_0\right\}^{\mathrm{T}} = \mathbf{0}$). Following (2.2) and (2.6) then it is possible to write that:

$$\mathbf{\Gamma} = \mathbf{\Lambda}^{\mathrm{T}} \left(\mathbf{r}^{'} - \mathbf{\Lambda}\, \mathbf{E}_1 \right) = \mathbf{\Lambda}^{\mathrm{T}} \underbrace{\begin{Bmatrix} 1 + u^{'} - \cos\theta \\ v^{'} - \sin\theta \\ \theta^{'} \end{Bmatrix}}_{\gamma} = \mathbf{\Lambda}^{\mathrm{T}} \begin{Bmatrix} \gamma_u \\ \gamma_v \\ \gamma_\theta \end{Bmatrix} . \tag{2.7}$$

Equation 2.7 refers to the transformation of the strain field γ, measured with respect to the fixed basis $\mathbf{e}_I$, to the moving basis $\mathbf{t}_I$. Noting this geometrical interpretation and bearing in mind the correspondence detailed between $\mathbf{N}$ and $\mathbf{n}$ in (2.5), the energetic conjugacy proposed in (2.4) is explained. Indeed, the success of the present formulation resides in the invariance property of the strain field, when measured with respect to the moving frame. The proof for the invariance of Γ_u and Γ_v can be found in [SVQ86b] whereas the invariance of Γ_θ is straightforward for the planar case.

2.3 A variational description for finite deformation

In order to construct finite element approximations for the solution of finite deformation problems, i.e. the one described in the previous section 2.2, it is necessary to write the formulation in the weak (or variational) form. These integrals forms are chosen to be written in the *reference* configuration. This approach allow us to treat variation or linearization steps simpler because the *reference* domain does not change during the deformation process.

In order to deduce the variational form, we introduce the total energy Π of the system in statics as [ZT00]

$$\Pi = \Psi - \Pi_{ext} \,, \tag{2.8}$$

with Ψ defined in (2.4) and Π_{ext} being the potential for the external work, both described in the *reference* configuration.

As we stated before, it will be assumed that strains are small, which allow us to express a linear elastic relation between $\mathbf{N}$ and $\mathbf{\Gamma}$ (the constitutive law):

$$\mathbf{N} = \mathbf{C_e}\, \mathbf{\Gamma} = \mathrm{diag} \left\{ \mathrm{E\,A} \quad \kappa\, \mathrm{G\,A} \quad \mathrm{E\,I} \right\} \mathbf{\Gamma} \,, \tag{2.9}$$

where E and G are respectively the beam's material Young's and shear modulus, A is the cross-sectional area and I is the moment of inertia about the beam's cross-section centroid. Equation (2.9) implies that stresses are constant along the cross-section, so it is common practice to include κ as a shear correction factor that accounts for shear variations along A.

Using the proposed constitutive law, then it is possible to write (2.8) as:

$$\Pi = \frac{1}{2} \int_{\mathrm{L}} \mathbf{C_e}\, \mathbf{\Gamma} \cdot \mathbf{\Gamma}\, \mathrm{d}X - \Pi_{ext} = \frac{1}{2} \int_{\mathrm{L}} \mathbf{\Gamma}^{\mathrm{T}}\, \mathbf{C_e}\, \mathbf{\Gamma}\, \mathrm{d}X - \Pi_{ext} \,. \tag{2.10}$$

With the proposed constitutive law, it is clear from (2.10) that Ψ results in a quadratic form in $\mathbf{\Gamma}$. Taking the variation of (2.10), it is found that:

$$\delta\Pi = \int_{\mathrm{L}} \delta\mathbf{\Gamma}^{\mathrm{T}} \underbrace{\mathbf{C_e}\,\mathbf{\Gamma}}_{\mathbf{N}} \,\mathrm{d}X - \delta\Pi_{ext}\,, \tag{2.11}$$

where now $\delta\Pi_{ext}$ denotes a term from end forces and loading along the beam length. Here, we will consider that loads do not depend on the deformed configuration. On the other hand, follower loads are configuration dependent and such treatment can be find in [SVQ86a] for the 3D finite strain beam.

The vector $\delta\mathbf{\Gamma}$ corresponds to the beam's virtual strains and is obtained from the variation of equation (2.6) as follows:

$$\delta\mathbf{\Gamma} = \delta\left(\left(\mathbf{\Lambda}\,\mathbf{\Lambda}_0\right)^{\mathrm{T}}\,\mathbf{r}'\right) = -\left(\mathbf{\Lambda}\,\mathbf{\Lambda}_0\right)^{\mathrm{T}}\,\mathbf{J}\,\mathbf{r}'\delta\theta + \left(\mathbf{\Lambda}\,\mathbf{\Lambda}_0\right)^{\mathrm{T}}\,\delta\mathbf{r}'\,, \tag{2.12}$$

with the following defined skew-symmetric matrix $\mathbf{J} = \begin{bmatrix} 0 & -1 & 0 \\ 1 & 0 & 0 \\ 0 & 0 & 0 \end{bmatrix}$ (see Appendix A for further details on the variation of rotations).

A finite element approximation for the displacements and rotation shall be introduced accordingly to:

$$\begin{Bmatrix} u \\ v \\ \theta \end{Bmatrix} \approx \mathbf{I}_\alpha(X) \begin{Bmatrix} u_\alpha \\ v_\alpha \\ \theta_\alpha \end{Bmatrix}\,, \tag{2.13}$$

where the shape functions $\mathbf{I}_\alpha(X)$ are standard Lagrangian polynomials and $\begin{Bmatrix} u_\alpha & v_\alpha & \theta_\alpha \end{Bmatrix}^{\mathrm{T}}$ correspond to $\alpha = 1, \ldots, n$ nodal values of the interpolated variables. Summation over repeated indices is implied and this convention will be followed from here on.

Recall that the same set of shape functions are used for each variable, and that elemental functions $\mathbf{I}_\alpha(X)$ of node α satisfy the completeness conditions:

$$\sum_{\alpha}^{n} \mathbf{I}_\alpha(X) = 1 \;\Rightarrow\; \sum_{\alpha}^{n} \mathbf{I}'_\alpha(X) = 1\,. \tag{2.14}$$

Using this approximation, the variational equation (2.11) may now be written for the finite element problem as:

$$\delta\Pi = \begin{bmatrix} \delta u_\alpha & \delta v_\alpha & \delta\theta_\alpha \end{bmatrix} \left(\int_{\mathrm{L}} \mathbf{B}_\alpha^{\mathrm{T}}\,\mathbf{n}\,\mathrm{d}X - \mathbf{f}_\alpha \right) = 0\,, \tag{2.15}$$

where the strain-displacement matrix is obtained by approximation of (2.12), and after some standard algebra manipulations results in:

$$\mathbf{B}_\alpha = \begin{bmatrix} \mathbf{I}_\alpha^{'} & 0 & \mathbf{I}_\alpha\, r_2^{'} \\ 0 & \mathbf{I}_\alpha^{'} & -\mathbf{I}_\alpha\, r_1^{'} \\ 0 & 0 & \mathbf{I}_\alpha^{'} \end{bmatrix} . \tag{2.16}$$

Regarding the external forces, the interpolation of $\delta\Pi_{ext}$ yields

$$\mathbf{f}_\alpha = \int_{\mathrm{L}} \begin{Bmatrix} \mathbf{I}_\alpha \left(\rho_0\, \mathrm{A}\, \mathbf{b} + \bar{\mathbf{T}}\right) \\ 0 \end{Bmatrix} \mathrm{d}X\,, \tag{2.17}$$

where we have considered for simplicity the beam is subjected to force vectors $\mathbf{b}$ and $\bar{\mathbf{T}}$, a body and a distributed load along the arc length parameter respectively, all defined in the *reference* configuration.

Let us remark that $\begin{bmatrix} \delta u_\alpha & \delta v_\alpha & \delta\theta_\alpha \end{bmatrix}$ are the beam nodal virtual displacements and rotation in the *reference* configuration, which are arbitrary except at the Dirichlet boundary. This implies that satisfying the finite element approximation of the variational equation (2.15), implies the satisfaction of equilibrium and the traction boundary conditions at each node of the beam. Therefore, the set of nodal beam equilibrium equations is conformed by:

$$\mathbf{g}_\alpha = \mathbf{g}_\alpha^e - \mathbf{f}_\alpha = \mathbf{0}\,,\ \alpha = 1, \ldots, n\ ; \tag{2.18}$$

where $\mathbf{g}_\alpha$ is the residual vector for node α and

$$\mathbf{g}_\alpha^e = \int_{\mathrm{L}} \begin{bmatrix} \mathbf{I}_\alpha^{'} & 0 & 0 \\ 0 & \mathbf{I}_\alpha^{'} & 0 \\ \mathbf{I}_\alpha\, r_2^{'} & -\mathbf{I}_\alpha\, r_1^{'} & \mathbf{I}_\alpha^{'} \end{bmatrix} \mathbf{n}\, \mathrm{d}X \tag{2.19}$$

is the elastic nodal force vector. Although the finite element problem is stated completely in (2.18), for the numerical solution of the nodal equilibrium equations, the linearization of the beam residuals will have to be computed. In Appendix B, a brief description of the Newton-Raphson method is presented together with the derivation of the system (2.18) tangent stiffness matrix.

2.4 Modelling smooth contact slidelines

In the context of Computer Aided Engineering (*CAE*), the geometry is usually modelled with *B*-Splines or *NURBS* (Non-Uniform Rational *B*-Splines). However, this information is often lost when the geometry is discretized using finite elements. Research has been recently done in a field that tries to skip the mesh generation. Instead of using an approximated geometry with finite elements, an exact description is done with *NURBS* and these ones are used as well as basis for the analysis. This topic has been denominated *Iso-geometric* analysis [HCB05], but since mesh generation is the approach mostly used, a method will be described here to transform a set of finite elements into a *B*-Splines curve [Muñ08]. The resulting interpolation will have the same number of elements but a different number of nodes and connectivity pattern.

2.4.1 *B*-Spline interpolation

The initial beam geometry will be discretized by a set of n_e cubic B-Splines, which results in a curve $\mathbf{C_e}(\xi) = B_{i,p}(\xi)\mathbf{P}_i$. The curve is shaped according to $n+1$ *control* points $\mathbf{P}_i$ and the corresponding basis function $B_{i,p}(\xi)$, defined over a parametric space $0 \leq \xi \leq 1$ and a polynomial order, which is chosen to be $p = 3$. For further details, see Ref. [PT97].

The support of each basis function is determined from a *knot* vector $\mathbf{k}$ of the form $\mathbf{k}^{\mathrm{T}} = \left\{ \underbrace{0,\ldots,0}_{p+1}, \xi_1, \ldots, \xi_{m-2p-1}, \underbrace{1,\ldots,1}_{p+1} \right\}_{m+1}$, which has $m+1$ *knot* values and $m = n+p+1$. The *knot* spans $[\xi_i, \xi_{i+1})$ are used to define the basis functions, that are constructed following a recursive formulae for **all** *knot* values in $\mathbf{k}$:

$$\begin{aligned} B_{i,0}(\xi) &= \begin{cases} 1 & \text{if } \xi_i \leq \xi < \xi_{i+1} \\ 0 & \text{otherwise} \end{cases} \\ B_{i,p}(\xi) &= \frac{\xi - \xi_i}{\xi_{i+p} - \xi_i} B_{i,p-1}(\xi) + \frac{\xi_{i+p-1} - \xi}{\xi_{i+p+1} - \xi_{i+1}} B_{i+1,p-1}(\xi) \end{aligned} \tag{2.20}$$

It is common practice to refer as the *speed*, the norm of the tangents to the parametrized curve $\left|\mathcal{C}'(\xi)\right|$. The most relevant properties of the B-Splines curves [Muñ08] are summarized as follows:

P1. Local support, as i.e. $B_{i,3}(\xi) = 0$ for $\xi \notin [\, \xi_i, \xi_{i+4} \,)$.

P2. As a consequence of *P1*, for a given span $[\, \xi_i, \xi_{i+1} \,)$, at most 4 $(p+1)$ basis functions are non-zero.

P3. Non-negativity of the basis functions, $B_{i,p}(\xi) \geq 0\,,\ \forall\, i, p$.

P4. The tangents of a B-Spline curve that passes through a control point $\mathbf{P}_k$ have the directions $\mathbf{P}_k - \mathbf{P}_{k-1}$ and $\mathbf{P}_{k+1} - \mathbf{P}_k$.

From properties *P3* and *P4*, a resulting B-Splines interpolation holds a smooth curve that start and end at the extremes control points, and approaches the control points in the interior.

2.4.2 Curve fitting

The construction of B-Splines curves that fit an arbitrary set of geometric data is known as *fitting*. Many work has been done on this field and it is only intended here to describe the method chosen to develop B-Spline interpolation from an existing finite element mesh. In the present case, for initially straight beams, the fitting problem is pretty simple. However, it will be referred here a method that can deal with a general curve in 3D.

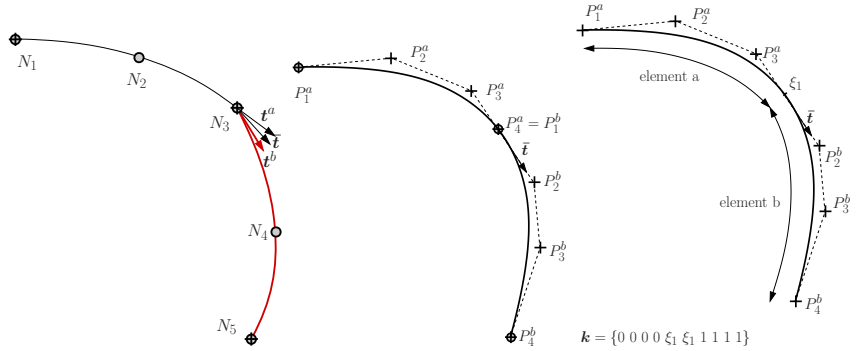

Figure 2.3: Definition of B-Spline from initial nodes of the beam.

It is first stated that the fitting problem in the present case categorizes as data *interpolation*, which means that the constructed curve will satisfy precisely the given geometry and to distinguish it from data *approximation*. Moreover, the method described in this sub-section is considered *local* rather than *global* interpolation. Local algorithms only use local data for each step, which makes them computationally less expensive and can also deal with cusps or straight line segments better. On the other hand, its more difficult to deal with the desire continuity at segment boundaries and multiple interior knots will usually result.

A C^1 continuity curve is the goal to construct in order to smooth the finite element contact transition. There is a possible choice between quadratic or cubic B-Splines for that purpose. However, the choice for cubic B-Splines resides in the fact that they can handle inflection points and collinearity without any special treatment [PT97]. The following algorithm is described in [PT97, pp. 395-405] as a *local cubic curve interpolation* and allows to construct a cubic C^1 B-Splines curve from a set two end-points $\mathbf{P}_0^e$ and $\mathbf{P}_3^e$ and their corresponding unit length tangent directions, $\mathbf{T}_0^e$ and $\mathbf{T}_3^e$ respectively.

Given n_e number of elements in a finite element mesh, a set of n_e Bézier segments $\mathcal{C}^e(\xi^e)$, with $0 \leq \xi^e \leq 1$ will be first constructed following the speed constant condition:

$$\left|\mathcal{C}'^e(0)\right| = \left|\mathcal{C}'^e(0.5)\right| = \left|\mathcal{C}'^e(1)\right| . \tag{2.21}$$

This construction is proved to be unique [PT97] and will be the basis for the intended B-Splines curve. The whole process is summary in the following step by step list:

1. An average unit length tangent direction is determined from the common nodes of adjacent elements, i.e. $\mathbf{T}_{avg} = 0.5(\mathbf{T}^A + \mathbf{T}^B)$ (see Figure 2.3a).

2. For each element e, a Bézier segment is constructed with four control points, $\mathbf{P}_0^e \ldots \mathbf{P}_3^e$, and the two at the extreme will coincide with the finite element end-nodes (see Figure 2.3b). Moreover, due to property *P4*, the control points at the middle are obtained using:

$$\mathbf{P}_1^e = \mathbf{P}_0^e + \frac{1}{3}\alpha\,\mathbf{T}_{0\,avg}^e\,;\ \mathbf{P}_2^e = \mathbf{P}_3^e - \frac{1}{3}\alpha\,\mathbf{T}_{3\,avg}^e\,, \tag{2.22}$$

where $\mathbf{T}_{0\,avg}^e = \mathbf{T}_{3\,avg}^{e-1}$ and $\mathbf{T}_{3\,avg}^e$ are the average tangent directions at adjacent elements. The construction is fully defined by the speed parameter α, which is derived using condition (2.21) and results to be the positive solution of the quadratic equation [PT97]:

$$a\,\alpha^2 + b\,\alpha + c = 0\,, \tag{2.23}$$

with $a = 16 - \left|\mathbf{T}_{3\,avg}^e + \mathbf{T}_{0\,avg}^e\right|^2$, $b = 12\,(\mathbf{P}_3^e - \mathbf{P}_0^e)\cdot\left(\mathbf{T}_{3\,avg}^e + \mathbf{T}_{0\,avg}^e\right)$ and $c = -36\,|\mathbf{P}_3^e - \mathbf{P}_0^e|^2$.

3. The set of knot values $\overline{\xi}^{\,e+1} = \overline{\xi}^{\,e} + |\mathbf{P}_1^e - \mathbf{P}_0^e|$ is computed. This yield to a uniform parametrization, where each Bézier segment have unitary speed at their end and mid-points with respect to the intervals $\left[\overline{\xi}^{\,e}, \overline{\xi}^{\,e+1}\right]$.

4. If the internal common nodes, $\mathbf{P}_3^1 \ldots \mathbf{P}_3^{n_e-1}$, are removed, a C^1 continuous cubic B-Spline curve is defined by the control points (see Figure 2.3c)

$$\underbrace{\mathbf{P}_0^1, \mathbf{P}_1^1, \mathbf{P}_2^1, \mathbf{P}_1^2, \mathbf{P}_2^2, \ldots, \mathbf{P}_1^{n_e}, \mathbf{P}_2^{n_e}, \mathbf{P}_3^{n_e}}_{2\,(n_e+1)}\,. \tag{2.24}$$

and the knots

$$\mathbf{k}^{\mathrm{T}} = \left\{ \underbrace{0,0,0,0, \frac{\overline{\xi}^{\,1}}{\overline{\xi}^{\,n_e}}, \frac{\overline{\xi}^{\,1}}{\overline{\xi}^{\,n_e}}, \frac{\overline{\xi}^{\,2}}{\overline{\xi}^{\,n_e}}, \frac{\overline{\xi}^{\,2}}{\overline{\xi}^{\,n_e}}, \ldots, \frac{\overline{\xi}^{\,n_e-1}}{\overline{\xi}^{\,n_e}}, \frac{\overline{\xi}^{\,n_e-1}}{\overline{\xi}^{\,n_e}}, 1,1,1,1}_{2\,(n_e+3)} \right\}. \tag{2.25}$$

If the above described steps are followed, a finite element mesh in a slideline has been transformed in a B-Splines curve parametrized via ξ, $0 \le \xi \le 1$. Each element e is defined by the knot span $\xi \in [\,\xi_{2e+2}, \xi_{2e+3}\,)$ and four control points $\mathbf{P}_2^{e-1}$, $\mathbf{P}_1^e$, $\mathbf{P}_2^e$ and $\mathbf{P}_2^{e+1}$. As an exception to the previous rule, the first and last elements will have control points $\mathbf{P}_0^1$, $\mathbf{P}_1^1$, $\mathbf{P}_2^1$ and $\mathbf{P}_2^2$ and $\mathbf{P}_2^{n_e-1}$, $\mathbf{P}_1^{n_e}$, $\mathbf{P}_2^{n_e}$ and $\mathbf{P}_3^{n_e}$ respectively (see Figure 2.3c). Moreover, the control points of each element will be consider as the new B-Splines nodes, since the knot span ensure (by means of property *P2*) there are only four non-zero basis functions. It is sufficient then to resort to the previous B-Spline construction of the domain and use the B-Spline basis functions as the shape functions $\mathbf{I}_\alpha(\xi)$ in the variational formulation. Therefore, cubic B-Spline interpolation of beams will parallel standard cubic Lagrangian finite elements, if the shape functions are modified properly. However, the latter implies two important modifications to be done compared to standard finite element procedures that will be described next.

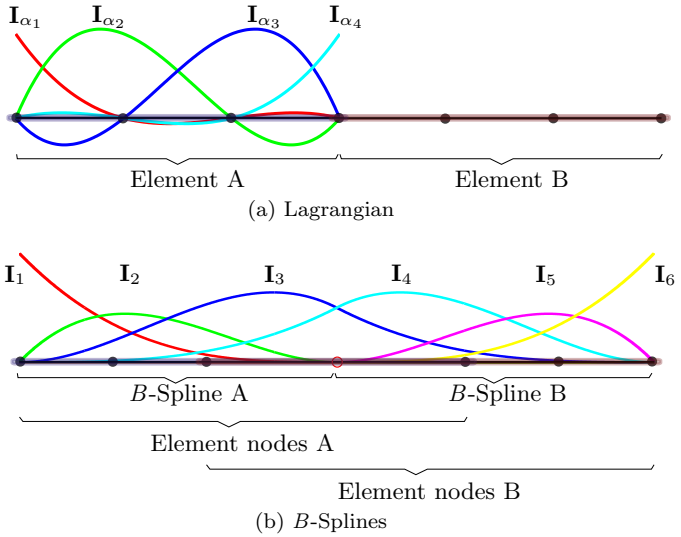

Figure 2.4: Connectivity of finite elements. Standard Lagrangian (a) and B-Splines (b).

When comparing B-Spline interpolation with standard finite element meshes, it is observed that connectivity will differ. Due to the support of B-Splines basis functions, the nodal connectivity will overlap different, i.e. in Figure 2.4b adjacent element has more than one common nodes. Regarding numerical integration, according to the degree of the B-Splines basis functions, at least 3 Gauss Points per element along the beam arc length direction has to be used to avoid *underintegration*. In addition, note that the parent domain for the whole set of B-Splines belongs to $\xi \in [0, 1]$ and this differ from standard iso-parametric finite elements. Therefore, the location of the Gauss Points for each element will differ in the B-Splines parent domain and additional storage of the elemental shape function values will be needed (but no additional computational effort is required).

Chapter 3

Time-integration

It is of prime interest in this thesis to describe the behaviour of sliding beams under the effect of inertial forces. In the beam equilibrium equations described in (2.11) non dynamic term is described. To do so, the equations of motion will be derived resorting to the Hamilton's principle and Lagrange equations. From this variational approach, the Newmark method [New59] will be presented as the proposed scheme to integrate in time the beam equations of motion. It is shown in [Muñ04] that the beam equations of motion in the continuum do conserve the mechanical properties (energy and momenta) in absence of external and dissipative loads. This motivates further analysis on the conserving properties of the fully discretized (in space and time) beam equations. For the Newmark method it will be shown that neither energy nor angular momenta are finally conserved, and numerical examples confirm these conclusions afterwards.

In the context of modified time integration schemes, there are possible alternatives that have been studied in order to achieve the constants of motion conservation in the non-linear regime. In some techniques, the conservation of energy is imposed upon a given algorithm through the use of Lagrange Multipliers, i.e. in [HCL78]. In a similar approach, but using penalty parameters, other energy conserving time integration has been developed (see i.e. [KC99]). On the other hand, here it will be followed the idea of keeping the minimum set of degrees of freedom and not coupling differential with *algebraic* equations. The conservation of energy is imposed between two subsequent time steps and therefore an incremental form of the beam equations of motion will arise. This approach will result in modified equilibrium equations (at a *mid-time* point) that will conserve the system energy. Moreover, in order to achieve angular momentum conservation, a *tangent-scaled* interpolation of the beam incremental rotations has to be implemented. The whole approach was first presented in [STD95] in the context of 3D nonlinear beams and here it will be used as a particular case for planar beams. In fact, an energy conserving time integration scheme for planar beams is described in [SS96], developed for linear finite elements and interpolation of *unscaledd* incremental rotations. It will be demonstrated here that the latter approach fails to conserve angular momentum.

Finally, many works has been also done in the context of conserving time integration schemes with an additional energy dissipation. In [BB99, AR01],

energy decaying algorithms have been constructed in order to eliminate undesirable high frequencies in a system response. This kind of approach will result more convenient to simulate dynamic problems where sudden motions or high frequency oscillations are likely to appear. They are though based on exact energy conserving algorithms.

3.1 Non-conserving schemes

3.1.1 A variational formulation for non-linear dynamics

Let us assume first the following definitions for a mechanical system in absence of dissipative loads. Consider $\mathbf{q}$ a vector of generalized coordinates (i.e. Cartesian) and $T(\dot{\mathbf{q}})$ the system kinetic energy. The potential elastic energy $\Psi(\mathbf{q})$ and the scalar potential associated with a conservative load $\Pi_{ext}(\mathbf{q})$ are the ones described previously in Section 2.3. The total energy of the system is now considered $\Pi(\mathbf{q}, \dot{\mathbf{q}}) = T + \Psi - \Pi_{ext}$, and a Lagrangian function is defined as $L(\mathbf{q}, \dot{\mathbf{q}}) = T - (\Psi - \Pi_{ext})$. The Hamilton's principle states that the true evolution of $\mathbf{q}(t)$ between two specified states at two specified times, $\mathbf{q}_1 = \mathbf{q}(t_1)$ and $\mathbf{q}_2 = \mathbf{q}(t_2)$, is a stationary point of the *action* functional defined as:

$$\mathcal{A} \equiv \int_{t_1}^{t_2} L(\mathbf{q}, \dot{\mathbf{q}}, t)\, \mathrm{d}t\,. \tag{3.1}$$

In terms of functional analysis, the Hamilton's principle implies that the true physical evolution of a system is solution of the variational equation:

$$\delta\mathcal{A} = 0\,. \tag{3.2}$$

In order to asses (3.2), let also consider that $\delta\mathbf{q}$ is a vector of small perturbations that vanishes at the end-points of the trajectory $\mathbf{q}(t_1) = \mathbf{q}(t_2) = \mathbf{0}$. Therefore, to the first order in the perturbation, (3.2) result:

$$\delta\mathcal{A} = \int_{t_1}^{t_2} \left(\delta\mathbf{q} \cdot \frac{\partial L}{\partial \mathbf{q}} + \dot{\delta\mathbf{q}} \cdot \frac{\partial L}{\partial \dot{\mathbf{q}}} \right) \mathrm{d}t = \int_{t_1}^{t_2} \delta\mathbf{q} \cdot \left(\frac{\partial L}{\partial \mathbf{q}} - \frac{\mathrm{d}}{\mathrm{d}t} \frac{\partial L}{\partial \dot{\mathbf{q}}} \right) \mathrm{d}t = 0\,;\ \forall \delta\mathbf{q}\,, \tag{3.3}$$

where integration by parts and boundary conditions have been applied to obtain the final expression above. Note that (3.3) is satisfied if and only if:

$$\frac{\partial L}{\partial \mathbf{q}} - \frac{\mathrm{d}}{\mathrm{d}t} \frac{\partial L}{\partial \dot{\mathbf{q}}} = 0\,, \tag{3.4}$$

which are known as the Lagrange equations for the variational problem. The equations of motion for the mechanical system are obtained applying the Virtual Work Principle and (3.4):

$$\delta\mathbf{q} \cdot \frac{\mathrm{d}}{\mathrm{d}t} \nabla_{\dot{\mathbf{q}}} T + \delta\mathbf{q} \cdot \nabla_{\mathbf{q}} \Psi - \delta\mathbf{q} \cdot \nabla_{\mathbf{q}} \Pi_{ext} = 0\,;\ \forall \delta\mathbf{q}\,. \tag{3.5}$$

Note from equation (3.5) that the second term yields $\delta\Psi - \delta\Pi_{ext}$ defined previously in (2.11). The first term will be named $\delta\mathcal{W}_{dyn}$ and deals with the inertial terms of the dynamic non-linear problem. In general, the kinetic energy for mechanical systems has a quadratic form. For the planar beam theory:

$$T = \frac{1}{2}\int_{\mathrm{L}} \dot{\mathbf{r}}^{\mathrm{T}}\, \mathbf{C_d}\, \dot{\mathbf{r}}\, \mathrm{d}X\,, \tag{3.6}$$

where $\mathbf{r}$ stands for the position vector defined in (2.2) and $\mathbf{C_d} = \mathrm{diag}\left\{\mathrm{A}_\rho \quad \mathrm{A}_\rho \quad \mathrm{I}_\rho\right\}$, with $\mathrm{A}_\rho = \mathrm{A}\,\rho_0$ and $\mathrm{I}_\rho = \mathrm{I}\,\rho_0$. The superimposed dot symbols ($\dot{}$) and ($\ddot{}$) denote here and onwards first and second time differentiation respectively.

3.1.2 The Newmark method

Since first and second time differentiation of the interpolated variables (see (2.13)) will naturally arise in the equation of motion, the numerical time integration will be introduced here. The Newmark algorithm was specially designed for the solution of second-order differential equations [New59], and is given by:

$$\begin{aligned}
\mathbf{r}_{n+1} &= \mathbf{r}_n + \dot{\mathbf{r}}_n\,\Delta t + \frac{1}{2}\,\ddot{\mathbf{r}}_n\,\Delta t^2 + \beta\,\Delta t^3\,\frac{\ddot{\mathbf{r}}_{n+1} - \ddot{\mathbf{r}}_n}{\Delta t} \\
\dot{\mathbf{r}}_{n+1} &= \dot{\mathbf{r}}_n + \ddot{\mathbf{r}}_n\,\Delta t + \gamma\,\Delta t^2\,\frac{\ddot{\mathbf{r}}_{n+1} - \ddot{\mathbf{r}}_n}{\Delta t}\,.
\end{aligned} \tag{3.7}$$

The scheme is originally designed for problems with translational degrees of freedom only. Note in (3.7), the position vector $\mathbf{r}$ - previously defined in (2.2) - includes the rotational degree of freedom θ. This can be done since non special treatment is needed for large rotations in the planar beam theory. The particular choice of $\beta = 1/4$ and $\gamma = 1/2$ constitutes the *trapezoidal* rule for numerical integration and is second order in accuracy. In *linear* problems, this is the highest accurate order that can be achieved for unconditional stability of the Newmark method [Muñ04]. However, this property will not be retained for non-linear dynamics and it will be shown by the numerical examples in Chapter 5.

The expressions in (3.7) can be reordered so the *unknowns* accelerations and velocities at time t_{n+1} are given as explicit functions of the *unknown* displacements $\mathbf{u}$ - previously defined in (2.2) - at time t_{n+1} and other *known* variables at time t_n:

$$\begin{aligned}
\ddot{\mathbf{r}}_{n+1} = \ddot{\mathbf{u}}_{n+1} &= \frac{1}{\beta\,\Delta t^2}\,(\mathbf{u}_{n+1} - \mathbf{u}_n) + \ddot{\tilde{\mathbf{u}}}_n \\
\dot{\mathbf{r}}_{n+1} = \dot{\mathbf{u}}_{n+1} &= \frac{\gamma}{\beta\,\Delta t}\,(\mathbf{u}_{n+1} - \mathbf{u}_n) + \dot{\tilde{\mathbf{u}}}_n\,,
\end{aligned} \tag{3.8}$$

where $\ddot{\tilde{\mathbf{u}}}_n$ and $\dot{\tilde{\mathbf{u}}}_n$ depend only on quantities that are given at time t_n:

$$\begin{aligned}\tilde{\ddot{\mathbf{u}}}_n &= -\frac{1}{\beta\,\Delta t}\,\dot{\mathbf{u}}_n + \frac{2\beta-1}{2\beta}\,\ddot{\mathbf{u}}_n \\ \tilde{\dot{\mathbf{u}}}_n &= \frac{\beta-\gamma}{\beta}\,\dot{\mathbf{u}}_n + \Delta t\,\frac{2\beta-\gamma}{2\beta}\,\ddot{\mathbf{u}}_n\,.\end{aligned} \tag{3.9}$$

If the finite element interpolation of displacements proposed in (2.13) is inserted in the velocity expression of (3.8), then it is possible to write the following:

$$\begin{aligned}\ddot{\mathbf{u}}_{n+1} &= \mathbf{I}_\alpha\left(\frac{1}{\beta}\,\frac{\mathbf{u}^\alpha_{n+1}-\mathbf{u}^\alpha_n}{\Delta t^2} + \tilde{\ddot{\mathbf{u}}}^\alpha_n\right) = \mathbf{I}_\alpha\,\ddot{\mathbf{u}}^\alpha_{n+1} \\ \dot{\mathbf{u}}_{n+1} &= \mathbf{I}_\alpha\left(\frac{\gamma}{\beta}\,\frac{\mathbf{u}^\alpha_{n+1}-\mathbf{u}^\alpha_n}{\Delta t} + \tilde{\dot{\mathbf{u}}}^\alpha_n\right) = \mathbf{I}_\alpha\,\dot{\mathbf{u}}^\alpha_{n+1}\,.\end{aligned} \tag{3.10}$$

The previous approximation will be used to discretize the virtual dynamic work given in (3.5):

$$\delta\mathcal{W}_{dyn} = \delta\mathbf{q}\cdot\frac{\mathrm{d}}{\mathrm{d}t}\nabla_{\dot{\mathbf{q}}}\,T = \delta\mathbf{u}^\alpha_{n+1}\cdot\frac{\mathrm{d}}{\mathrm{d}t}\int_{\mathrm{L}}\mathbf{I}_\alpha\,\mathbf{C_d}\,\mathbf{I}_\beta\,\dot{\mathbf{u}}^\beta_{n+1}\,\mathrm{d}X\,. \tag{3.11}$$

The nodal dynamic force vector is finally obtained from (3.11) and is written as follows:

$$\mathbf{g}^d_\alpha = \int_{\mathrm{L}}\underbrace{\mathbf{I}_\alpha\,\mathbf{C_d}\,\mathbf{I}_\beta\,\mathrm{d}X}_{\mathbf{M}_{\alpha\beta}}\,\ddot{\mathbf{u}}^\beta_{n+1} \tag{3.12}$$

For the dynamic analysis, the Newmark method has been introduced and together with the finite element interpolation, a whole set of discretized nodal equations of motion is obtained by:

$$\mathbf{g}_\alpha = \mathbf{g}^d_\alpha + \mathbf{g}^e_\alpha - \mathbf{f}_\alpha = \mathbf{0}\,,\ \alpha = 1,\ldots,n\,. \tag{3.13}$$

In the same way developed for the static case, the solution of the non-linear system of equations in (3.13) is done through the Newton-Raphson method. The linearization of the dynamic nodal beam residual results from (3.8) and (3.12) in the following simple expression:

$$\boldsymbol{\Delta}\mathbf{g}^d_\alpha = \frac{1}{\beta\,\Delta t^2}\mathbf{M}_{\alpha\beta}\,\boldsymbol{\Delta}\mathbf{u}^\beta_{n+1} = \mathbf{K}^{\alpha\beta}_{mass}\,\boldsymbol{\Delta}\mathbf{u}^\beta_{n+1}\,. \tag{3.14}$$

3.2 Conserving schemes - An incremental formulation

3.2.1 The mid-point time-stepping rule

An implicit time-stepping scheme is presented, and consists of the following two simple rules for the mid-point acceleration and velocity respectively:

$$\ddot{\mathbf{u}}_{n+\frac{1}{2}} = \frac{\dot{\mathbf{u}}_{n+1} - \dot{\mathbf{u}}_n}{\Delta t} \; ; \; \dot{\mathbf{u}}_{n+\frac{1}{2}} = \frac{\mathbf{u}_{n+1} - \mathbf{u}_n}{\Delta t} \, , \tag{3.15}$$

where the term *mid-point* refers in general to a situation in time, e.g.

$$\dot{\mathbf{u}}_{n+\frac{1}{2}} = \frac{\dot{\mathbf{u}}_{n+1} + \dot{\mathbf{u}}_n}{2} \, . \tag{3.16}$$

This algorithm was applied in the context of rigid body dynamics and proof to conserve exactly the energy and momenta [SW91]. Reordering terms in equations (3.15) and (3.16), yields the velocity update

$$\dot{\mathbf{u}}_{n+1} = \frac{2}{\Delta t} \left(\mathbf{u}_{n+1} - \mathbf{u}_n - \frac{\Delta t}{2} \dot{\mathbf{u}}_n \right) \, . \tag{3.17}$$

while the midpoint acceleration can be rewritten substituting (3.17) into (3.15):

$$\ddot{\mathbf{u}}_{n+\frac{1}{2}} = \frac{2}{\Delta t^2} \left(\mathbf{u}_{n+1} - \mathbf{u}_n - \Delta t \dot{\mathbf{u}}_n \right) \, . \tag{3.18}$$

3.2.2 Modified mid-point equilibrium equations

Definitions for the system energy presented in 3.1 will be considered. The conservation of energy between two consecutive time steps t_{n+1} and t_n is imposed using the increments of kinetic, elastic and a potential of the external loads respectively:

$$\Delta \Pi = \Pi_{n+1} - \Pi_n = \Delta T + \Delta \Psi - \Delta \Pi_{ext} = 0 \, . \tag{3.19}$$

Denote the symbol Δ is used for incremental variations, such that $\Delta(\bullet) = (\bullet)_{n+1} - (\bullet)_n$, and should not be confused here or elsewhere with the bold character $\mathbf{\Delta}$, which stands for iterative changes. Let remark that (3.19) resembles (3.5), but in contrast, the latter states a zero energy infinitesimal variation. The aim of the present conserving scheme will be to approximate the increments in equation (3.19) as an inner product of the nodal incremental displacements vector $\Delta \mathbf{u}_\alpha$ and a modified vector of nodal residuals $\mathbf{g}^{\Delta}_{\alpha_{n+\frac{1}{2}}}$. In a similar way to the variational formulation given in (3.5):

$$\Delta \Pi \approx \Delta \mathbf{u}_\alpha \cdot \mathbf{g}^{\Delta}_{\alpha_{n+\frac{1}{2}}} = \Delta \mathbf{u}_\alpha \cdot (\mathbf{g}^{\Delta,\, d}_{\alpha_{n+\frac{1}{2}}} + \mathbf{g}^{\Delta,\, e}_{\alpha_{n+\frac{1}{2}}} - \mathbf{f}^{\Delta}_{\alpha_{n+\frac{1}{2}}}) = 0 \, , \tag{3.20}$$

whereas the proposed algorithm will clearly acquire energy conservation if the previous is satisfied.

The particular form in which the incremental displacements and rotations $\Delta\mathbf{u}_\alpha$ in (3.20) are interpolated can furnish additional conserving properties to the algorithm. This topic will be further explored when dealing with the conservation of angular momentum. Moreover, with respect to the modified mid-point nodal equilibrium equations $\mathbf{g}^{\Delta}_{\alpha\,n+\frac{1}{2}}$ in (3.20), the idea was first presented in [ST92]. It has been proved in their work that all the conserving properties in mechanics can be satisfied in the context of non-linear elastodynamics as well. Together with the mid-point time-stepping rule, already presented in subsection 3.2.1, they proposed a modification of the second Piola-Kirchhoff stress tensor in the equilibrium equations. An average of the latter tensor at consecutive time steps t_{n+1} and t_n came up instead. The simplicity of the method is remarkable and has established a tendency on which different finite elements for non-linear dynamics were developed.

Increment of kinetic energy

Recalling the definition of kinetic energy T in (3.6) and a finite element interpolation of displacements in (2.13), the increment of T over a time step Δt can be written as:

$$\Delta T = \frac{1}{2}\left(\dot{\mathbf{u}}^{\alpha}_{n+1}\cdot\mathbf{M}_{\alpha\beta}\,\dot{\mathbf{u}}^{\beta}_{n+1} - \dot{\mathbf{u}}^{\alpha}_{n}\cdot\mathbf{M}_{\alpha\beta}\,\dot{\mathbf{u}}^{\beta}_{n}\right). \tag{3.21}$$

The increment in (3.21) can be rewritten as a product of a sum and a difference, and using after that the mid-point rule velocity update and acceleration, from (3.17) and (3.15) respectively:

$$\Delta\mathbf{u}_\alpha\cdot\mathbf{g}^{\Delta,\,d}_{\alpha\,n+\frac{1}{2}} = \frac{1}{2}\left(\dot{\mathbf{u}}^{\alpha}_{n+1}+\dot{\mathbf{u}}^{\alpha}_{n}\right)\cdot\mathbf{M}_{\alpha\beta}\,\left(\dot{\mathbf{u}}^{\beta}_{n+1}-\dot{\mathbf{u}}^{\beta}_{n}\right) = \Delta\mathbf{u}_\alpha\cdot\mathbf{M}_{\alpha\beta}\,\ddot{\mathbf{u}}^{\beta}_{n+\frac{1}{2}}\,. \tag{3.22}$$

Increment of the potential elastic energy

Using the definition stated in (2.10), the increment of the elastic potential is given in the following expression, where again the difference of quadratic forms is factorized:

$$\begin{aligned}\Delta\Psi &= \frac{1}{2}\int_{\mathrm{L}}\left(\mathbf{C_e}\,\mathbf{\Gamma}_{n+1}\cdot\mathbf{\Gamma}_{n+1} - \mathbf{C_e}\,\mathbf{\Gamma}_{n}\cdot\mathbf{\Gamma}_{n}\right)\mathrm{d}X\\ &= \int_{\mathrm{L}}\left(\mathbf{\Gamma}_{n+1}-\mathbf{\Gamma}_{n}\right)\cdot\mathbf{C_e}\left(\frac{\mathbf{\Gamma}_{n+1}+\mathbf{\Gamma}_{n}}{2}\right)\mathrm{d}X = \int_{\mathrm{L}}\Delta\mathbf{\Gamma}\cdot\mathbf{N}_{n+\frac{1}{2}}\,\mathrm{d}X\\ &= \int_{\mathrm{L}}\mathbf{\Lambda}_0^{\mathrm{T}}\,\left[(\mathbf{\Lambda}^{\mathrm{T}}\,\mathbf{r}')_{n+1} - (\mathbf{\Lambda}^{\mathrm{T}}\,\mathbf{r}')_{n}\right]\cdot\mathbf{N}_{n+\frac{1}{2}}\,\mathrm{d}X\,,\end{aligned} \tag{3.23}$$

and the definition of the strain measure - see equation (2.6) - has been used in the last equality. If the rotational part of $\Delta\mathbf{\Gamma}$ in (3.23) is computed, it simply

yields $\Delta\theta^{'}$ for the planar beam theory. However, the translational part of $\Delta\boldsymbol{\Gamma}$ needs to be rewritten as a product of a *mid-point term* $(\bullet)_{n+\frac{1}{2}}$ times a vector function of the incremental displacements $\Delta\mathbf{u}$. For that purpose, let introduce $\tilde{\mathbf{r}}$ to refer to the translational part of the position vector $\mathbf{r}$ defined in (2.2). The same meaning will be noted for $\Delta\tilde{\boldsymbol{\Gamma}}$, which will finally be expand following:

$$\tilde{\boldsymbol{\Lambda}}_0^{\mathrm{T}} \left[(\tilde{\boldsymbol{\Lambda}}^{\mathrm{T}} \tilde{\mathbf{r}}^{'})_{n+1} - (\tilde{\boldsymbol{\Lambda}}^{\mathrm{T}} \tilde{\mathbf{r}}^{'})_{n} \right] = \tilde{\boldsymbol{\Lambda}}_0^{\mathrm{T}} \left(\tilde{\boldsymbol{\Lambda}}_{n+\frac{1}{2}}^{\mathrm{T}} \Delta\tilde{\mathbf{r}}^{'} + \Delta\tilde{\boldsymbol{\Lambda}}^{\mathrm{T}} \tilde{\mathbf{r}}^{'}_{n+\frac{1}{2}} \right) . \tag{3.24}$$

Note the first summand of (3.24) fits the shape intended for the mid-point modifications but the second still have to be transformed. The following identity will be used:

$$\Delta\tilde{\boldsymbol{\Lambda}} = 2 \, \tan\left(\Delta\theta/2\right) \, \tilde{\mathbf{J}} \, \tilde{\boldsymbol{\Lambda}}_{n+\frac{1}{2}} \, , \tag{3.25}$$

which is in fact the application of the Cayley transform [Muñ04] applied to the planar case. Finally, the modified mid-point increment of elastic potential energy is written by substitution of (3.24) and (3.25) into (3.23):

$$\Delta\Psi = \int_{\mathrm{L}} \left\{ \begin{array}{c} \Delta\tilde{\mathbf{r}}^{'} \cdot \tilde{\boldsymbol{\Lambda}}_{n+\frac{1}{2}} \, \tilde{\boldsymbol{\Lambda}}_0 \, \tilde{\mathbf{N}}_{n+\frac{1}{2}} \\ \omega^{'} \, \mathrm{M}_{n+\frac{1}{2}} - \omega \, \frac{\tan(\omega/2)}{\omega/2} \left[\tilde{\mathbf{r}}^{'}_{n+\frac{1}{2}} \right]_{\times} \cdot \tilde{\boldsymbol{\Lambda}}_{n+\frac{1}{2}} \, \tilde{\boldsymbol{\Lambda}}_0 \, \tilde{\mathbf{N}}_{n+\frac{1}{2}} \end{array} \right\} \mathrm{d}X \, . \tag{3.26}$$

Denote in the previous that $\left[(\tilde{\bullet}) \right]_{\times} = \tilde{\mathbf{J}} \, (\tilde{\bullet})$ and $\omega = \Delta\theta$ has been introduced as the *unscaled* incremental rotation. The distinction will be make against $\underline{\omega}$, the *scaled* incremental rotation which is given by

$$\underline{\omega} = 2 \, \tan\left(\omega/2\right) \, , \tag{3.27}$$

and yields another form of the incremental elastic potential:

$$\Delta\underline{\Psi} = \int_{\mathrm{L}} \left\{ \begin{array}{c} \Delta\tilde{\mathbf{r}}^{'} \cdot \tilde{\boldsymbol{\Lambda}}_{n+\frac{1}{2}} \, \tilde{\boldsymbol{\Lambda}}_0 \, \tilde{\mathbf{N}}_{n+\frac{1}{2}} \\ \underline{\omega}^{'} \left(1 + \frac{\underline{\omega}^2}{4} \right)^{-1} \mathrm{M}_{n+\frac{1}{2}} - \underline{\omega} \left[\tilde{\mathbf{r}}^{'}_{n+\frac{1}{2}} \right]_{\times} \cdot \tilde{\boldsymbol{\Lambda}}_{n+\frac{1}{2}} \, \tilde{\boldsymbol{\Lambda}}_0 \, \tilde{\mathbf{N}}_{n+\frac{1}{2}} \end{array} \right\} \mathrm{d}X \, , \tag{3.28}$$

where differentiation of (3.27) with respect to the arc length parameter has been used:

$$\underline{\omega}^{'} = \left[1 + \tan^2\left(\omega/2\right) \right] \, \omega^{'} = \overbrace{\left(1 + \frac{\underline{\omega}^2}{4} \right)}^{\mathrm{s}^{-1}(\underline{\omega})} \, \omega^{'} \, . \tag{3.29}$$

It still remains to be applied the interpolation of the incremental displacements and rotation, that will yield to the discrete form of (3.23). We here have

developed two possible choices for the interpolation of the incremental rotation, either ω or $\underline{\omega}$. Let us note that interpolation of the latter will lead additionally to conservation of angular momentum (see Appendix D). We therefore will use the following discretization:

$$\Delta\underline{\mathbf{u}} \equiv \begin{Bmatrix} \Delta\tilde{\mathbf{u}} \\ \underline{\omega} \end{Bmatrix} \approx \mathbf{I}_\alpha \, \Delta\underline{\mathbf{u}}_\alpha \,, \tag{3.30}$$

and remark that $\Delta\tilde{\mathbf{r}} = \Delta\tilde{\mathbf{u}}$. Using (3.30) into (3.28), the modified mid-point nodal elastic residual is obtained:

$$\Delta\underline{\Psi} = \Delta\underline{\mathbf{u}}_\alpha \cdot \underline{\mathbf{g}}^{\Delta,\,e}_{\alpha\,n+\frac{1}{2}} = \Delta\underline{\mathbf{u}}_\alpha \cdot \int_{\mathrm{L}} \begin{bmatrix} \mathbf{I}'_\alpha \, \tilde{\mathbb{1}} & 0 \\ -\mathbf{I}_\alpha \left[\tilde{\mathbf{r}}'_{n+\frac{1}{2}}\right]^{\mathrm{T}}_{\times} & \mathbf{I}'_\alpha \end{bmatrix} \begin{Bmatrix} \tilde{\mathbf{\Lambda}}_{n+\frac{1}{2}} \, \tilde{\mathbf{\Lambda}}_0 \, \tilde{\mathbf{N}}_{n+\frac{1}{2}} \\ \mathrm{s}(\underline{\omega}) \, \mathrm{M}_{n+\frac{1}{2}} \end{Bmatrix} \mathrm{d}X \,. \tag{3.31}$$

Increment of a potential for the external loads

Since we consider only conservative and constant loads, an increment on the external potential is simply determined by

$$\Delta\Pi_{ext} = \Delta\mathbf{u}_\alpha \cdot \mathbf{f}^{\Delta}_{\alpha\,n+\frac{1}{2}} = \Delta\mathbf{u}_\alpha \cdot \mathbf{f}_\alpha \,, \tag{3.32}$$

with $\mathbf{f}_\alpha$ defined in (2.17).

Solution of the dynamic conservative system

The increment of energy has been approximated as $\Delta\Pi \approx \Delta\mathbf{u}_\alpha \cdot \mathbf{g}^{\Delta}_{\alpha\,n+\frac{1}{2}}$, and we have derived the expressions to build the nodal residual non-linear equations:

$$\mathbf{g}^{\Delta}_{\alpha\,n+\frac{1}{2}} = \mathbf{0} \,;\; \alpha = 1, \ldots, n \;, \tag{3.33}$$

which yield the condition of energy conservation for any $\Delta\mathbf{u}_\alpha$. Moreover, it is demonstrated in Appendix D that by using $\underline{\mathbf{g}}^{\Delta,\,e}_{\alpha\,n+\frac{1}{2}}$, this scheme also conserves linear and angular momenta. Let us remark that the latter condition requires the interpolation of tangent scaled rotations and accordingly the following should be addressed to the mid-time integration scheme:

$$\dot{\underline{\mathbf{u}}}_{n+\frac{1}{2}} = \begin{Bmatrix} \dfrac{\Delta\tilde{\mathbf{u}}}{\Delta t} \\ \dfrac{\underline{\omega}}{\Delta t} \end{Bmatrix} . \tag{3.34}$$

The Newton-Raphson method is used to solve (3.33) for each particular time step, with the particularity that an *unsymmetric* tangent stiffness matrix results from the linearization of $\underline{\mathbf{g}}^{\Delta,\,e}_{\alpha\,n+\frac{1}{2}}$ (see Appendix B).

Chapter 4

The *master-slave* sliding contact

In this chapter we will apply the master-slave approach in order to describe a *kinematically rigorous* translational joint [MJ04], here referred to as a *sliding* joint. We will next explain what we mean by the former definition, which has basically used to distinguish the present approach from another one that is only kinematically approximate.

Originally [CJ96], the master-slave method only related the degrees of freedom of a *slave* **node** to an extended set of *master and released* degrees of freedom, which were specific to only one **node** in the *master* finite element. In cases where the master element deformation is significant, this leads to unrealistic configurations. For example, with the *node-to-node* (NN) [Muñ04] description, a joint originally placed at the middle node of an horizontal beam in Figure 4.1a will slide along the nodal tangent to the beam. This, as can be clearly seen from deformed configurations 1 and 2 of Figure 4.1a, will lead to a kinematically inconsistent result.

In order to amend the previous disjunction and *rigorously* model the kinematics of a *sliding* joint, a formulation that relates the behaviour of a *slave* **node** to the set of *master and released* variables at all nodes of the master **element** was first presented in [MJ04]. We will here refer the previous as a *node-to-element* (NE) [Muñ04] approach, and with this technique we will model the sliding joints in the present chapter. The basic contact assumption will be that a slave node at such a joint, will follow without any friction, the deformed line of cross-section centroids of the master beam element. An example of deformations obtained by the NE approach is sketched in Figure 4.1b, where it can be compared as well with 4.1a, corresponding results from the NN case.

We remark that the treatment of sliding contact with other methods, primarily Lagrange multipliers or augmented Lagrange formulations, has been reported in [BB01, AP98], among others. The choice of the master-slave method is based on previous work where it has been proved its advantages when modeling permanent, such as sliding, contact [MJ04]. We address that the previous allows us to avoid issues about contact detection and assume as well that contact forces

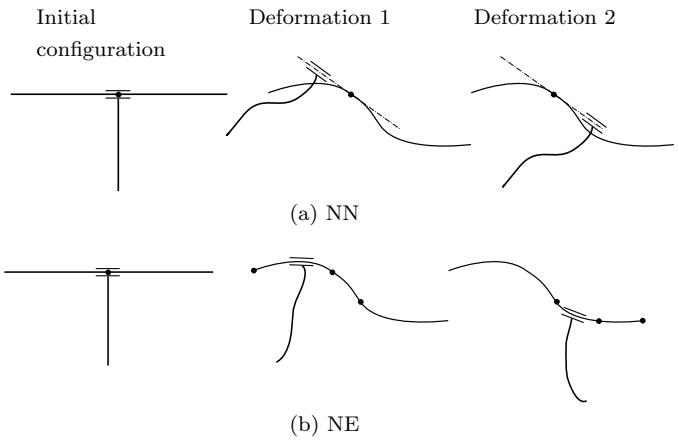

(a) NN

(b) NE

Figure 4.1: Sketched results comparison between NN and NE methods

might be of either direction. In addition, we intend to smooth the contact element transition by the introduction of B-Splines interpolation. We state that to the author's knowledge this has not been tested before in the context of sliding beams.

Furthermore, we will combine the master-slave method (in an incremental form) together with the conservative time-integration developed in Section 3.2. With the previous master-slave technique, either energy or momentum conserving algorithms have been achieved in sliding contact problems, among others, in the context of joint modeling for 3D geometrically exact beams [MJ06]. We will propose and implement, for the planar case, a new algorithm that will preserve both energy and momenta, through a modified mid-point relaxed contact condition and equilibrium equations [SM11]. In this incremental formulations, special care will be exercised to retain the conserving properties developed first for a contact point sliding within a single element, to the case when the contact point jumps to an adjacent element.

We present again [AP98], and also cite [Bau00] as references on conserving algorithms in the context of sliding contact. The first one describes general contact in elastodynamics with an augmented Lagrangian formulation, and the last resort to Lagrange multipliers within 3D beams in combination with energy conservation or decay. Our choice in the master-slave context is based on sorting out the problems inherit by the use of penalty parameters or Lagrange multipliers as already mentioned before.

We will resume in this Chapter the key ideas of the master-slave method in order to present in the end, our contribution to the energy-momentum conserving algorithm, but we refer the reader to [Muñ04], where the theory can be found in more detail. The present Chapter is divided into two Sections, in Section 4.1 we will present the variational master-slave formulation and Section 4.2 will introduce an incremental formulation. The latter is developed in order to cope with conserving time integration, and the technique will reassemble the one developed in Section 3.2.

4.1 Sliding joints using NE contact

The present Section deals with a variational formulation of sliding contact with the master-slave method, implemented for planar beams. Due to the nature of the formulation, it can be coupled together with the Newmark method (see Section 3.1) to reproduce the dynamic response of a system. The outline for this section follows like this, first the kinematic assumptions of a system with two beams in sliding contact are presented in Subsection 4.1.1. In addition, the master-slave relationship is derived in Subsection 4.1.2 for the continuum, giving rise to the infinitesimal form of the sliding contact condition. Furthermore, we will introduce the finite element interpolation in Subsection 4.1.3 to discretize the previous, allowing us to finally present the weak form of the nodal equilibrium equations for the whole system under sliding contact. It will be described as well that the formulation deals with contact transitions along a discretized *slideline* of master elements by the definition of a *coupling element* [Muñ04]. We finally describe in Subsection 4.1.4 a few issues regarding the computational implementation of the method, such as the linearization of the master-slave residuals and the treatment of contact transition between finite elements.

4.1.1 Kinematics of a sliding joint

In general, a joint is considered as a flexible attachment between two elements of a system. In a finite element model, the kinematic relationship between two nodes, from different elements but connected to the same joint, can be given as an algebraic equation. In the master-slave approach for the sliding joint, we will relate the degrees of freedom of a slide node (the *slave* node) to the degrees of freedom of all the nodes at a *master* element, through the released degrees of freedom (relative displacements of the slave node with respect to the master element, measured in the moving frame).

We will use the following definitions:

$$\mathbf{r}_m \equiv \begin{Bmatrix} \tilde{\mathbf{r}}_m \\ \theta_m \end{Bmatrix} \; ; \; \mathbf{r} \equiv \begin{Bmatrix} \tilde{\mathbf{r}} \\ \theta \end{Bmatrix} \; , \tag{4.1}$$

to refer to the master and slave nodal variables respectively, defined in the fixed basis $\mathbf{e}_i$. In addition, we will denote by

$$\mathbf{r}_R \equiv \begin{Bmatrix} \tilde{\mathbf{r}}_R \\ \theta_R \end{Bmatrix} \; , \tag{4.2}$$

the released nodal variables, which are given for the moving basis $\mathbf{t}_i$. Note that, from here onwards, kinematic variables without a subscript will assumed to be slave quantities.

Let us note that the idea of introducing released rotations is key in the modeling of joints for 3D beams. In the planar case, non distinction can be made for the rotation with respect to the moving or the fixed frame. However, we have introduced the released rotation for completeness. In fact, we will

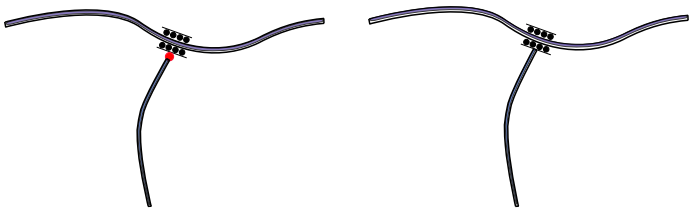

(a) Free rotation (b) Fixed rotation

Figure 4.2: Plane sliding joint type

distinguish the two possible configurations, either free or fix, the rotation make take in a planar sliding joint (see Figure 4.2).

To start with the sliding kinematics, let us first consider two beams $\mathcal{B}^A$ and $\mathcal{B}^B$ that at time t are in contact, at respective points of the centroid axis A_1 and B_1 (see Figure 4.3). The contact conditions will be written in terms of the translations and the rotation as follows:

$$\tilde{\mathbf{r}}(X_{A_1}, t) = \tilde{\mathbf{r}}(X_{B_1}, t) \tag{4.3a}$$

$$\theta(X_{A_1}, t) = \theta(X_{B_1}, t) + \theta_{rel}\,, \tag{4.3b}$$

where the constant θ_{rel} is the relative rotation between the two beams at the initial configuration, i.e. due to additive planar rotations: $\theta_{rel} = \theta_0(X_{A_1}) - \theta_0(X_{B_1})$. We will also note that this contact condition, for the planar rotation, implies a joint that transmits moment and therefore we are considering the case sketched in Figure 4.2b.

The model we will consider for the sliding contact resorts to four basic hypothesis that will be enumerated as follows:

H1: At the contact point, beam $\mathcal{B}^A$ exercise a force $\overline{\mathbf{n}}_{B_1}$ on point B_1 of beam $\mathcal{B}^B$ such that the third Newton law is valid:

$$\overline{\mathbf{n}}_{B_1} = -\overline{\mathbf{n}}_{A_1}\,, \tag{4.4}$$

being $\overline{\mathbf{n}}_{A_1}$ the force exercise by $\mathcal{B}^B$ on point A_1 of beam $\mathcal{B}^A$.

H2: Analogous to *H1*, but relating the planar moment we will assume that:

$$\overline{m}_{B_1} = -\overline{m}_{A_1}\,. \tag{4.5}$$

H3: Since none frictionless contact is considered along a slideline, forces along the tangent direction to the centroid lines of beams $\mathcal{B}^A$ and $\mathcal{B}^B$ will be zero:

$$\overline{\mathbf{n}}_{A_1} \cdot \tilde{\mathbf{r}}'_{A_1} = \overline{\mathbf{n}}_{B_1} \cdot \tilde{\mathbf{r}}'_{B_1} = 0\,. \tag{4.6}$$

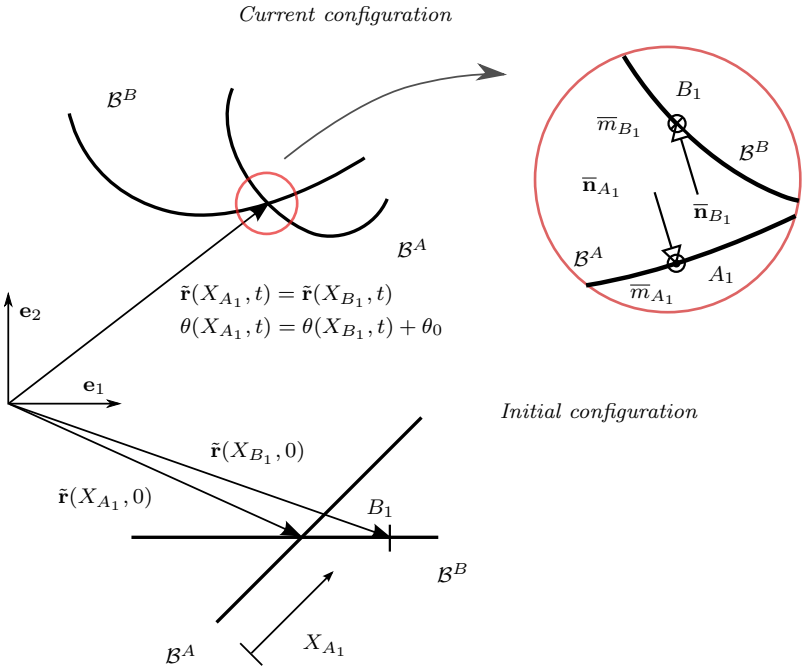

Figure 4.3: Contact kinematics at time t for beams $\mathcal{B}^A$ and $\mathcal{B}^B$

H4: In case the joint rotation is released (see Figure 4.2a), none friction moment will be associated to its movement. Again, an equivalent hypothesis to *H3* for the planar moment is valid:

$$\overline{m}_{A_1} = \overline{m}_{B_1} = 0\,. \tag{4.7}$$

4.1.2 The master-slave relationship

Let us first consider that the contact condition previously defined in a deformed configuration, is perturbed by a kinematically admissible virtual displacement $\epsilon\,\delta\mathbf{u}$ [Muñ04]. Since we have stated that permanent contact will be modelled, is assumed that point A_1 will remain in contact with beam $\mathcal{B}^B$. However, the contact point in the latter will change due to sliding and, in the perturbed configuration, contact will be established at point B_2 (see Figure 4.4).

We will rewrite the contact conditions given in (4.3) to the perturbed configuration as

$$\tilde{\mathbf{r}}_\epsilon(X_{A_1},t) = \tilde{\mathbf{r}}_\epsilon(X_{B_2},t) \tag{4.8a}$$
$$\theta_\epsilon(X_{A_1},t) = \theta_\epsilon(X_{B_2},t)\,, \tag{4.8b}$$

which in fact provide the following relationships between virtual quantities:

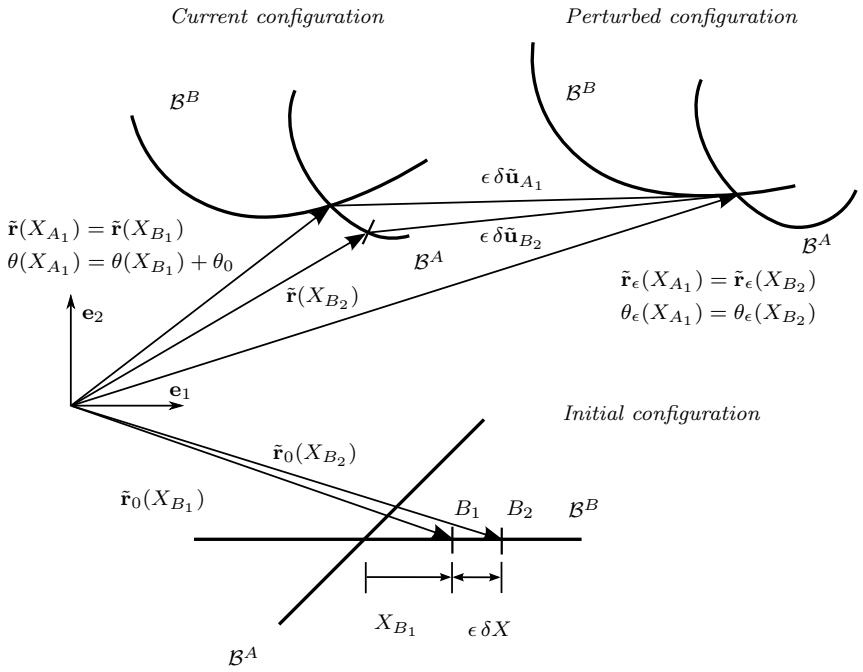

Figure 4.4: Admissible perturbed contact configuration for beams $\mathcal{B}^A$ and $\mathcal{B}^B$

$$
\begin{aligned}
\delta\tilde{\mathbf{r}}_{A_1} &\equiv \left.\frac{\mathrm{d}}{\mathrm{d}\epsilon}\right|_{\epsilon=0} \tilde{\mathbf{r}}_\epsilon(X_{A_1}) = \left.\frac{\mathrm{d}}{\mathrm{d}\epsilon}\right|_{\epsilon=0} [\tilde{\mathbf{r}}(X_{B_1} + \epsilon\,\delta X) + \epsilon\,\delta\tilde{\mathbf{u}}(X_{B_1} + \epsilon\,\delta X)] \\
&= \tilde{\mathbf{r}}^{'}(X_{B_1})\,\delta X + \delta\tilde{\mathbf{u}}_{B_1}\,, \\
\delta\theta_{A_1} &\equiv \left.\frac{\mathrm{d}}{\mathrm{d}\epsilon}\right|_{\epsilon=0} \theta_\epsilon(X_{A_1}) = \left.\frac{\mathrm{d}}{\mathrm{d}\epsilon}\right|_{\epsilon=0} [\theta(X_{B_1} + \epsilon\,\delta X) + \epsilon\,\delta\theta(X_{B_1} + \epsilon\,\delta X)] \\
&= \theta^{'}(X_{B_1})\,\delta X + \delta\theta_{B_1}\,,
\end{aligned}
$$

where the time index t has been dropped to easy the notation and we denote δX a variation of the contact point on the reference configuration. Defining $\tilde{\mathbf{r}}^{'}_{B_1} \equiv \tilde{\mathbf{r}}^{'}(X_{B_1})$ and $\theta^{'}_{B_1} \equiv \theta^{'}(X_{B_1})$ we arrive from the previous result to the master-slave relationships

$$\delta\tilde{\mathbf{u}}_{A_1} = \tilde{\mathbf{r}}^{'}_{B_1}\,\delta X + \delta\tilde{\mathbf{u}}_{B_1}\,, \tag{4.9a}$$

$$\delta\theta_{A_1} = \theta^{'}_{B_1}\,\delta X + \delta\theta_{B_1}\,. \tag{4.9b}$$

4.1.3 Equilibrium equations in sliding contact

Let us consider first the discrete weak form G^h of the equilibrium equations for the two beams in sliding contact. Recall G^h corresponds to the finite element

interpolation defined in (2.13), such that $\mathbf{u}^h = \mathbf{I}_\alpha\, \mathbf{u}_\alpha$ and

$$G^h(\mathbf{r}, \delta\mathbf{u}^h) \equiv \sum_{I=A,B} \delta\mathbf{u}^I \cdot \mathbf{g}^I - \theta'_{B_1}\, \overline{m}_{A_1}\, \delta X = 0\,, \tag{4.10}$$

where $\delta\mathbf{u}^I = \begin{Bmatrix} \delta\mathbf{u}^I_1 & \dots & \delta\mathbf{u}^I_{n_I} \end{Bmatrix}$ is the vector of nodal virtual displacements, $\mathbf{g}^I = \begin{Bmatrix} \mathbf{g}_{1,\,I} & \dots & \mathbf{g}_{n_I,\,I} \end{Bmatrix}$ the nodal residual vector, and both of them correspond to a discrete beam I. Denote such residual comprises the dynamic, elastic and external nodal force vectors $\mathbf{g}^d_{\alpha,\,I}$, $\mathbf{g}^e_{\alpha,\,I}$ and $\mathbf{f}_{\alpha,\,I}$ respectively, and are given in equation (3.13).

We remark the complete derivation of (4.10) can be found in [MJ04]. Their followed procedure considers first the weak form of local equilibria in $\mathcal{B}^A$ and $\mathcal{B}^B$ separately, together with the work done by $\overline{\mathbf{n}}_{I_1}$ and $\overline{m}_{I_1}$, their corresponding contact concentrated force and torque respectively. Finally, by the introduction of the infinitesimal sliding condition (4.9), the contact hypothesis *H1-H3* and using the proposed finite element interpolation, the complete nodal weak form of the system G^h yields.

With the finite element interpolation, the master-slave relationship (4.9) may be rewritten as

$$\delta\mathbf{u}_{n_A} = \begin{Bmatrix} \tilde{\mathbf{r}}'_{B_1} \\ \theta'_{B_1} \end{Bmatrix} (\delta\tilde{\mathbf{u}}_R \cdot \mathbf{E}_1) + \mathbf{I}^B_\alpha\, \delta\mathbf{u}_\alpha\,, \tag{4.11}$$

where $\tilde{\mathbf{u}}_R = \begin{Bmatrix} \delta X & 0 \end{Bmatrix}$ is the vector of *released* translations, and we have assumed that the sliding point A_1 at a finite element A corresponds to node n_A all throughout the motion. The *master* and *master and released* vectors of virtual displacements and rotations are defined respectively as

$$\delta\mathbf{u}^A \equiv \begin{Bmatrix} \delta\mathbf{u}^A_1 \\ \vdots \\ \delta\mathbf{u}^A_{n_A} \end{Bmatrix} \;\text{ and }\; \delta\mathbf{u}^A_{Rm} \equiv \begin{Bmatrix} \delta\mathbf{u}_R \\ \delta\mathbf{u}^A_1 \\ \vdots \\ \delta\mathbf{u}^A_{n_A} \\ \delta\mathbf{u}^B_1 \\ \vdots \\ \delta\mathbf{u}^B_{n_B} \end{Bmatrix}, \tag{4.12}$$

Using (4.12), we can relate the previous vectors as follows

$$\delta\mathbf{u}^A = \mathbf{N}^*_\delta\, \delta\mathbf{u}^A_{Rm}\,, \tag{4.13}$$

where, denoting by $\overline{\mathbf{0}}$ the 3×3 zero matrix, then

$$\mathbf{N}^*_\delta = \begin{bmatrix} \overline{\mathbf{0}} & \mathbb{1} & \dots & \overline{\mathbf{0}} & \overline{\mathbf{0}} & \overline{\mathbf{0}} & \dots & \overline{\mathbf{0}} \\ \vdots & \vdots & \ddots & \vdots & \vdots & \vdots & \ddots & \vdots \\ \overline{\mathbf{0}} & \overline{\mathbf{0}} & \dots & \mathbb{1} & \overline{\mathbf{0}} & \overline{\mathbf{0}} & \dots & \overline{\mathbf{0}} \\ \mathbf{R}^*_{\delta\,B} & \overline{\mathbf{0}} & \dots & \overline{\mathbf{0}} & \overline{\mathbf{0}} & \mathbf{I}^B_1\,\mathbb{1} & \dots & \mathbf{I}^B_{n_B}\,\mathbb{1} \end{bmatrix} \;\text{ and }\; \mathbf{R}^*_{\delta\,B} = \begin{bmatrix} \tilde{\mathbf{r}}'_{B_1} \otimes \mathbf{E}_1 & 0 \\ \theta'_{B_1}\,\mathbf{E}_1 & 0 \end{bmatrix}. \tag{4.14}$$

We will now insert the master-slave relationship (4.14) into the weak form (4.10), which leads to

$$G^h(\mathbf{r}, \delta\mathbf{u}^h) = \delta\mathbf{u}^A_{Rm} \cdot \mathbf{N}^{*\,\mathrm{T}}_{\delta}\, \mathbf{g}^A + \delta\mathbf{u}^B \cdot \mathbf{g}^B - \theta'_{B_1}\, \overline{m}_{A_1}\, \delta X = 0\,, \tag{4.15}$$

but recalling that the rotational part of the nodal residual $\mathbf{g}_{n_A}$ yields the equivalence $g^m_{n_A} = \overline{m}_{A_1}$, then we finally arrive to

$$G^h(\mathbf{r}, \delta\mathbf{u}^h) = \delta\mathbf{u}^A_{Rm} \cdot \mathbf{N}^{\mathrm{T}}_{\delta}\, \mathbf{g}^A + \delta\mathbf{u}^B \cdot \mathbf{g}^B = 0\,, \tag{4.16}$$

with

$$\mathbf{N}_\delta = \begin{bmatrix} \overline{\mathbf{0}} & \mathbb{1} & \dots & \overline{\mathbf{0}} & \overline{\mathbf{0}} & \overline{\mathbf{0}} & \dots & \overline{\mathbf{0}} \\ \vdots & \vdots & \ddots & \vdots & \vdots & \vdots & \ddots & \vdots \\ \overline{\mathbf{0}} & \overline{\mathbf{0}} & \dots & \mathbb{1} & \overline{\mathbf{0}} & \overline{\mathbf{0}} & \dots & \overline{\mathbf{0}} \\ \mathbf{R}_{\delta\, B} & \overline{\mathbf{0}} & \dots & \overline{\mathbf{0}} & \overline{\mathbf{0}} & \mathbf{I}^B_1\, \mathbb{1} & \dots & \mathbf{I}^B_{n_B}\, \mathbb{1} \end{bmatrix} \text{ and } \mathbf{R}_{\delta\, B} = \begin{bmatrix} \tilde{\mathbf{r}}'_{B_1} \otimes \mathbf{E}_1 & 0 \\ \mathbf{0} & 0 \end{bmatrix}. \tag{4.17}$$

It can be observed that through the master-slave relationship, the the virtual work performed by the beam element A has been expressed as the dot product of $\delta\mathbf{u}^A_{Rm}$, a set of *master and released* degrees of freedom, and its work-conjugate extended residual, given by

$$\mathbf{g}^A_{Rm} \equiv \mathbf{N}^{\mathrm{T}}_{\delta}\, \mathbf{g}^A = \begin{Bmatrix} \mathbf{R}^{\mathrm{T}}_{\delta\, B}\, \mathbf{g}_{n_A} \\ \mathbf{g}_{1,\,A} \\ \vdots \\ \mathbf{g}_{n_A-1,\,A} \\ \mathbf{0} \\ \mathbf{L}^{\mathrm{T}}_{\delta\, B}\, \mathbf{g}_{n_A} \end{Bmatrix}, \text{ with } \mathbf{L}_{\delta\, B} \equiv \begin{bmatrix} \mathbf{I}^B_1\, \mathbb{1} & \dots & \mathbf{I}^B_{n_B}\, \mathbb{1} \end{bmatrix}. \tag{4.18}$$

Considering now the virtual work performed by the finite element B, together with (4.18), then the new equilibrium equations for the whole system with sliding contact yields:

$$\mathbf{g}_{\alpha,\,A} = \mathbf{0}\,, \qquad \alpha = 1, \dots, n_A - 1\,, \tag{4.19a}$$

$$\mathbf{R}^{\mathrm{T}}_{\delta\, B}\, \mathbf{g}_{n_A,A} = \mathbf{0}\,, \tag{4.19b}$$

$$\mathbf{g}_{\alpha,\,B} + \mathbf{I}^B_\alpha\, \mathbf{g}_{n_A,A} = \mathbf{0}\,, \qquad \alpha = 1, \dots, n_B\,. \tag{4.19c}$$

Denote equations (4.19a) are the standard equilibrium equations for all nodes on element A with exception of node n_A. The second equation, (4.19b), enforces none work along the direction of released translations $\tilde{\mathbf{u}}^A_R$, consequently to our bilateral frictionless hypothesis. Finally, equations (4.19c) establish the equilibrium at the master nodes, given by the residuals of the master element B nodes $\mathbf{g}_{\alpha,\,B}$ plus the contribution of the sliding node residuals $\mathbf{g}_{n_A,A}$, weighted by shape functions $\mathbf{I}^B_\alpha$ computed at the corresponding element.

Modeling the sliding joint with its rotation free

We have previously derived the master-slave relationship for a fixed rotation in the sliding joint. If a free rotation is consider instead, and resorting to hypothesis *H4*, non contact moment can be exercised by such a joint in the planar case. We will now rewrite the contact condition related to the joint rotation and that will result as well in slightly changes of the master-slave residuals. Since we consider this type of joint (refer to Figure 4.2) has more practical applications, it will be the one implemented in the numerical examples of Chapter 5.

The contact condition for the released planar joint rotation gives a trivial relation:

$$\theta(X_{A_1}, t) = \theta_R(t)\,, \tag{4.20}$$

which simply relates the infinitesimal rotations

$$\delta\theta_{A_1} = \delta\theta_R\,. \tag{4.21}$$

Using the previous, together with the infinitesimal translations condition (4.9a), then the master-slave relationship yields

$$\delta\mathbf{u}_{n_A} = \begin{Bmatrix} \tilde{\mathbf{r}}'_{B_1} \\ 0 \end{Bmatrix} (\delta\tilde{\mathbf{u}}_R \cdot \mathbf{E}_1) + \begin{Bmatrix} \mathbf{0} \\ \delta\theta_R \end{Bmatrix} + \mathbf{I}^B_\alpha\, \delta\tilde{\mathbf{u}}_\alpha\,. \tag{4.22}$$

Since we have that $\overline{m}_{A_1} = 0$, for the present joint it will result that $\mathbf{N}^R_\delta \equiv \mathbf{N}^*_\delta = \mathbf{N}_\delta$, with

$$\mathbf{N}^R_\delta = \begin{bmatrix} \overline{\mathbf{0}} & \mathbb{1} & \dots & \overline{\mathbf{0}} & \overline{\mathbf{0}} & \overline{\mathbf{0}} & \dots & \overline{\mathbf{0}} \\ \vdots & \vdots & \ddots & \vdots & \vdots & \vdots & \ddots & \vdots \\ \overline{\mathbf{0}} & \overline{\mathbf{0}} & \dots & \mathbb{1} & \overline{\mathbf{0}} & \overline{\mathbf{0}} & \dots & \overline{\mathbf{0}} \\ \mathbf{R}^R_{\delta\, B} & \overline{\mathbf{0}} & \dots & \overline{\mathbf{0}} & \overline{\mathbf{0}} & \mathbf{I}^B_1\, \tilde{\mathbb{1}} & \dots & \mathbf{I}^B_{n_B}\, \tilde{\mathbb{1}} \end{bmatrix}, \quad \mathbf{R}^R_{\delta\, B} = \begin{bmatrix} \tilde{\mathbf{r}}'_{B_1} \otimes \mathbf{E}_1 & 0 \\ \mathbf{0} & 1 \end{bmatrix}, \tag{4.23}$$

and $\tilde{\mathbb{1}} = \operatorname{diag}\{1 \quad 1 \quad 0\}$.

The new equilibrium equations will result in

$$\mathbf{g}_{\alpha,\,A} = \mathbf{0}\,, \qquad \alpha = 1, \dots, n_A - 1\,, \tag{4.24a}$$

$$\mathbf{R}^{R^{\mathrm{T}}}_{\delta\, B}\, \mathbf{g}_{n_A, A} = \mathbf{0}\,, \tag{4.24b}$$

$$\mathbf{g}_{\alpha,\,B} + \mathbf{I}^B_\alpha\, \mathbf{g}^f_{n_A, A} = \mathbf{0}\,, \qquad \alpha = 1, \dots, n_B\,. \tag{4.24c}$$

We will remark the differences with (4.19) reside in (4.24b), which enforces none work associated with the released translations and rotation $\mathbf{u}^A_R$, whereas equations (4.24c) establish the equilibrium at the master nodes, given by residuals $\mathbf{g}_{\alpha,\,B}$ plus a weighted contribution *only* of the sliding nodal *force* residuals $\mathbf{g}^f_{n_A, A}$.

The contact *coupling element*

Let us define a *coupling element* [Muñ04] an hypothetic element that contains the displacement vector $\mathbf{u}^A_{Rm}$, with $3 \times (n_A + n_B + 1)$ degrees of freedom: displacements and rotations of elements A and B, and the released degrees of freedom from the slave node n_A. Note that coupling element residual $\mathbf{g}^A_{Rm}$ has been defined in (4.18), and depends not only on element A residual $\mathbf{g}^A$ but also the terms $\mathbf{R}_{\delta B}$ and $\mathbf{L}_{\delta B}$ which depend on element B. Since these last terms are not limited to a single element on a slideline, by computing them at the contact point of a new contacted element, different coupling elements will deal with the contact transition. We will expand the topic of dynamically changing the coupling element in the next Subsection.

4.1.4 Aspects on the NE computational implementation

Newton-Raphson solution and update

The non-linear vector equation

$$\mathbf{g} = \mathbf{0} \tag{4.25}$$

yields for $\mathbf{g}$ the *global* residual of the structure, which is obtained after the assembling of all elemental residuals, including $\mathbf{g}^A_{Rm}$. Note that the last one has to be assembled following the pattern given by the coupling element $\mathbf{u}^A_{Rm}$. An iterative Newton-Raphson procedure will be employed to solve (4.25). Within this scheme (refer to Appendix B), the global tangent operator $\mathbf{K} = \nabla_{\mathbf{u}}\,\mathbf{g}$ will contain additional terms that arise from the linearization of the coupling element. Indeed, such linearization leads to $\boldsymbol{\Delta}\mathbf{g}_{Rm} = \nabla_{\mathbf{u}_{Rm}}\,\mathbf{g}^A_{Rm} = \mathbf{K}_{cp}\,\boldsymbol{\Delta}\mathbf{u}_{Rm}$, where $\mathbf{K}_{cp}$ is the local tangent operator of the coupling element and may be expressed as

$$\mathbf{K}_{cp} = \mathbf{N}_\delta^{\mathrm{T}}\,\mathbf{K}_A\,\mathbf{N}_\delta^* + \begin{bmatrix} \mathbf{K}_{RR} & \mathbf{0}_{3\times 3N_A} & \mathbf{K}_{Rm} \\ \mathbf{0}_{3N_A\times 3} & \mathbf{0}_{3N_A\times 3N_A} & \mathbf{0}_{3N_A\times 3N_B} \\ \mathbf{K}_{mR} & \mathbf{0}_{3N_B\times 3N_A} & \mathbf{0}_{3N_B\times 3N_B} \end{bmatrix} \tag{4.26}$$

The previous result has been derived in Appendix C. We denote that $\mathbf{K}_{cp}$ has coupling terms between degrees of freedom of element A and master element B and therefore, special care must be exercised whenever the contact point switches from one element to another along the slideline, as we will described in the following part.

Regarding the update process during the iterative solution, special care must be taken in order to preserve the sliding contact condition. This is done by including a consistent update of the slave kinematics, once the iterative changes $\boldsymbol{\Delta}X$ and $\boldsymbol{\Delta}\theta_R$ has been obtained from the solution of (4.25), following the process summarized in Tables 4.1 and 4.2 for a fixed or released joint rotation respectively. The master and released variables are updated following standard procedures, as well as the inertial forces should be computed after velocities and accelerations are updated following i.e. in this variational approach, Newmark method 3.1.

$X_B^{i+1} = X_B^i + \mathbf{\Delta} X$	
Translations	Rotations
$\tilde{\mathbf{r}}_{n_A}^{i+1} = \tilde{\mathbf{r}}(X_B^{i+1}) = \mathbf{I}_\alpha(X_B^{i+1})\,\tilde{\mathbf{r}}_\alpha$	$\theta_{n_A}^{i+1} = \theta(X_B^{i+1}) + \theta_0 = \mathbf{I}_\alpha(X_B^{i+1})\,\theta_\alpha + \theta_0$

Table 4.1: Updating the kinematics of slave node. Planar joint rotation fixed

$X_B^{i+1} = X_B^i + \mathbf{\Delta} X$	
Translations	Rotations
$\tilde{\mathbf{r}}_{n_A}^{i+1} = \tilde{\mathbf{r}}(X_B^{i+1}) = \mathbf{I}_\alpha(X_B^{i+1})\,\tilde{\mathbf{r}}_\alpha$	$\theta_{n_A}^{i+1} = \theta_{n_A}^{i+1} + \mathbf{\Delta}\theta_R$

Table 4.2: Updating the kinematics of slave node. Free planar joint rotation

Contact element transition

With a proper definition of the coupling element, we will here show how the formulation can deal with a straightforward contact transition between elements along a *slideline*. For example, in Figure 4.5, it is assumed that at times t_1 and t_2, the element A has its contact point established with adjacent elements B and C respectively. In the reference configuration (see Figure 4.5), the contacted element can be easily obtained from the value of X_R and the initial mesh element sizes.

If the transition of the contact point occurs during the iterative process, the generic definition of the coupling element will allow to consider that a new element is contacted, simply by changing the computation of $\mathbf{R}_{\delta B}$ and $\mathbf{L}_{\delta B}$, i.e. referring again to Figure 4.5: $\mathbf{R}_{\delta C}$ and $\mathbf{L}_{\delta C}$. If the topology of the elements in the slideline is the same, the size of the coupling element will not change, but let us remark that the extended residual and the coupling terms of $\mathbf{K}_{cp}$ will have to be assembled adequately.

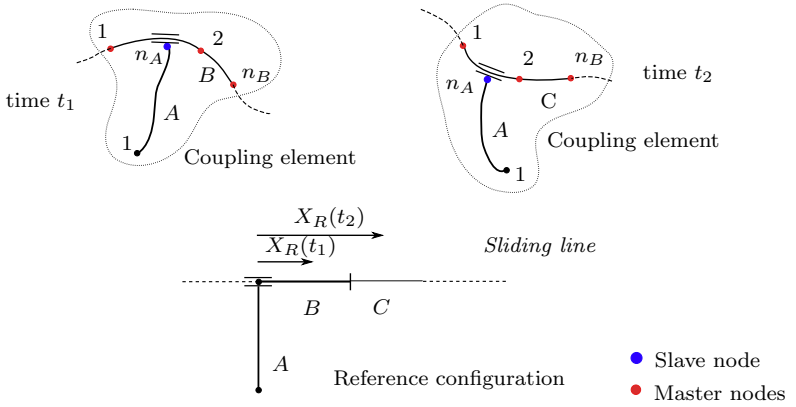

Figure 4.5: Scheme of a coupling element and a contact element transition

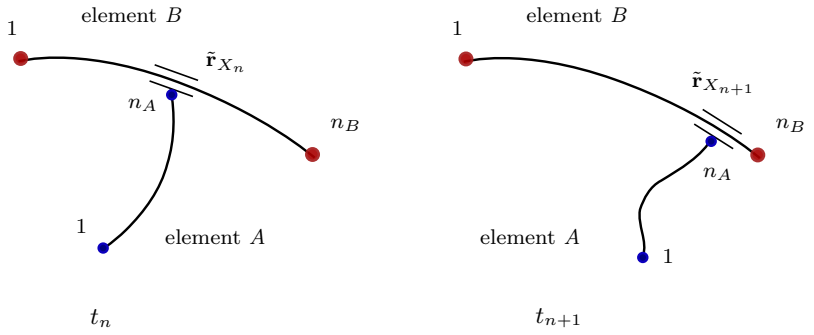

Figure 4.6: Sketch mesh in a non-transition case between Δt

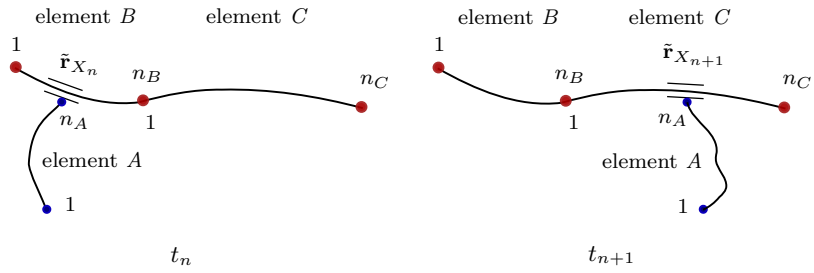

Figure 4.7: Sketch mesh in a transition case between Δt

4.2 Conserving contact using NE sliding

We will here present a technique that will adapt the variational NE approach for sliding contact, into an incremental formulation that will be connected with a conserving time integration scheme. However, we will need to distinguish first two possible situations, depicted in Figures 4.6 and 4.7. In the first case, the contact point slides within only one element *(NT)*, but in the other, it moves to an adjacent element *(T)*.

Such distinction is essential in the present approach since the coupling element may vary its topology, as well as the requirements for the conservation properties may change when transition occurs T. We denote by n_A, n_B and n_C the number of nodes of elements A, B and C respectively. Note that, as in the previous Section, we have assumed that the slave node is n_A, and we have plotted in Figure 4.6 and 4.7 the slave nodes in blue in contrast to the master ones shown in red.

The sliding kinematic conditions for a slave node n_A, resorting to interpolating functions $\mathbf{I}_\alpha$, may be written as follows:

$$
\begin{aligned}
& & \underline{t_n} & & \underline{t_{n+1}} & \\
NT: & \quad \tilde{\mathbf{r}}_{n_A,n} = \tilde{\mathbf{r}}_{X_n} = \mathbf{I}^{\alpha}_{X_n}\, \tilde{\mathbf{r}}_{j,n} & \quad \tilde{\mathbf{r}}_{n_A,n+1} = \tilde{\mathbf{r}}_{X_{n+1}} = \mathbf{I}^{\alpha}_{X_{n+1}}\, \tilde{\mathbf{r}}_{j,n+1} & \quad (4.27a) \\
T: & \quad \tilde{\mathbf{r}}_{n_A,n} = \tilde{\mathbf{r}}_{X_n} = \mathbf{I}^{\alpha}_{X_n}\, \tilde{\mathbf{r}}^{B}_{j,n} & \quad \tilde{\mathbf{r}}_{n_A,n+1} = \tilde{\mathbf{r}}_{X_{n+1}} = \mathbf{I}^{\alpha}_{X_{n+1}}\, \tilde{\mathbf{r}}^{C}_{j,n+1}\,, & \quad (4.27b)
\end{aligned}
$$

where we have added a superscript to the nodal positions in (4.27b) in order to distinguish the element to which they belong.

Incremental relationships in absence of contact transition (NT)

Whenever there are translations with no contact transition NT, the incremental displacement of node n_A may be written as

$$\begin{aligned}\Delta\tilde{\mathbf{r}}_{n_A} &= \tilde{\mathbf{r}}_{n_A,n+1} - \tilde{\mathbf{r}}_{n_A,n} = \mathbf{I}^{\alpha}_{X_{n+1}}\,\tilde{\mathbf{r}}_{\alpha,n+1} - \mathbf{I}^{\alpha}_{X_n}\,\tilde{\mathbf{r}}_{j,n} \\ &= \mathbf{I}^{\alpha}_{X\,\frac{1}{2}}\,\Delta\tilde{\mathbf{r}}_{\alpha} + \Delta\mathbf{I}^{\alpha}\,\tilde{\mathbf{r}}_{\alpha,n+\frac{1}{2}}\,, \end{aligned} \tag{4.28}$$

accounting with the following definitions:

$$\mathbf{I}^{\alpha}_{X\,\frac{1}{2}} \equiv \frac{1}{2}\left(\mathbf{I}^{\alpha}_{X_{n+1}} + \mathbf{I}^{\alpha}_{X_n}\right); \quad \Delta\mathbf{I}^{\alpha} \equiv \mathbf{I}^{\alpha}_{X_{n+1}} - \mathbf{I}^{\alpha}_{X_n}; \quad \Delta\tilde{\mathbf{r}}_{\alpha} \equiv \tilde{\mathbf{r}}_{\alpha,n+1} - \tilde{\mathbf{r}}_{\alpha,n}\,.$$

We refer the reader to [MJ06], where a graphical interpretation analysis of (4.28) has been done. It has been clearly shown that the increments $\Delta\tilde{\mathbf{r}}_{t_n}$ and $\Delta\tilde{\mathbf{r}}_{t_{n+1}}$ are due to the variation of the contact point coordinate at respecting times t_n and t_{n+1}, whereas ΔX_n and ΔX_{n+1} are the increments of the position vectors due to time variation at coordinates X_n and X_{n+1} respectively. In fact, using an interpolation of the previous increments through a parameter $\gamma \in \Re$:

$$\Delta\tilde{\mathbf{r}}_{n_A} = (1-\gamma)\,\left(\Delta\tilde{\mathbf{r}}_{t_n} + \Delta\tilde{\mathbf{r}}_{X_{n+1}}\right) + \gamma\,\left(\Delta\tilde{\mathbf{r}}_{X_n} + \Delta\tilde{\mathbf{r}}_{t_{n+1}}\right) \tag{4.29}$$

which follows that (4.28) is nothing but the special case of (4.29) for $\gamma = \frac{1}{2}$.

Having in mind as well, that our goal is to find the incremental form of the master-slave relationship, then the following vectors can be rewritten:

$$\Delta\tilde{\mathbf{r}}_{t_n} = \frac{1}{\Delta X}\,\left(\Delta\tilde{\mathbf{r}}_{t_n}\otimes\mathbf{E}_1\right)\,\Delta\tilde{\mathbf{r}}_R\,; \quad \Delta\tilde{\mathbf{r}}_{t_{n+1}} = \frac{1}{\Delta X}\,\left(\Delta\tilde{\mathbf{r}}_{t_{n+1}}\otimes\mathbf{E}_1\right)\,\Delta\tilde{\mathbf{r}}_R \tag{4.30}$$

Inserting equations (4.30) into (4.28) and using the standard nodal interpolation, the master-slave relationship for translations (and case NT) is obtained in the incremental form:

$$\Delta\tilde{\mathbf{r}}_{n_A} = \frac{1}{\Delta X}\,\left(\Delta\mathbf{I}^{\alpha}\,\tilde{\mathbf{r}}_{j,n+\frac{1}{2}}\otimes\mathbf{E}_1\right)\,\Delta\tilde{\mathbf{r}}_R + \mathbf{I}^{\alpha}_{X\,\frac{1}{2}}\,\Delta\mathbf{r}_j\,, \tag{4.31}$$

where we remark $\gamma = 0.5$ has been used for the interpolation defined in (4.29).

Incremental relationships with contact transition (T)

We will consider now the case which contact conditions are given by (4.27b). We will again propose an interpolation of increments such like (4.29), using

$\gamma = 0.5$ but considering now that position vectors from different elements will have to be taken into account. This yields a different master-slave relationship for incremental translations than in (4.31):

$$\Delta\tilde{\mathbf{r}}_{n_A} = \frac{1}{\Delta X}\left[\left(\mathbf{I}^{\alpha}_{X_{n+1}}\,\tilde{\mathbf{r}}^{C}_{\alpha,n+\frac{1}{2}} - \mathbf{I}^{\alpha}_{X_n}\,\tilde{\mathbf{r}}^{B}_{\alpha,n+\frac{1}{2}}\right)\otimes\mathbf{E}_1\right]\Delta\tilde{\mathbf{r}}_R + 0.5\,\mathbf{I}^{\alpha}_{X_{n+1}}\,\Delta\tilde{\mathbf{r}}^{C}_{\alpha} + 0.5\,\mathbf{I}^{\alpha}_{X_n}\,\Delta\tilde{\mathbf{r}}^{B}_{\alpha}\,. \tag{4.32}$$

We remark that the topology now for the coupling element will change since *two* elements C and B present their incremental displacements $\Delta\tilde{\mathbf{r}}^{C}_{\alpha}$ $\Delta\tilde{\mathbf{r}}^{B}_{\alpha}$ in the master-slave relationship.

An incremental form for the master-slave relationship

Having studied the relationships for translations in the previous Subsections, either for NT or T conditions of the contact point transition within elements, and assuming now that the sliding joint planar rotation will be released, we will present here the master-slave incremental relationship, using the results derived, mainly equations (4.31) and (4.32).

Let us first define, as we have done in previous Section for infinitesimal displacements, the vector of *slave incremental displacements* $\Delta\mathbf{u}^{A}$ and the vector of *released and master incremental displacements* $\Delta\mathbf{u}^{A}_{Rm}$ as

$$\Delta\mathbf{u}^{A} \equiv \begin{Bmatrix} \Delta\mathbf{u}^{A}_{1} \\ \vdots \\ \Delta\mathbf{u}^{A}_{n_A} \end{Bmatrix} \text{ and } \Delta\mathbf{u}^{A}_{Rm} \equiv \begin{Bmatrix} \Delta\mathbf{u}_{R} \\ \Delta\mathbf{u}^{A}_{1} \\ \vdots \\ \Delta\mathbf{u}^{A}_{n_A} \\ \Delta\mathbf{u}^{B}_{1} \\ \vdots \\ \Delta\mathbf{u}^{B}_{n_B} \end{Bmatrix}, \tag{4.33}$$

with $\Delta\mathbf{u}_R = \begin{Bmatrix}\Delta\tilde{\mathbf{r}}_R & \Delta\theta_R\end{Bmatrix}$. Let us remark that the superscript I corresponds in vector $\Delta\mathbf{u}^{A}_{Rm}$ corresponds to the contacted element at time $n+1$, and recall that when the transition occurs, then we will consider the relationship as it two elements were in contact, leading to a bigger coupling element. This approach, though it requires modifications on the data structure with respect to the variational approach, will lead to an incremental formulation that can conserve energy and momentum.

It is now clear that equations (4.31) and (4.32) provide with the necessary relationships to build the transformation matrix $\mathbf{N}_{\Delta}$ such that

$$\Delta\mathbf{u}^{A} = \mathbf{N}_{\Delta}\,\Delta\mathbf{u}^{A}_{Rm}\,, \tag{4.34}$$

with

No Transition (NT)		Transition (T)
$\mathbf{I}_X^\alpha$	$\mathbf{I}_{X\,\frac{1}{2}}^\alpha$	$0.5\mathbf{I}_{X_{n+1}}^{\alpha,\,C}$; $0.5\mathbf{I}_{X_n}^{\alpha,\,B}$
$\Delta\tilde{\mathbf{r}}_X$	$\Delta\mathbf{I}^\alpha\,\tilde{\mathbf{r}}_{\alpha,n+\frac{1}{2}}$	$\Delta\tilde{\mathbf{r}}_{BC_{n+\frac{1}{2}}} = \left(\mathbf{I}_{X_{n+1}}^\alpha\,\tilde{\mathbf{r}}_{\alpha,n+\frac{1}{2}}^C - \mathbf{I}_{X_n}^\alpha\,\tilde{\mathbf{r}}_{\alpha,n+\frac{1}{2}}^B\right)$
γ	0.5	0.5

Table 4.3: Values for the incremental NE approaches E_C and M_C in matrices $\mathbf{N}_\Delta$ and $\mathbf{R}_\Delta$

$$\mathbf{N}_\Delta = \begin{bmatrix} \overline{\mathbf{0}} & \mathbb{1} & \dots & \overline{\mathbf{0}} & \overline{\mathbf{0}} & \overline{\mathbf{0}} & \dots & \overline{\mathbf{0}} \\ \vdots & \vdots & \ddots & \vdots & \vdots & \vdots & \ddots & \vdots \\ \overline{\mathbf{0}} & \overline{\mathbf{0}} & \dots & \mathbb{1} & \overline{\mathbf{0}} & \overline{\mathbf{0}} & \dots & \overline{\mathbf{0}} \\ \mathbf{R}_\Delta & \overline{\mathbf{0}} & \dots & \overline{\mathbf{0}} & \overline{\mathbf{0}} & \mathbf{I}_X^1\,\tilde{\mathbb{1}} & \dots & \mathbf{I}_X^{n_I}\,\tilde{\mathbb{1}} \end{bmatrix}, \tag{4.35}$$

and the matrix $\mathbf{R}_\Delta$ given by

$$\mathbf{R}_\Delta = \begin{bmatrix} \frac{1}{\Delta X}\,\Delta\tilde{\mathbf{r}}_X \otimes \mathbf{E}_1 & 0 \\ \mathbf{0} & 1 \end{bmatrix}. \tag{4.36}$$

Note that different expressions for $\mathbf{I}_X^\alpha$, $\Delta\tilde{\mathbf{r}}_X$ and γ will lead to different strategies in the incremental master-slave NE approach. We will present our choice in Table 4.3, with $\gamma = 0.5$ maintained for both NT and T cases, which furnishes the best approximation to the angular momentum conserving condition [Muñ04], as we will later discuss.

4.2.1 An energy conserving approach

The incremental NE sliding approach has been derived with an exact contact condition, which states that, no matter about the contact point transition within elements, the kinematics of the slave node will be given by:

$$\tilde{\mathbf{r}}_{n_A,\,n+1} = \mathbf{I}_{X_{n+1}}^{\alpha\,I}\,\tilde{\mathbf{r}}_{\alpha,\,n+1}^I\,, \tag{4.37}$$

with I the element contacted at time t_{n+1}. In order to preserve the energy conservation of the time integration scheme, it will be mandatory to update the slave kinematics using (4.37) [MJ06]. However, since the angular momentum condition is given by:

$$\tilde{\mathbf{r}}_{n_A,\,n+\frac{1}{2}} = \mathbf{I}_{X_{n+\frac{1}{2}}}^{\alpha\,I}\,\tilde{\mathbf{r}}_{\alpha,\,n+\frac{1}{2}}^I\,, \tag{4.38}$$

when no element transition occurs at element I and:

$$\tilde{\mathbf{r}}_{n_A,\,n+\frac{1}{2}} = 0.5\,\mathbf{I}_{X_{n+1}}^{\alpha\,I_{n+1}}\,\tilde{\mathbf{r}}_{\alpha,\,n+\frac{1}{2}}^{I_{n+1}} + 0.5\,\mathbf{I}_{X_n}^{\alpha\,I_n}\,\tilde{\mathbf{r}}_{\alpha,\,n+\frac{1}{2}}^{I_n}\,, \tag{4.39}$$

	No Transition (NT)	Transition (T)
$\mathbf{I}_X^\alpha$	$\mathbf{I}_{X\frac{1}{2}}^\alpha$	$0.5\mathbf{I}_{X_{n+1}}^{\alpha,C};\ 0.5\mathbf{I}_{X_n}^{\alpha,B}$
$\Delta\tilde{\mathbf{r}}_X$	$2\left(\mathbf{I}_{X\frac{1}{2}}^\alpha\,\tilde{\mathbf{r}}_{\alpha,n}-\tilde{\mathbf{r}}_{n_A,n}\right)$	$2\left(0.5\,\mathbf{I}_{X_{n+1}}^\alpha\,\tilde{\mathbf{r}}_{\alpha,n}^C+0.5\,\mathbf{I}_{X_n}^\alpha\,\tilde{\mathbf{r}}_{\alpha,n}^B-\tilde{\mathbf{r}}_{n_A,n}\right)$

Table 4.4: Values for the incremental NE approach $E\&M_C$ in matrices $\mathbf{N}_\Delta$ and $\mathbf{R}_\Delta$

with I_{n+1} the slideline element in contact at t_{n+1} and analogous, I_n the previous contacted element at t_n.

The previous discrepancy made the present algorithm E_C to be energy conserving, with an exact contact kinematic condition, but fails to preserve angular momentum.

4.2.2 An angular momentum conserving approach

In the previous case, we will update the kinematics of the slave node following the angular momentum conditions, either (4.38) or (4.39), depending on the contact point transition condition. However, since the equilibrium equations has been derived through a master-slave relationship *on an exact* contact condition, this algorithm M_C will be the contrary example to E_C. We state that the angular momentum conserving condition for the slave node is satisfied, but at the expense of loosing the energy conserving properties of the time integration scheme.

4.2.3 The energy and momentum conserving approach

With the intention of assessing the paradox between E_C and M_C, a new algorithm that preserves energy and momenta has been built [SM11]. Since the angular momentum condition is unavoidable, we have developed the master-slave relationship *starting* from the mid-point relaxed condition (4.38) instead of the exact contact conditions of (4.27a) and (4.27b). In such a way, the slave node kinematics are updated following the angular momentum conserving condition and at the same time the energy conserving condition given by the master-slave relationships is fulfilled. We remark the update kinematics for the slave node will be given by (4.38) and (4.39), depending on the transition condition, and the master-slave residuals can be derived from the summary in Table 4.4.

Chapter 5

Numerical examples

In the present Chapter we will present a series of numerical examples that implement in a *MATLAB* code, the different theories developed through all the rest of the previous chapters. There are five different beam problems that have been taken from the literature and adapted in some cases to our planar formulation. We intend with these examples, either to verify our formulations comparing them to previous work, or to benchmark with a model problem the performance of different algorithms.

The convergence for all the finite element computations reported herein, is established on the basis of the L_2 norm of the residual nodal vector, and a full Newton-Raphson iterative solution procedure is employed. A convergence force tolerance $\epsilon_f = 1E-10$ will be considered unless a different one is specified, and non convergence will be stated after the maximum number of iterations $\text{Ite}_{max} = 20$ is reached at a given time step.

It is emphasized as well that the deformed shapes in all figures reported here are given at the same scale as the initial geometry of the beams, that is to say, non magnification factors are employed to show structural deformations.

We will start first with a single example on statics in Section 5.1. We will verify the quadratic convergence in the solution of the beams residuals, using different orders of Lagrangian standard interpolation and testing as well the performance of the B-Splines. In Section 5.2 and 5.3 two examples of dynamics will be shown, and conserving properties of the different time integration schemes will be discussed. Finally, Section 5.4 and 5.5 will present a two beam system in sliding contact with different load cases and supports. We will asses there the role of contact smoothing, as well as testing the performance of different conserving algorithms in the stability of the non-linear solution.

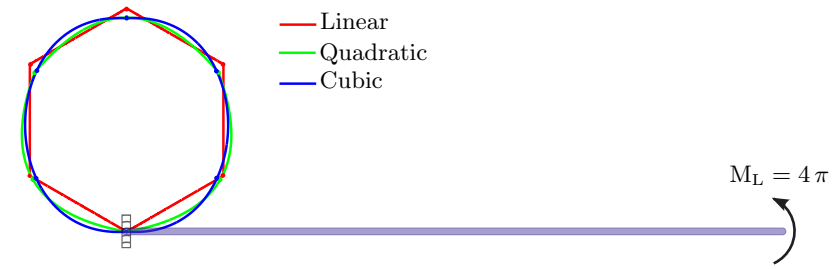

(a) Lagrangian interpolation

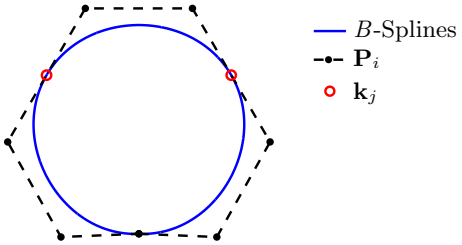

(b) B-Splines interpolation

Figure 5.1: Cantilever beam deformation. Interpolation comparison

5.1 Pure bending of a cantilever beam

A similar example to the problem presented in [SVQ86a] is here described. In addition, we well test as well, different orders for standard Lagrangian and B-Splines interpolations. An initial straight beam of unit length and bending stiffness $\mathrm{E\,I} = 2$ is subjected to a concentrated moment $\mathrm{M_L}$ at its end. The exact solution to this problem is a circumference arch with radius $\rho_C = \mathrm{E\,I}/\mathrm{M_L}$ [SVQ86a]. An end moment $\mathrm{M_L} = 4\,\pi$ is applied in a single load step, and will force the rod to wind around itself into a closed circle. Let us remark that regarding numerical integration, different Gaussian quadrature rules have been used depending on the interpolation's order. In the linear case, a one point rule has been used to avoid *shear locking* effects, for the quadratic order, a two point rule is implemented, and three points are applied for the cubic and B-Splines interpolations.

In Figure 5.1a we present in scale the initial configuration of the cantilever beam, as well as the comparison of deformed results from different finite element interpolations. We have used different orders of standard Lagrangian interpolation, maintaining the total number of nodes constant. Therefore, results are shown for five, three and two; linear, quadratic and cubic elements respectively. Moreover, in Figure 5.1b we show the same problem solution but modelled with three B-Spline elements, joined at knot values $\mathbf{k}_j$, plotted in red. We have also depicted in black their nodal configuration, given by control points $\mathbf{P}_i$, connected together by the *control polygon*.

In Figure 5.2 we present the different solutions convergence rate, and it is shown that near equilibrium, quadratic convergence is achieved. We note that

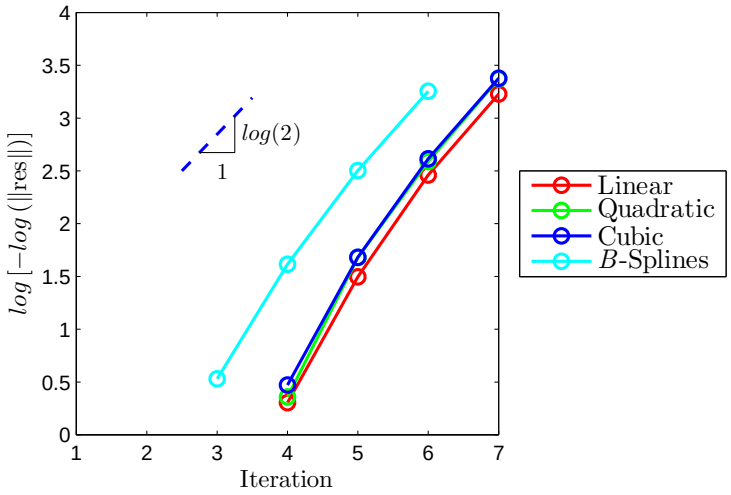

Figure 5.2: Bending problem: comparison in the evolution of the L_2 norm of the residual for different interpolations

in Figure 5.2 the values for which the logarithm is not defined have not been plotted, and the solution for B-Splines requires one iteration less than the other interpolations.

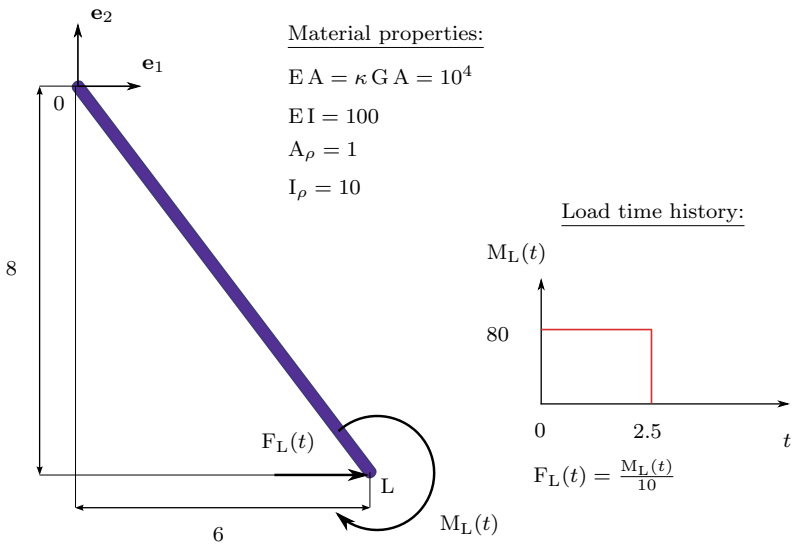

Figure 5.3: The *flying spaghetti*. Initial configuration and data

5.2 The *flying spaghetti*

The present numerical example has been extracted from [SVQ86c]. We will reproduce the mechanical and geometric properties exactly as it has been reported, but will include modifications in the finite element interpolation and a comparison between time integration schemes. A flexible rod with free ends, initially placed in an inclined position, is subjected to a torque and force applied simultaneously at one end (see Figure 5.3). The external force and moment are removed at the same time $t = 2.5$, and consequently a free flight occurs immediately after, which is simulated till $t = 7.5$. We will apply a time step increment $\Delta t = 0.1$, and the obtained sequence of motion will be likely to the one shown in Figure 5.4, which in fact has been modelled using five B-Spline elements and a Newmark method.

We will first test the performance in the Newmark method, using different finite element interpolation but a similar number of degrees of freedom. For example, the five B-Splines case depicted in Figure 5.4 is compared to a four cubic Lagrangian, in order to maintain similar total number of nodes. We have found that none time step halving is required in the B-Splines case to complete the total simulation time. On the other hand, convergence difficulties has been reported at times $t = 5.2$, $t = 5.6$, $t = 6.5$, $t = 7.0$, and $t = 7.2$ when the same algorithm is used with cubic Lagrangian interpolation, taking nine time steps more than the expected to end the simulation.

In Figure 5.5, we present the evolution of energy and angular momentum in the Newmark method for the *flying spaghetti* in free flight, and the plots show that none of these quantities are conserved. We compare as well the energy and angular momentum values computed for the different interpolations. The energy results for the present example show the effects of time step reduction for cubic elements, where smaller time increments had to be taken to avoid instabilities. On the other hand, energy seems to remain bounded when Newmark method is

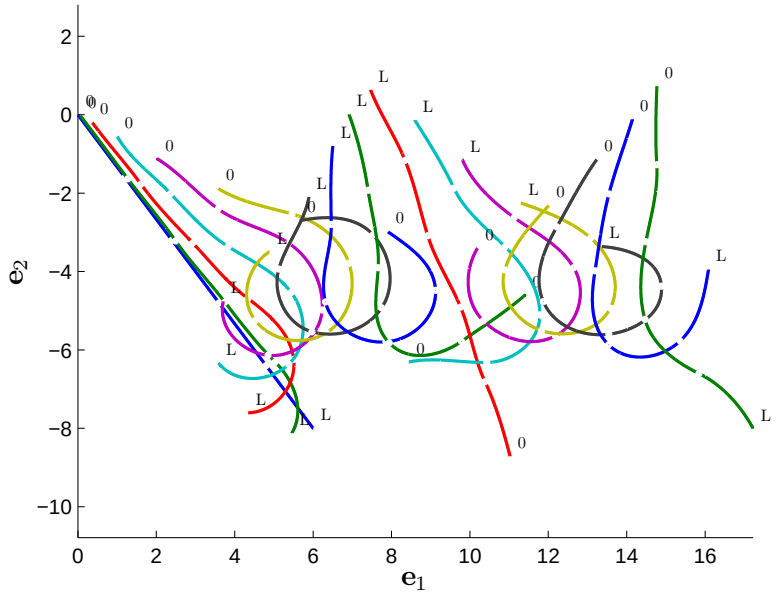

Figure 5.4: *Flying spaghetti* motion after each five time increments

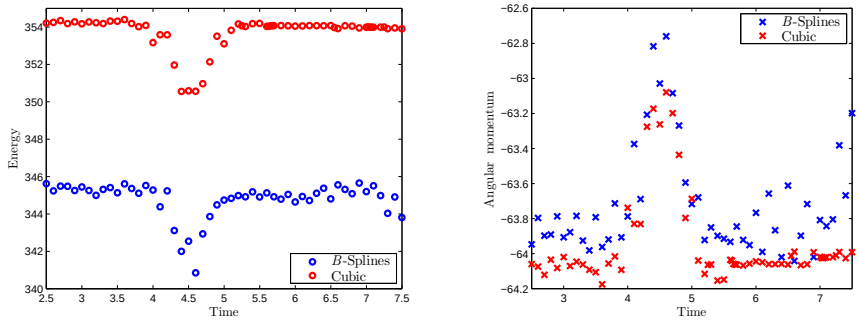

(a) Total energy (b) Angular momentum

Figure 5.5: The *flying spaghetti*. Energy and angular momentum during free flight

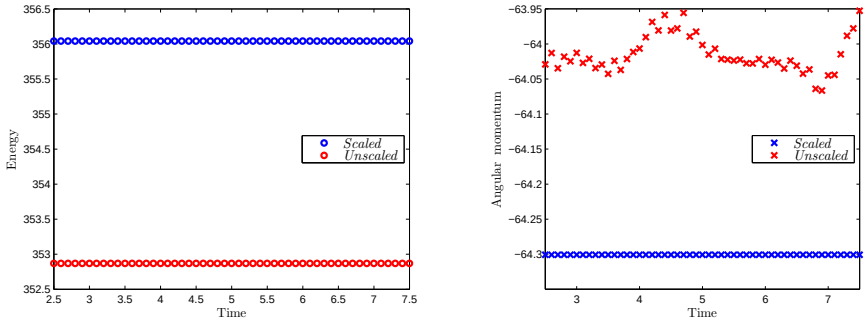

(a) Total energy (b) Angular momentum

Figure 5.6: The *flying spaghetti* with conserving time integration. Energy and angular momentum during free flight

employed with B-Splines, a fact that becomes even more noticeable when mesh refinement is applied. A test with five cubic finite elements fails to converge at $t = 4.9$ after five successive time step halvings, and this behaviour is worsen when the mesh is further refined. However, we have encountered that simulation ends without any time step halving even for 15 B-Splines.

We conclude the present example of non-linear dynamics showing the conserving properties of the modified mid-point time integration schemes described in Section 3.2. We take the same discretization previously described of five B-Spline elements and the *flying spaghetti* is run to compare results from the conserving algorithms that use *unscaledd* or *scaled* rotations. In Figure 5.6, energy and angular momentum time evolution is plotted. The results confirm that energy conservation is achieved by both schemes, whereas only the interpolation of *tangent scaled* incremental rotations leads to conservation of momenta (see Appendix D). Let us finally remark that the previous two schemes do not significantly differ in the computation of results (see i.e. energy differences in Figure 5.6a).

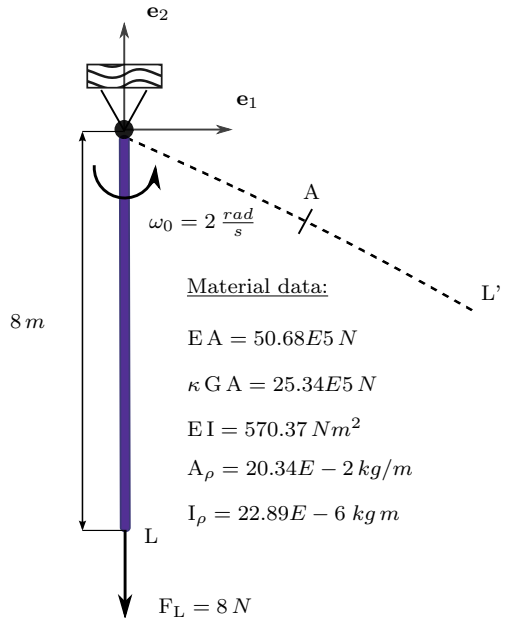

Figure 5.7: A flexible pendulum. Initial configuration and data

5.3 A flexible pendulum

The example in this Section takes the same initial data and beam properties proposed in [SS96]. A simple beam pendulum is placed initially in vertical position and an angular velocity ω_0 is consistently applied to all nodes. The pendulum's tip is subjected to a constant force $\mathrm{F_L}$, and no body forces are considered. The structural behaviour of this system will be studied till the simulation end time $t = 10\,s$.

In [SS96], they developed a conservative mid-point time integration scheme specifically for C_0 planar beam elements, and interpolation of *unscaled* incremental rotations. In that context, they successfully tested the energy conserving scheme against Newmark method. The former algorithm showed that despite its *unsymmetric* stiffness matrix, it worked more efficient than the latter, as much bigger time steps could be taken in non-linear dynamics problems. In our case, based on the previous background, we will test B-Splines and interpolation of *tangent scaled* incremental rotations. The latter, as we have already mentioned before, leads to an energy and momenta - E&M - conserving algorithm. Simulations are run for all cases with spatial discretization of five B-Splines. The conservative time scheme will use a time step $\Delta t = 0.4\,s$ whereas $\Delta t = 0.05\,s$ will be applied for the Newmark scheme - NWM -. With respect to the convergence force tolerance, $\epsilon_f = 1E-8$ will be used for both time integration schemes.

In Figure 5.8 we present the sequence of motion of deformed configurations of the beam pendulum, using the conserving time integration scheme. Furthermore, we test the performance of E&M against NWM, by comparing their

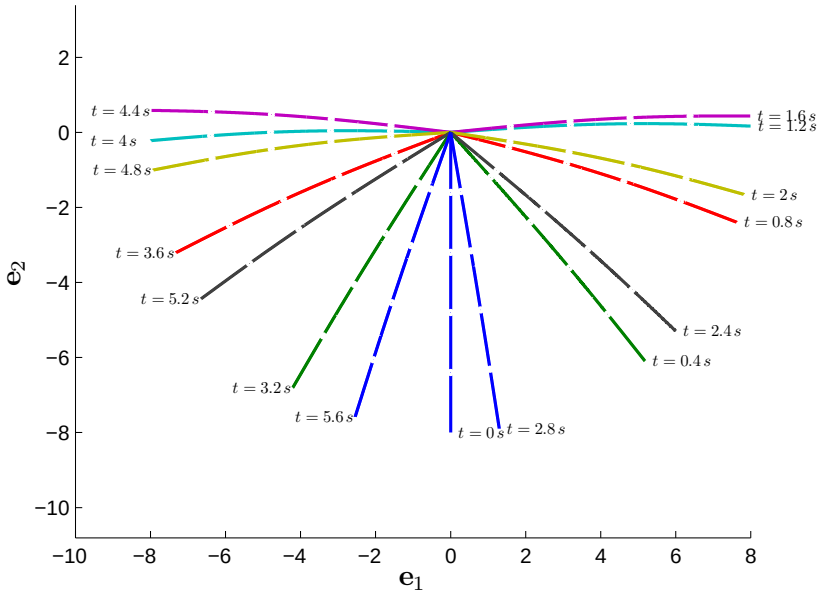

Figure 5.8: Beam pendulum motion. First consecutive fourteen time increments

resulting energy and angular momentum evolution of the system, in Figure 5.9. NWM failed to converge after five successive time step halvings at time $t = 7.43$. In fact, is seen in Figure 5.9a that the energy gradually became unstable before the NWM algorithm completely failed. This has been observed in [SS96] as well, which makes NWM unsuitable even for a time adaptive scheme. On the other hand, E&M complete the analysis using a time step eight times bigger for the whole simulation history. As it is clear seen in 5.9a and 5.9b respectively, with E&M the total energy of the system remains constant and the angular momentum is conserved.

We finally present in Figure 5.10 the evolution of some variables of structural analysis, such as the tip rotation θ_{L} and the bending moment at point A. We have included as well in the plots, an interpolation of the E&M results in black. We conclude that the conserving scheme, despite its long time increments, reproduces structural analysis variables with acceptable accuracy.

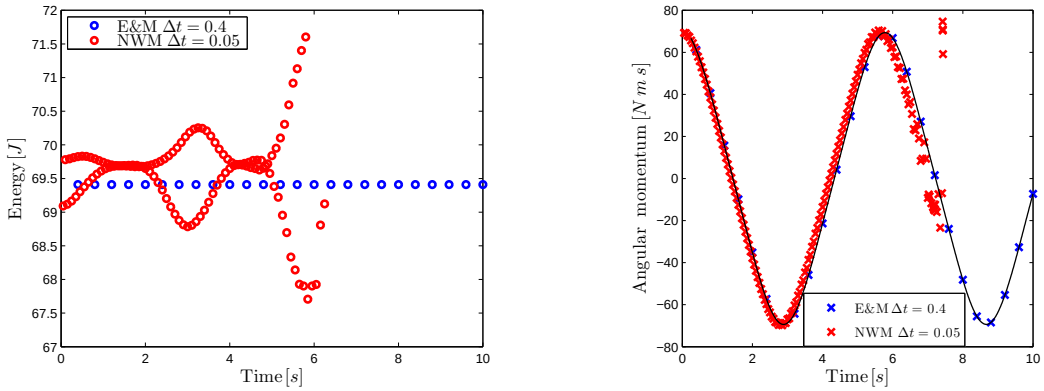

(a) Total energy

(b) Angular momentum

Figure 5.9: Beam pendulum energy and angular momentum. Time integration comparison

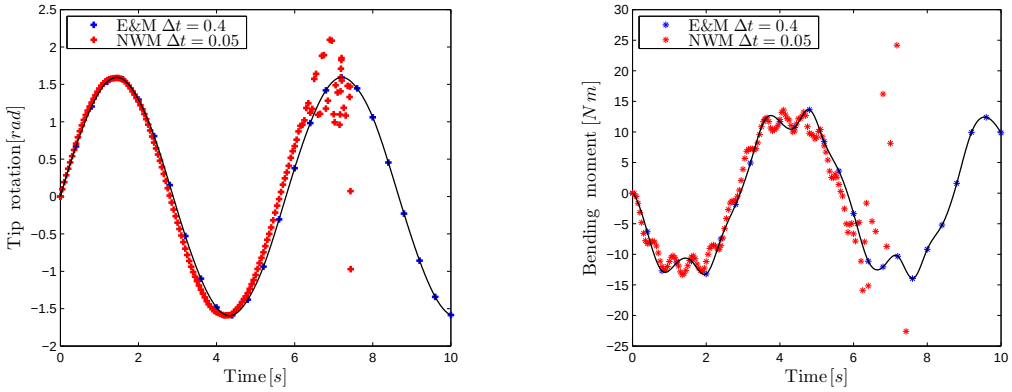

(a) Tip rotation

(b) Bending moment

Figure 5.10: Beam pendulum tip rotation and bending moment. Time integration comparison

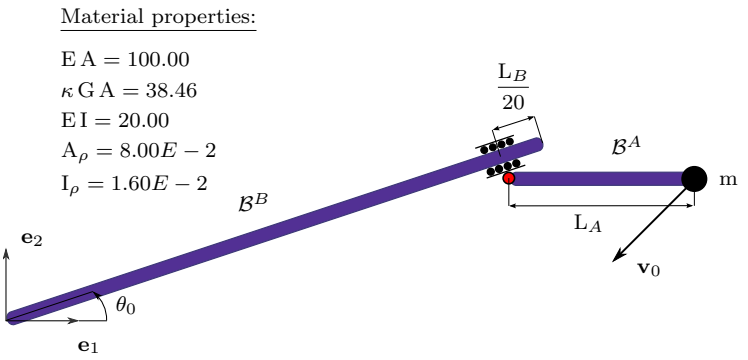

Figure 5.11: A free moving mass attached to sliding beams. Initial configuration and problem data

5.4 Free mass in sliding flight

The present example has been adapted from [MJ06] to our planar case formulations. The system is formed by two beams connected with a sliding joint, with its rotation free, and a mass m $= 1\,kg$ attached to one beam's tip. The initial configuration is depicted in Figure 5.11, as well as mechanical properties, which are shared for both beams. However, the geometrical design differs, beam $\mathcal{B}^A$ total length is L$_\text{A}$ = 1 and for beam $\mathcal{B}^B$ corresponds L$_\text{B}$ $= \sqrt{10}$ and an initial rotation $\theta_0 = \arctan 1/3\,rad$. An initial velocity $\mathbf{v}_0 = \begin{Bmatrix} -10 & -10 \end{Bmatrix}^\text{T}$ is applied to the mass at $\mathcal{B}^A$ tip. Since no external loads are applied to the system, the actual physics of this problem must conserve energy and momenta. We remark this problem has no practical relevance, but it will test the conserving properties of incremental NE sliding formulations proposed in Section 4.2.

In the following simulations, we will discretize beams $\mathcal{B}^A$ and $\mathcal{B}^B$ with three and five B-Spline elements respectively, and the analysis will be run until $t = 0.36$, which is the approximate time when $\mathcal{B}^A$ reaches $\mathcal{B}^B$ tip. Three different incremental formulations within the NE sliding contact approach will be tested using time increment $\Delta t = 0.02$, referring to them as E$_\text{C}$, M$_\text{C}$ and E&M$_\text{C}$, which respectively stands for energy, momentum and energy-momentum conserving schemes (see Subsections 4.2.1, 4.2.2 and 4.2.3 respectively for further references). The whole set of algorithms are able to reach the end time for the prescribed Δt without any need of time step halving. However, if we compare the energy and angular momentum time progression in Figure 5.13, the distinguishing characteristics of the three algorithms are clearly shown.

In Figure 5.12, it is shown the sequence of free sliding motion of the beams' and mass system. The depicted plot has been taken from the E$_\text{C}$ algorithm results. We remark that although results from the different conserving schemes in question do not differ significantly at first sight, the only scheme that preserves the *exact* contact conditions in the E$_\text{C}$ (we refer the reader to 4.2.1 for further details). On the other hand, M$_\text{C}$ and E&M$_\text{C}$ use a *relaxed* sliding contact condition, as it is shown in Figure 5.13 for the E&M$_\text{C}$ free flight sequence. Such non-exact contact state, though it is confined, can still be well distinguished in the detail at Figure 5.13a.

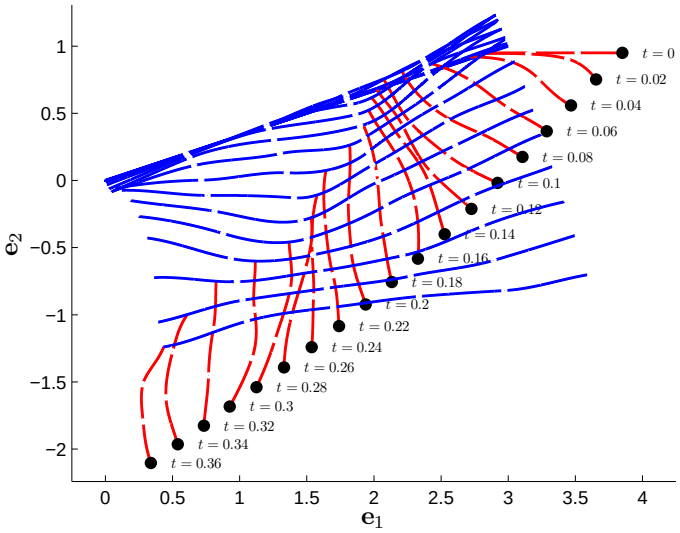

Figure 5.12: The free sliding mass system motion

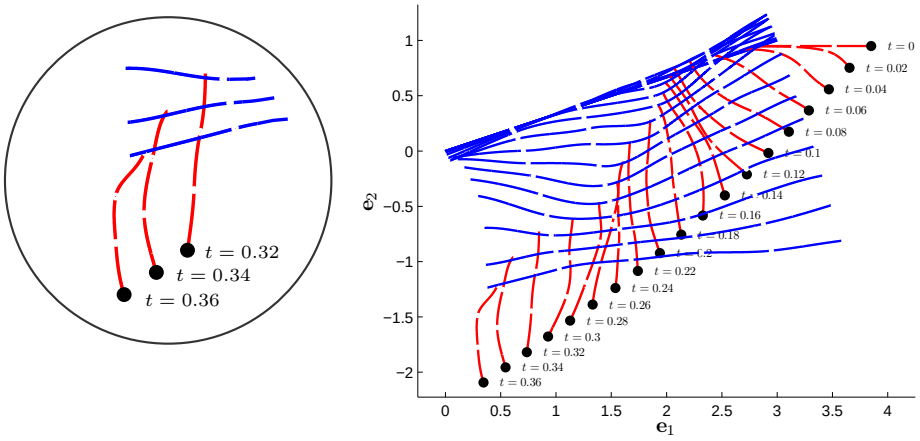

(a) Relaxed contact detail

(b) Sliding motion with E&M$_C$

Figure 5.13: The free sliding mass system motion. Detail of relaxed contact constrains

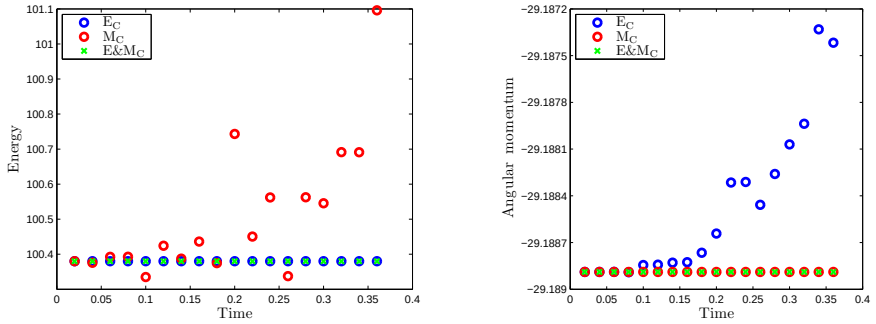

(a) Total energy

(b) Angular momentum

Figure 5.14: The free sliding mass problem. Comparison of conserving properties in modified NE sliding schemes

In Figure 5.14 we present, as anticipated before, the evolution of the conserving properties of the three incremental NE sliding contact approaches. In Figure 5.14a, we show that energy remains constant for E_C and $E\&M_C$. However, the angular momentum in 5.14b is only conserved for M_C and $E\&M_C$. The previous show that a relaxed contact condition and a consequent modification of the master-slave relationship (see 4.2.3) preserves the conserving properties of the modified mid-point time integration scheme given in 3.2.2. This can be consider one of our contributions in the present work, recalling that to the author's knowledge, non energy and momentum conservation has been reported yet for sliding contact within a NE approach.

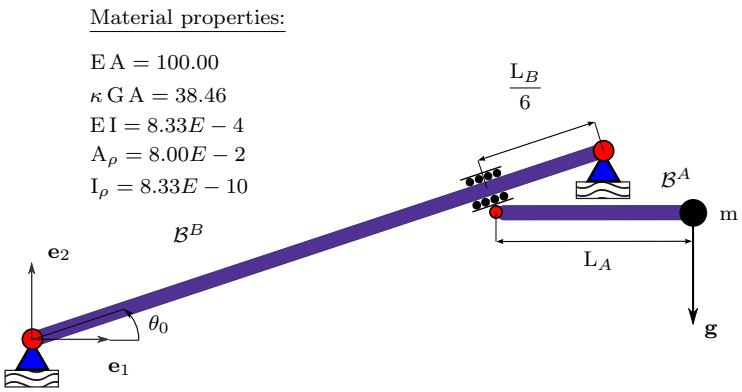

Figure 5.15: Initial configuration and problem data for the aerial runway example

5.5 A planar aerial runway

The example here is formed, like in previous Section 5.4, by a system of two beams in sliding contact and a mass $\mathrm{m} = 1\,kg$ attached to the free end of beam $\mathcal{B}^A$. The initial configuration is given in Figure 5.15, where the mass is subjected to the gravitational field $\mathbf{g} = \begin{Bmatrix} 0 & -9.8 \end{Bmatrix}^{\mathrm{T}}$ and beam $\mathcal{B}^B$ is simply supported at both ends. The beams dimensions $\mathrm{L_A}$ and $\mathrm{L_B}$, together with θ_0 initial rotation are the same used before (refer to Section 5.4). However, the initial position of $\mathcal{B}^A$ has been changed as depicted in Figure 5.15. Note as well in Figure 5.15, the material properties, shared by both beams, which are much more flexible than in the *free mass in sliding flight* problem. In fact, our intention with the present example is to model (in a planar configuration) an *aerial runway*. A real mechanical device like that, for leisure purposes, has been drawn in Figure 5.16 [1]. This example has been adapted from [MJ04], where it was presented for 3D sliding beams. Our aim here is to asses the effects of sliding contact at the finite element transitions, either modelled by standard Lagrangian or B-Splines interpolations. The problem is of particular interest since strong variations of the tangent to the deformed line of centroids is expected along the beam's arc length.

The simulation of the problem will be run during the first 1.9 seconds. An initial time increment $\Delta t = 0.1$ will be used, which may be eventually reduced due to time step halvings, and no convergence of the problem will be stated after five successive time step halvings. We propose four different discretizations that, in order to keep similar (or equal if possible) the total number of degrees of freedom, result in table 5.1. We will test the different finite element interpolations performance in the solution of the aerial runway, using for benchmarking the NE incremental approach $\mathrm{E_C}$, which preserves the exact contact condition.

We will first present in Figure 5.17, the sequence of motions for the aerial runway using B-Splines. The plot is shown in four different snapshots, each of them containing the system deformation at five consecutive time increments $\Delta t = 0.1$. Let us note that at intermediate configurations during the iterative

[1] Vectorized draw from `http://www.ludusleisure.co.uk/downloads/swings/Aerial-Runway.jpg`.

Figure 5.16: A typical aerial runway device

	Number of elements	
Element type	$\mathcal{B}^A$	$\mathcal{B}^B$
B-Splines	3	5
Cubic	2	4
Quadratic	3	6
Linear	6	12

Table 5.1: Number of elements per beam used for the aerial runway problem

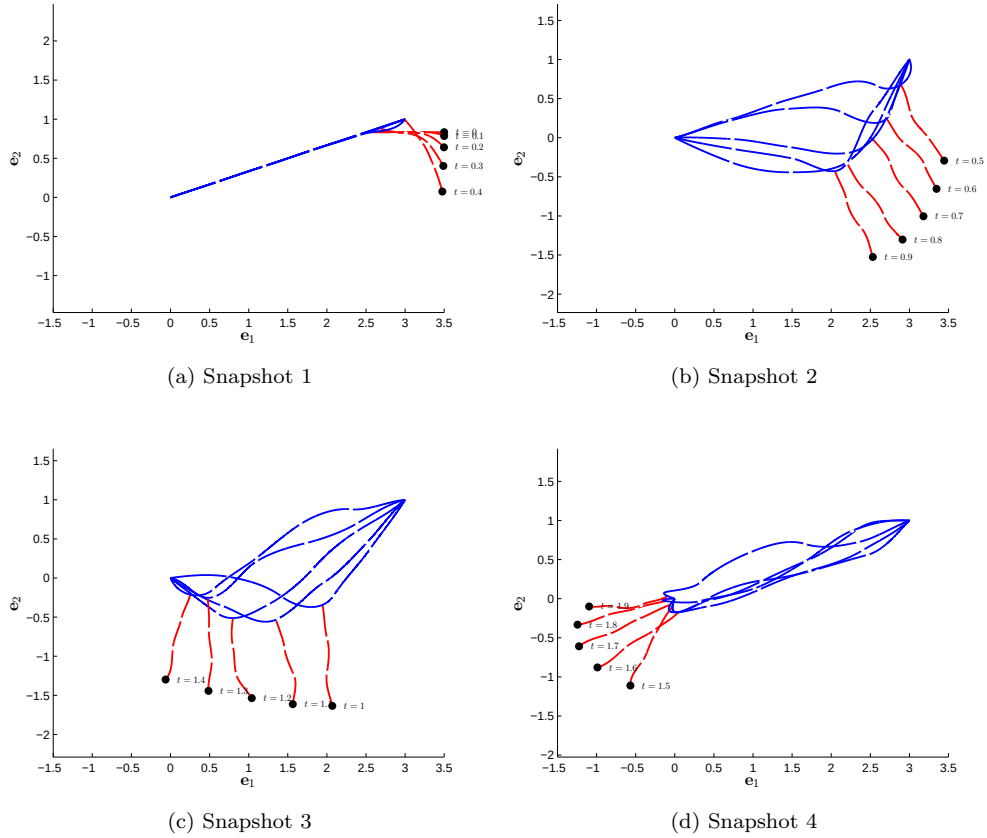

(a) Snapshot 1

(b) Snapshot 2

(c) Snapshot 3

(d) Snapshot 4

Figure 5.17: Planar aerial runway B-Splines model. Sequences of the system motion in four snapshots

solution process, beam $\mathcal{B}^A$ released translations may result outside $\mathcal{B}^B$ domain. We remark that time step halving (up to a minimum $\Delta t = 0.0125$) was employed, though it is not shown in Figure 5.17, in order to maintain the sliding contact between beams. Despite that, the simulation reaches the end time successfully for the *smooth* slideline discretized with B-Splines.

On the other hand, we have implemented as well standard Lagrangian finite elements of different orders (refer to Table 5.1) such that the aerial runway simulation is run with the same solution parameters just mentioned before. We have confirmed that a discrete non-smooth (Lagrangian) interpolation of the slideline has a detrimental effect on the convergence, regardless of the order of the interpolation. In Figure 5.18, the different results are shown in a sequence of deformed configurations of the beam system. However, we have found that for all Lagrangian discretizations, the analysis fails to converge between times $t = 0.6$ and $t = 0.7$, that is precisely when element transition occurs. Let us finally note as well, that intermediate time steps halvings has been computed during the numerical solution, but are not shown in the plot for clarity.

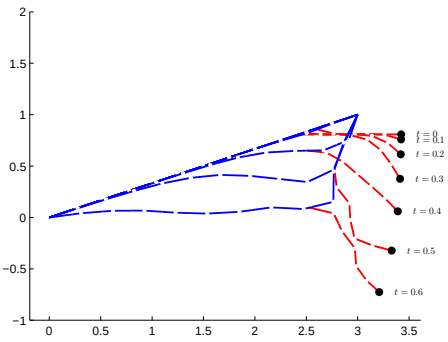

(a) Linear

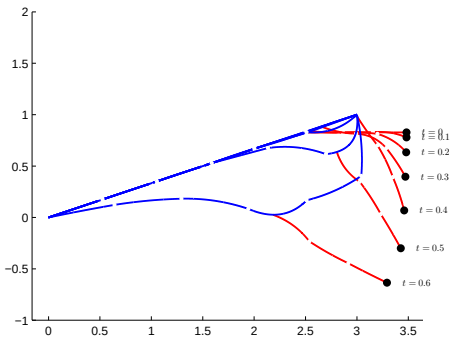

(b) Quadratic

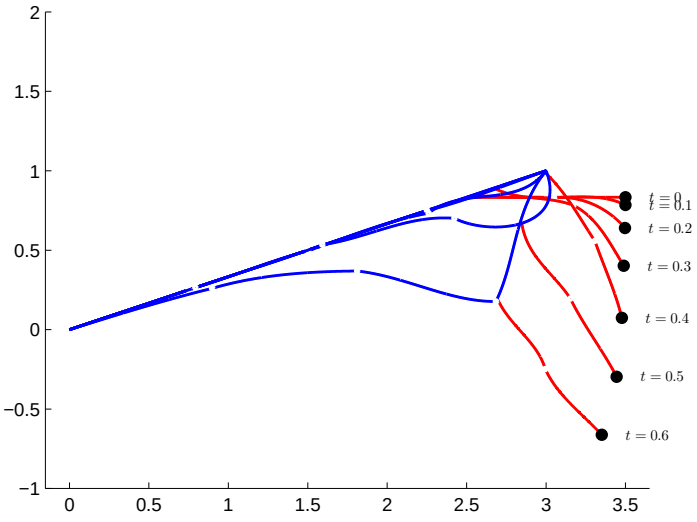

(c) Cubic

Figure 5.18: Planar aerial runway. Comparison of non-smooth contact using Lagrangian interpolation

Chapter 6

Conclusions

6.1 Contribution of the present thesis

The modelling of sliding contact for a geometrically exact planar beam using a *node-to-element* (NE) master-slave approach has been successfully implemented. In addition, we have included B-Splines interpolation with the intention of smoothing the contact slideline and results have shown its advantages compared with standard Lagrangian interpolation. Conserving time integration has been explored as well in the previous context, and the main contribution in the topic has been the energy and momentum conserving scheme, which properties has been auspiciously tested.

In previous work, the same master-slave NE approach has been implemented for the modelling of joints in 3D geometrically exact beams [CJ96, MJ04, MJ06]. Despite that our work has been based on a simpler model, which do not have the complexities of of large 3D rotations, we believe that the achievements of this thesis, mainly the use of B-Splines interpolation, can be extended to the 3D case without posing any further theoretical difficulty.

Although the scope of this work has been to model conservative time integration, in the context of beam sliding contact, we have found that the dynamic response of beams integrated with Newmark method, behaves more stable when B-Splines interpolation is used. The latter can be seen more like a by product rather than a thesis scope.

We may finally summarize the contributions done in the present work:

1. B-Splines interpolation has been tested in a variety of model problems and gave a successfull response mainly in the solution of sliding contact in beams, given the smooth discretization of contact loads at elements transitions they provide. Moreover, the solution in non-linear dynamics under Newmark method have always behaved more stable with B-Splines interpolation compared with standard Lagrangian interpolation (up to order three).

2. In the context of conservative time-integration of beams in sliding con-

tact, using the master-slave method, an algorithm that conserves energy and momentum has been developed and implemented. Their conserving properties have been confirmed in a series of numerical examples.

3. Recalling the definition of the *coupling element* in the NE master-slave incremental approach [MJ06], an extension of this idea that couples more than a master element to the slave node has been developed and implemented. The previous has allowed us to preserve the conserving properties of the incremental master-slave formulation at the elements contact transitions.

6.2 Further work

The energy-momentum conserving algorithm presented for sliding beams does not fulfilled the exact contact constrains. At this expense, it has not been tested how much the relaxed contact kinematics may vary from the exact ones, and if such may present a detrimental effect in the iterative solution of the non-linear equations.

With respect to an algorithm that may be able to exactly conserve the energy, momentum and the contact constrains using the master-slave method for geometrically exact beams, it has not been explored yet. An idea on that direction may well be to leave the interpolation parameter γ (see (4.29)) as an extra variable to the problem, and add consequently the algebraic equation of the slave nodal condition for angular momentum conservation.

Appendix A

Variation of rotations

Let $\mathbf{v}$ a unitary 3D vector that can be expressed as a rotation in an arbitrary Euclidean system of coordinates $\mathbf{e}_{\mathrm{i}}$, such that i.e. $\mathbf{v} = \mathbf{\Lambda}\,\mathbf{e}_1$

Taking a variation of $\mathbf{v}$ [Muñ04] then:

$$\delta\mathbf{v} = \delta\mathbf{\Lambda}\,\mathbf{e}_1 = [\delta\mathbf{\Theta}]_\times\ \mathbf{v}\,, \tag{A.1}$$

where $[(\bullet)]_\times$ denotes the skew-symmetric matrix form of a vector such that $[(\bullet)]_\times\ \mathbf{a} = \bullet \times \mathbf{a}$. It holds therefore that:

$$[\delta\mathbf{\Theta}]_\times = \begin{bmatrix} 0 & -\delta\theta_3 & \delta\theta_2 \\ \delta\theta_3 & 0 & -\delta\theta_1 \\ -\delta\theta_2 & \delta\theta_1 & 0 \end{bmatrix} \tag{A.2}$$

Note (A.1) holds the variation of rotations equation:

$$\boxed{\delta\mathbf{\Lambda} = [\delta\mathbf{\Theta}]_\times\ \mathbf{\Lambda}}, \tag{A.3}$$

and let also remark the following properties:

$$\delta\left(\mathbf{\Lambda}^{\mathrm{T}}\right) = (\delta\mathbf{\Lambda})^{\mathrm{T}} = \mathbf{\Lambda}^{\mathrm{T}}\ [\delta\mathbf{\Theta}]_\times^{\mathrm{T}} = -\mathbf{\Lambda}^{\mathrm{T}}\ [\delta\mathbf{\Theta}]_\times \overbrace{=}^{\text{true in 2D}} -\,[\delta\mathbf{\Theta}]_\times\ \mathbf{\Lambda}^{\mathrm{T}} \tag{A.4}$$

Denote that in the 2D case $\delta\theta_3 = \delta\theta$, with θ the angle defined in Figure 2.1. This means that (A.2) will be simplified as:

$$[\delta\mathbf{\Theta}]_\times^{2D} = \begin{bmatrix} 0 & -\delta\theta & 0 \\ \delta\theta & 0 & 0 \\ 0 & 0 & 0 \end{bmatrix} = \mathbf{J}\,\delta\theta\,. \tag{A.5}$$

Appendix B

Solution of the discretized beam equations

An overview on the Newton-Raphson method

Many numerical techniques has been developed in the context of solution for nonlinear systems, see i.e. [ZT00]. Let formulate the problem as the solution of the discretized beam equations (see Section 2.3)

$$\mathbf{g}_\alpha(\mathbf{u}^\beta_{n+1}) = \mathbf{g}^e_\alpha(\mathbf{u}^\beta_{n+1}) - \mathbf{f}^\alpha_{n+1} = \mathbf{0}\,,\ \alpha,\beta = 1,\ldots,n\,, \tag{B.1}$$

which starts from a nearby nodal solution at

$$\mathbf{u}^\beta_{n+1} = \mathbf{u}^\beta_n\,,\ \mathbf{g}_\alpha(\mathbf{u}^\beta_n) = \mathbf{0}\,,\ \mathbf{f}^\alpha_{n+1} = \mathbf{f}^\alpha_n\,, \tag{B.2}$$

and arises from changes in the nodal forcing function $\mathbf{f}^\alpha_n$ (load steps):

$$\mathbf{f}^\alpha_{n+1} = \mathbf{f}^\alpha_n + \Delta\mathbf{f}^\alpha_n\,. \tag{B.3}$$

So far, the objective will be to determine the change in the set of nodes $\Delta\mathbf{u}^\beta_n$ such that

$$\mathbf{u}^\beta_{n+1} = \mathbf{u}^\beta_n + \Delta\mathbf{u}^\beta_n\,. \tag{B.4}$$

The Newton-Raphson iterative method is the one that will be described here. It is based mainly on the first order approximation of (B.1) (recall that non follower loads are modelled), given by:

$$\mathbf{g}_\alpha(\mathbf{u}^{i+1}_{\beta_{n+1}}) \approx \mathbf{g}_\alpha(\mathbf{u}^i_{\beta_{n+1}}) + \boldsymbol{\Delta}\mathbf{g}^e_\alpha(\mathbf{u}^i_{\beta_{n+1}}) = \mathbf{0}\,. \tag{B.5}$$

The iteration counter i is distinguished from the discrete time parameter n [1] and usually starts by assuming that

$$\mathbf{u}^1_{\beta\,n+1} = \mathbf{u}^\beta_n\,, \tag{B.6}$$

in which $\mathbf{u}^\beta_n$ is a converged nodal solution at a previous load step. Moreover, the jacobian matrix (or stiffness matrix in structural terms) corresponding to a tangent direction is given by:

$$\boldsymbol{\Delta}\mathbf{g}^e_\alpha = \mathbf{K}^{\alpha\beta}_{\mathrm{T}}\,\boldsymbol{\Delta}\mathbf{u}_\beta\,. \tag{B.7}$$

The nodal iterative correction for the method is compute as:

$$\mathbf{u}^{i+1}_{\beta\,n+1} = \mathbf{u}^i_{\beta\,n+1} + \boldsymbol{\Delta}\mathbf{u}^i_{\beta\,n}\,, \tag{B.8}$$

and relies on the solution of the linear system given in (B.5):

$$\mathbf{K}^{\alpha\beta}_{\mathrm{T}}(\mathbf{u}^i_{\beta\,n+1})\,\boldsymbol{\Delta}\mathbf{u}^i_{\beta\,n} = -\mathbf{g}_\alpha(\mathbf{u}^i_{\beta\,n+1})\,. \tag{B.9}$$

Linearization of the beam's variational elastic residual

For the derivation of the tangent stiffness matrix, consider first (B.7) and after refering to (2.19) is obtained:

$$\mathbf{K}^{\alpha\beta}_{\mathrm{T}}\,\boldsymbol{\Delta}\mathbf{u}_\beta = \underbrace{\int_{\mathrm{L}} \mathbf{B}^{\mathrm{T}}_\alpha\,\boldsymbol{\Lambda}\boldsymbol{\Lambda}_0\,\boldsymbol{\Delta}\mathbf{N}\,\mathrm{d}X}_{\mathbf{K}_{\mathrm{M}}} + \underbrace{\int_{\mathrm{L}} \boldsymbol{\Delta}(\mathbf{B}^{\mathrm{T}}_\alpha\,\boldsymbol{\Lambda}\boldsymbol{\Lambda}_0)\,\mathbf{N}\,\mathrm{d}X}_{\mathbf{K}_{\mathrm{G}}} \tag{B.10}$$

Note $\mathbf{K}_{\mathrm{M}}$ results from the linearization of the *spatial* stress-couple resultant $\mathbf{n}$ and is known as the material part of $\mathbf{K}_{\mathrm{T}}$. In addition, $\mathbf{K}_{\mathrm{G}}$ is known as the geometric part of $\mathbf{K}_{\mathrm{T}}$ and arises from the linearization of the strain-displacement matrix. The material tangent stiffness matrix results to be symmetric, it can be derived considering (2.9) and (2.15), and the computation is performed using:

$$\mathbf{K}^{\alpha\beta}_{\mathrm{M}} = \int_{\mathrm{L}} \mathbf{B}^{\mathrm{T}}_\alpha\,\boldsymbol{\Lambda}\boldsymbol{\Lambda}_0\,\mathbf{C}\,(\boldsymbol{\Lambda}\boldsymbol{\Lambda}_0)^{\mathrm{T}}\,\mathbf{B}_\beta\,\mathrm{d}X \tag{B.11}$$

For the geometric tangent stiffness matrix, the derivation is a little more involved and will be described as a special case of the 3D beam theory (see [SVQ86a]).

Let first take a digression to remark that in the 3D case there is a distinction between the *spatial* stress and couple resultant that will be named as $\mathbf{n}_{3\mathrm{D}}$ and $\mathbf{m}_{3\mathrm{D}}$ respectively, together with the position vector $\mathbf{r}_{3\mathrm{D}}$. Each of them will have

[1] Note, from here and through all this work, the difference used in notation between an iterative $\boldsymbol{\Delta}$ or an incremental Δ variation.

three components, and should not be confused with $\mathbf{n}$ and $\mathbf{r}$, defined in (2.5) and (2.2) respectively for the planar case. Following [SVQ86a], the geometric tangent stiffness matrix is given by:

$$\mathbf{K}_{\mathrm{G}}^{\alpha\beta} = \int_{\mathrm{L}} \mathbf{\Phi}_{\alpha}^{\mathrm{T}}\, \mathbf{G}\, \mathbf{\Phi}_{\beta}\, \mathrm{d}X \tag{B.12}$$

where $\mathbf{\Phi}_{\alpha}$ is a discretized differential matrix operator defined as follows:

$$\mathbf{\Phi} = \begin{bmatrix} \mathbf{I}'_{\alpha}\, \mathbb{1} & \mathbf{0} \\ \mathbf{0} & \mathbf{I}'_{\alpha}\, \mathbb{1} \\ \mathbf{0} & \mathbf{I}_{\alpha}\, \mathbb{1} \end{bmatrix} \tag{B.13}$$

and $\mathbf{G}$ is a so-called geometric stiffness matrix, which take for the 3D beam theory the following form:

$$\mathbf{G} = \begin{bmatrix} \mathbf{0} & \mathbf{0} & -\left[\mathbf{n}_{3\mathrm{D}}\right]_{\times} \\ \mathbf{0} & \mathbf{0} & -\left[\mathbf{m}_{3\mathrm{D}}\right]_{\times} \\ \left[\mathbf{n}_{3\mathrm{D}}\right]_{\times} & \mathbf{0} & \left[\mathbf{r}'_{3\mathrm{D}}\right]_{\times}\, \left[\mathbf{n}_{3\mathrm{D}}\right]_{\times} \end{bmatrix} \tag{B.14}$$

Having considered equations (B.12), (B.13) and (B.14) the following '[2,2]' submatrix [2] is derived as the expression for the geometric tangent stiffness matrix of 3D beams:

$$\mathbf{K}_{\mathrm{G}}^{\alpha\beta} = \int_{\mathrm{L}} \begin{bmatrix} \mathbf{0} & -\left[\mathbf{n}_{3\mathrm{D}}\right]_{\times} \mathbf{I}'_{\alpha} \mathbf{I}_{\beta} \\ \left[\mathbf{n}_{3\mathrm{D}}\right]_{\times} \mathbf{I}_{\alpha} \mathbf{I}'_{\beta} & -\left[\mathbf{m}_{3\mathrm{D}}\right]_{\times} \mathbf{I}'_{\alpha} \mathbf{I}_{\beta} + \left[\mathbf{r}'_{3\mathrm{D}}\right]_{\times}\, \left[\mathbf{n}_{3\mathrm{D}}\right]_{\times} \mathbf{I}_{\alpha} \mathbf{I}_{\beta} \end{bmatrix} \mathrm{d}X \tag{B.15}$$

For the planar beam formulation, (B.15) will be reduced to a special case where the following identities are considered (see Appendix A):

$$\left[\mathbf{m}_{3\mathrm{D}}\right]_{\times} = \emptyset\,;\ \left[(\bullet)_{3\mathrm{D}}\right]_{\times} = \mathbf{J}^{\mathrm{T}}\, (\bullet)\,. \tag{B.16}$$

Finally, an expression for the computation of the geometric tangent stiffness matrix of planar beams is given by:

$$\mathbf{K}_{\mathrm{G}}^{\alpha\beta} = \int_{\mathrm{L}} \begin{bmatrix} 0 & 0 & -f_v\, \mathbf{I}'_{\alpha}\, \mathbf{I}_{\beta} \\ 0 & 0 & f_u\, \mathbf{I}'_{\alpha}\, \mathbf{I}_{\beta} \\ -f_v\, \mathbf{I}_{\alpha}\, \mathbf{I}'_{\beta} & f_u\, \mathbf{I}_{\alpha}\, \mathbf{I}'_{\beta} & -\left(f_u\, r'_1 + f_v\, r'_2\right)\, \mathbf{I}_{\alpha}\, \mathbf{I}_{\beta} \end{bmatrix} \mathrm{d}X \tag{B.17}$$

Note that (B.17) is a symmetric matrix. Nevertheless, (B.15) describes generally an unsymmetric matrix. It is demonstrated in [SVQ86a] that the symmetry of $\mathbf{K}_{\mathrm{G}}$ is recovered at a state of equilibrium in the continuum. However, this is not in general valid if a finite element discretization is used [Cri97].

[2] Note this compact notation holds a 6×6 matrix

Linearization of the beam's incremental residuals

We will present here the linearization of the dynamic and elastic nodal residuals developed in Subsection 3.2.2, where non contribution to the tangent stiffness matrix from the external loads are considered. Recall that interpolation of tangent scaled rotations leads to the following formulation:

$$\underline{\mathbf{g}}^{\Delta,\,d}_{\alpha\,n+\frac{1}{2}} = \mathbf{M}_{\alpha\beta}\,\ddot{\mathbf{u}}^{\beta}_{n+\frac{1}{2}}\,, \tag{B.18a}$$

$$\underline{\mathbf{g}}^{\Delta,\,e}_{\alpha\,n+\frac{1}{2}} = \int_{\mathrm{L}} \begin{bmatrix} \mathbf{I}'_{\alpha}\,\tilde{\mathbf{\Lambda}}_{n+\frac{1}{2}}\,\tilde{\mathbf{\Lambda}}_{0} & 0 \\ -\mathbf{I}_{\alpha}\,\left[\tilde{\mathbf{r}}'_{n+\frac{1}{2}}\right]^{\mathrm{T}}_{\times}\,\tilde{\mathbf{\Lambda}}_{n+\frac{1}{2}}\,\tilde{\mathbf{\Lambda}}_{0} & \mathbf{I}'_{\alpha}\,\mathrm{s}(\underline{\omega}) \end{bmatrix} \mathbf{N}_{n+\frac{1}{2}}\,\mathrm{d}X\,, \tag{B.18b}$$

where $\mathrm{s}(\underline{\omega})$ is the function such that $\boldsymbol{\Delta}\theta = \mathrm{s}(\underline{\omega})\boldsymbol{\Delta}\underline{\omega}$ and the linearization has to be performed consequently with respect to $\boldsymbol{\Delta}\underline{\mathbf{u}} = \mathbf{I}_{\beta}\,\boldsymbol{\Delta}\underline{\mathbf{u}}_{\beta}$.

Dynamic nodal residual

Let us first note the equivalence $\underline{\mathbf{g}}^{\Delta,\,d}_{\alpha\,n+\frac{1}{2}} = \mathbf{g}^{\Delta,\,d}_{\alpha\,n+\frac{1}{2}}$, from equations (3.22) and (B.18a). This equality results from the time stepping condition stated in (3.34), which simply allow us to derive from (3.22) that

$$\boldsymbol{\Delta}\mathbf{u}_{\alpha}\cdot\mathbf{g}^{\Delta,\,d}_{\alpha\,n+\frac{1}{2}} = \boldsymbol{\Delta}\underline{\mathbf{u}}_{\alpha}\cdot\underbrace{\mathbf{g}^{\Delta,\,d}_{\alpha\,n+\frac{1}{2}}}_{\underline{\mathbf{g}}^{\Delta,\,d}_{\alpha\,n+\frac{1}{2}}}\,. \tag{B.19}$$

Despite the equivalence in equation (B.19), let us remark that from the implementational point of view it is different to compute $\ddot{\mathbf{u}}^{\beta}_{n+\frac{1}{2}}$ if *unscaled* or *scaled* incremental rotations are interpolated.

Regarding the linearization of (B.18a), we will use from (3.34) that

$$\boldsymbol{\Delta}\ddot{\mathbf{u}}^{\beta}_{n+\frac{1}{2}} = \frac{\boldsymbol{\Delta}\dot{\underline{\mathbf{u}}}^{\beta}_{n+1}}{\Delta t} = \frac{2}{\Delta t^{2}}\,\boldsymbol{\Delta}\underline{\mathbf{u}}_{\beta}\,, \tag{B.20}$$

which can be used directly in (B.18a) to derive

$$\boldsymbol{\Delta}\underline{\mathbf{g}}^{\Delta,\,d}_{\alpha\,n+\frac{1}{2}} = \frac{2}{\Delta t^{2}}\,\mathbf{M}_{\alpha\beta}\,\boldsymbol{\Delta}\,\underline{\mathbf{u}}_{\beta}\,. \tag{B.21}$$

Similarly, it is possible to verify that

$$\boldsymbol{\Delta}\mathbf{g}^{\Delta,\,d}_{\alpha\,n+\frac{1}{2}} = \frac{2}{\Delta t^{2}}\,\mathbf{M}_{\alpha\beta}\,\boldsymbol{\Delta}\,\mathbf{u}_{\beta}\,. \tag{B.22}$$

Elastic nodal residual

For the linearization of the present residual, we will first aim to writte the relation between *independent* and *interpolated* variables from B.18b:

$$\begin{Bmatrix} \boldsymbol{\Delta}\tilde{\mathbf{u}}^{'} \\ \boldsymbol{\Delta}\theta^{'} \\ \boldsymbol{\Delta}\theta \end{Bmatrix} = \begin{Bmatrix} \boldsymbol{\Delta}\tilde{\mathbf{u}}^{'} \\ \mathrm{s}^{'}(\underline{\omega})\,\boldsymbol{\Delta}\underline{\omega} + \mathrm{s}(\underline{\omega})\,\boldsymbol{\Delta}\underline{\omega}^{'} \\ \mathrm{s}(\underline{\omega})\,\boldsymbol{\Delta}\underline{\omega} \end{Bmatrix} = \mathbf{B}_{\beta}^{\Delta}\,\boldsymbol{\Delta}\underline{\mathbf{u}}_{\beta}\,, \tag{B.23}$$

with matrix $\mathbf{B}_{\beta}^{\Delta}$ defined like:

$$\mathbf{B}_{\beta}^{\Delta} = \begin{bmatrix} \mathbf{I}_{\beta}^{'}\,\tilde{\mathbb{1}} & 0 \\ \mathbf{0} & \mathbf{I}_{\beta}\,\mathrm{s}^{'}(\underline{\omega}) + \mathbf{I}_{\beta}^{'}\,\mathrm{s}(\underline{\omega}) \\ \mathbf{0} & \mathbf{I}_{\beta}\,\mathrm{s}(\underline{\omega}) \end{bmatrix}. \tag{B.24}$$

In order to obtain the linearization of the second term in the integral from (B.18b), we first aim to write $\boldsymbol{\Delta\Gamma}_{n+1}$ as a function of the increments described in (B.23):

$$\begin{aligned} \boldsymbol{\Delta\Gamma}_{n+1} &= \begin{Bmatrix} \boldsymbol{\Delta}\left(\tilde{\boldsymbol{\Lambda}}_{n+1}\,\tilde{\boldsymbol{\Lambda}}_{0}\right)^{\mathrm{T}}\,\tilde{\mathbf{r}}_{n+1}^{'} + \left(\tilde{\boldsymbol{\Lambda}}_{n+1}\,\tilde{\boldsymbol{\Lambda}}_{0}\right)^{\mathrm{T}}\,\boldsymbol{\Delta}\tilde{\mathbf{r}}^{'} \\ \boldsymbol{\Delta}\theta^{'} \end{Bmatrix} \\ &= \begin{Bmatrix} \left(\tilde{\boldsymbol{\Lambda}}_{n+1}\,\tilde{\boldsymbol{\Lambda}}_{0}\right)^{\mathrm{T}}\left(-\left[\tilde{\mathbf{r}}_{n+1}^{'}\right]_{\times}\boldsymbol{\Delta}\theta + \boldsymbol{\Delta}\tilde{\mathbf{r}}^{'}\right) \\ \boldsymbol{\Delta}\theta^{'} \end{Bmatrix} \\ &= \left(\tilde{\boldsymbol{\Lambda}}_{n+1}\,\tilde{\boldsymbol{\Lambda}}_{0}\right)^{\mathrm{T}} \underbrace{\begin{bmatrix} \tilde{\mathbb{1}} & 0 & -\left[\tilde{\mathbf{r}}_{n+1}^{'}\right]_{\times} \\ \mathbf{0} & 1 & 0 \end{bmatrix}}_{\mathbb{1}_{\tilde{\mathbf{r}}}} \begin{Bmatrix} \boldsymbol{\Delta}\tilde{\mathbf{u}}^{'} \\ \boldsymbol{\Delta}\theta^{'} \\ \boldsymbol{\Delta}\theta \end{Bmatrix} = \left(\tilde{\boldsymbol{\Lambda}}_{n+1}\,\tilde{\boldsymbol{\Lambda}}_{0}\right)^{\mathrm{T}}\mathbb{1}_{\tilde{\mathbf{r}}} \begin{Bmatrix} \boldsymbol{\Delta}\tilde{\mathbf{u}}^{'} \\ \boldsymbol{\Delta}\theta^{'} \\ \boldsymbol{\Delta}\theta \end{Bmatrix}. \end{aligned} \tag{B.25}$$

An expression for $\boldsymbol{\Delta}\mathbf{N}_{n+\frac{1}{2}}$ can be directly derived using (B.25) and (B.23) as follows:

$$\boldsymbol{\Delta}\mathbf{N}_{n+\frac{1}{2}} = \frac{1}{2}\,\boldsymbol{\Delta}\mathbf{N}_{n+1} = \frac{1}{2}\,\mathbf{C}_{\mathbf{e}}\,\boldsymbol{\Delta\Gamma}_{n+1} = \frac{1}{2}\,\mathbf{C}_{\mathbf{e}}\left(\tilde{\boldsymbol{\Lambda}}_{n+1}\,\tilde{\boldsymbol{\Lambda}}_{0}\right)^{\mathrm{T}}\mathbb{1}_{\tilde{\mathbf{r}}}\,\mathbf{B}_{\beta}^{\Delta}\,\boldsymbol{\Delta}\underline{\mathbf{u}}_{\beta}\,. \tag{B.26}$$

In addition, we will account on the following equations to derive the linearization of the first term in (B.18b):

$$\boldsymbol{\Delta\Lambda}_{n+\frac{1}{2}} = \frac{1}{2}\,\mathrm{s}(\underline{\omega})\,\tilde{\mathbf{J}}\,\tilde{\boldsymbol{\Lambda}}_{n+1}\,\boldsymbol{\Delta}\underline{\omega}\,, \tag{B.27}$$

$$\boldsymbol{\Delta}\mathrm{s}(\underline{\omega}) = -\frac{1}{2}\,\mathrm{s}^{2}(\underline{\omega})\,\underline{\omega}\,\boldsymbol{\Delta}\underline{\omega}\,. \tag{B.28}$$

Resorting finally to

$$\boldsymbol{\Delta}\underline{\mathbf{g}}^{\Delta,\,e}_{\alpha\;n+\frac{1}{2}} = \mathbf{K}^{\Delta,\,e}_{\alpha\beta}\,\boldsymbol{\Delta}\underline{\mathbf{u}}_{\beta}\,, \tag{B.29}$$

the unsymmetric stiffness matrix $\mathbf{K}^{\Delta,\,e}_{\alpha\beta}$ results:

$$\mathbf{K}^{\Delta,\,e}_{\alpha\beta} = \frac{1}{2}\int_{\mathrm{L}}\begin{bmatrix} \mathbf{I}'_{\alpha}\tilde{\boldsymbol{\Lambda}}_{n+\frac{1}{2}}\tilde{\boldsymbol{\Lambda}}_{0} & 0 \\ -\mathbf{I}_{\alpha}\left[\tilde{\mathbf{r}}'_{n+\frac{1}{2}}\right]^{\mathrm{T}}_{\times}\tilde{\boldsymbol{\Lambda}}_{n+\frac{1}{2}}\tilde{\boldsymbol{\Lambda}}_{0} & \mathbf{I}'_{\alpha}\mathrm{s}(\underline{\omega}) \end{bmatrix}\mathbf{C}_{\mathbf{e}}\left(\tilde{\boldsymbol{\Lambda}}_{n+1}\tilde{\boldsymbol{\Lambda}}_{0}\right)^{\mathrm{T}}\mathbb{1}_{\tilde{\mathbf{r}}}\,\mathbf{B}^{\Delta}_{\beta}\,\mathrm{d}X + \tag{B.30}$$

$$+\frac{1}{2}\int_{\mathrm{L}}\begin{bmatrix} \mathbf{0} & \mathbf{I}'_{\alpha}\mathbf{I}_{\beta}\left[\tilde{\boldsymbol{\Lambda}}_{n+1}\tilde{\boldsymbol{\Lambda}}_{0}\tilde{\boldsymbol{\Delta}\mathbf{N}}_{n+\frac{1}{2}}\right]_{\times}\mathrm{s}(\underline{\omega}) \\ \mathbf{I}_{\alpha}\mathbf{I}'_{\beta}\left[\tilde{\boldsymbol{\Lambda}}_{n+\frac{1}{2}}\tilde{\boldsymbol{\Lambda}}_{0}\tilde{\boldsymbol{\Delta}\mathbf{N}}_{n+\frac{1}{2}}\right]^{\mathrm{T}}_{\times} & -\mathbf{I}_{\alpha}\mathbf{I}_{\beta}\left[\tilde{\mathbf{r}}'_{n+\frac{1}{2}}\right]^{\mathrm{T}}_{\times}\left[\tilde{\boldsymbol{\Lambda}}_{n+1}\tilde{\boldsymbol{\Lambda}}_{0}\tilde{\boldsymbol{\Delta}\mathbf{N}}_{n+\frac{1}{2}}\right]_{\times} - \mathbf{I}'_{\alpha}\mathbf{I}_{\beta}\mathrm{s}^{2}(\underline{\omega})\underline{\omega}\mathrm{M}_{n+\frac{1}{2}} \end{bmatrix}\mathrm{d}X\,.$$

Appendix C

Linearization of master-slave residuals

Variational formulation

The linearization of the extended residual $\mathbf{g}^A_{Rm} = \mathbf{N}_\delta^{\mathrm{T}}\,\mathbf{g}^A$ will be split in two terms:

$$\boldsymbol{\Delta}(\mathbf{N}_\delta^{\mathrm{T}}\,\mathbf{g}^A) = \mathbf{N}_\delta^{\mathrm{T}}\,\boldsymbol{\Delta}\mathbf{g}^A + (\boldsymbol{\Delta}\mathbf{N}_\delta^{\mathrm{T}})\,\mathbf{g}^A \tag{C.1}$$

where we will consider $\mathbf{N}_\delta$, together with $\mathbf{R}_{\delta\,B}$ and $\mathbf{L}_{\delta\,B}$ defined in (4.23), which stands for the released planar sliding joint rotation.

The first term in (C.1) can be expressed using the Jacobian matrix of the single element A, $\mathbf{K}_A$, such that:

$$\boldsymbol{\Delta}\mathbf{g}^A = \mathbf{K}_A\,\boldsymbol{\Delta}\mathbf{u}^A = \mathbf{K}_A\,\mathbf{N}_\delta\,\boldsymbol{\Delta}\mathbf{u}^A_{Rm} \tag{C.2}$$

where equation (4.23) has been used to relate the vector of iterative changes of released and master variables. We therefore have, remarking again for a released planar joint rotation, that the first term in (C.1) yields

$$\mathbf{N}_\delta^{\mathrm{T}}\,\boldsymbol{\Delta}\,\mathbf{g}^A = \mathbf{N}_\delta^T\,\mathbf{K}_A\,\boldsymbol{\Delta}\mathbf{u}^A = \mathbf{N}_\delta^T\,\mathbf{K}_A\,\mathbf{N}_\delta\,\boldsymbol{\Delta}\mathbf{u}^A_{Rm}\,. \tag{C.3}$$

The second term on (C.1) is a bit more involved, and using first (4.23) for the definition of $\mathbf{N}_\delta$, the development of the product $(\boldsymbol{\Delta}\mathbf{N}_\delta^{\mathrm{T}})\,\mathbf{g}^A$ results:

$$(\boldsymbol{\Delta}\mathbf{N}_\delta^{\mathrm{T}})\,\mathbf{g}^A = \left\{\begin{array}{c} \mathbf{E}_1 \otimes \boldsymbol{\Delta}\tilde{\mathbf{r}}'_B\,\mathbf{g}^f_{n_A} \\ \mathbf{0}_{3\times(n_A+1)} \\ \boldsymbol{\Delta}(\mathbf{I}^B_1)\,\mathbf{g}^f_{n_A} \\ \vdots \\ \boldsymbol{\Delta}(\mathbf{I}^B_{n_B})\,\mathbf{g}^f_{n_A} \end{array}\right\}. \tag{C.4}$$

Deriving from (C.4) the following term

$$\boldsymbol{\Delta}\tilde{\mathbf{r}}_B^{'} = \boldsymbol{\Delta}(\mathbf{I}_\alpha^{'B}\,\tilde{\mathbf{r}}_\alpha) = \mathbf{I}_\alpha^{'B}\,\boldsymbol{\Delta}\tilde{\mathbf{r}}_\alpha + \mathbf{I}_\alpha^{''B}\,\tilde{\mathbf{r}}_\alpha\,\boldsymbol{\Delta}X = \mathbf{I}_\alpha^{'B}\,\boldsymbol{\Delta}\tilde{\mathbf{r}}_\alpha + \tilde{\mathbf{r}}_B^{''} \otimes \mathbf{E}_1\,\boldsymbol{\Delta}\tilde{\mathbf{r}}_R\,,$$

the computation of $(\boldsymbol{\Delta}\mathbf{N}_\delta^{\mathrm{T}})\,\mathbf{g}^A$ turns into (4.26), where the following definitions have been implicitly made:

$$\begin{aligned}
\mathbf{K}_{RR} &= \begin{bmatrix} \left(\tilde{\mathbf{r}}_B^{''} \cdot \mathbf{g}_{n_A}^f\right) \mathbf{E}_1 \otimes \mathbf{E}_1 & 0 \\ \mathbf{0} & 0 \end{bmatrix} \\
\mathbf{K}_{Rm} &= \begin{bmatrix} \mathbf{E}_1 \otimes \mathbf{g}_{n_A}^f & 0 \\ \mathbf{0} & 0 \end{bmatrix} \begin{bmatrix} \mathbf{I}_1^{'B}\,\tilde{\mathbb{1}} & \dots & \mathbf{I}_{n_B}^{'B}\,\tilde{\mathbb{1}} \end{bmatrix} \\
\mathbf{K}_{mR} &= \mathbf{K}_{Rm}^{\mathrm{T}}
\end{aligned} \tag{C.5}$$

Appendix D

Demonstration of conserving properties

Tangent scaled rotations - Conservation of momenta

Recall the nodal residuals given by interpolation of tangent scaled incremental rotations conform the following non-linear system of equations:

$$\underline{\mathbf{g}}^{\Delta}_{\alpha\,n+\frac{1}{2}} = \underline{\mathbf{g}}^{\Delta,\,d}_{\alpha\,n+\frac{1}{2}} + \underline{\mathbf{g}}^{\Delta,\,e}_{\alpha\,n+\frac{1}{2}} - \mathbf{f}_{\alpha} = \mathbf{0}\,;\; \alpha = 1, \ldots, n\;. \tag{D.1}$$

The dynamic, elastic and external force vectors were developed in the Subsection 3.2.2 and may be written respectively as

$$\underline{\mathbf{g}}^{\Delta,\,d}_{\alpha\,n+\frac{1}{2}} = \frac{1}{\Delta t}\int_{\mathrm{L}} \mathbf{I}_{\alpha}\,\Delta\mathbf{l}\,\mathrm{d}X\,, \tag{D.2a}$$

$$\underline{\mathbf{g}}^{\Delta,\,e}_{\alpha\,n+\frac{1}{2}} = \int_{\mathrm{L}} \begin{bmatrix} \mathbf{I}'_{\alpha}\,\tilde{\mathbb{1}} & 0 \\ -\mathbf{I}_{\alpha}\left[\tilde{\mathbf{r}}'_{n+\frac{1}{2}}\right]^{\mathrm{T}}_{\times} & \mathbf{I}'_{\alpha} \end{bmatrix} \begin{Bmatrix} \tilde{\mathbf{\Lambda}}_{n+\frac{1}{2}}\,\tilde{\mathbf{\Lambda}}_{0}\,\tilde{\mathbf{N}}_{n+\frac{1}{2}} \\ \mathrm{s}(\underline{\omega})\,\mathrm{M}_{n+\frac{1}{2}} \end{Bmatrix} \mathrm{d}X\,, \tag{D.2b}$$

$$\mathbf{f}_{\alpha} = \int_{\mathrm{L}} \begin{Bmatrix} \mathbf{I}_{\alpha}\left(\mathrm{A}_{\rho}\,\mathbf{b} + \bar{\mathbf{T}}\right) \\ 0 \end{Bmatrix} \mathrm{d}X\,, \tag{D.2c}$$

where the definition of the vector of *local specific momenta* $\mathbf{l}$ has been used in (D.2a) for a demonstration purpose:

$$\mathbf{l} = \begin{Bmatrix} \mathbf{l}_f \\ \mathrm{l}_m \end{Bmatrix} \equiv \begin{Bmatrix} \mathrm{A}_{\rho}\,\dot{\tilde{\mathbf{u}}} \\ \mathrm{I}_{\rho}\,\dot{\theta} \end{Bmatrix}\,. \tag{D.3}$$

Equation (D.2a) can be derived from the increment of kinetic energy - see (3.22) -, using the time stepping condition (3.34) and replacing with (D.3) as follows:

$$\Delta T = \int_{\mathrm{L}} \left(\mathrm{A}_\rho \, \dot{\tilde{\mathbf{u}}}_{n+\frac{1}{2}} \cdot \Delta\dot{\tilde{\mathbf{u}}} + \mathrm{I}_\rho \, \dot{\theta}_{n+\frac{1}{2}} \, \Delta\dot{\theta} \right) \mathrm{d}X = \frac{1}{\Delta t} \int_{\mathrm{L}} \left(\Delta\tilde{\mathbf{u}} \cdot \mathrm{A}_\rho \, \Delta\dot{\tilde{\mathbf{u}}} + \underline{\omega} \, \mathrm{I}_\rho \, \Delta\dot{\theta} \right) \mathrm{d}X$$
$$= \frac{1}{\Delta t} \int_{\mathrm{L}} \Delta\underline{\mathbf{u}} \cdot \Delta\mathbf{l} \, \mathrm{d}X \, . \tag{D.4}$$

Replacing the expressions (D.2a), (D.2b) and (D.2c) in equation (D.1), we obtain

$$\underline{\mathbf{g}}^{\Delta}_{\alpha_{n+\frac{1}{2}}} = \begin{Bmatrix} \underline{\mathbf{g}}^{\Delta,\, f}_{\alpha_{n+\frac{1}{2}}} \\ \underline{g}^{\Delta,\, m}_{\alpha_{n+\frac{1}{2}}} \end{Bmatrix} = \mathbf{0} \tag{D.5}$$
$$= \int_{\mathrm{L}} \begin{Bmatrix} \mathbf{I}_\alpha \, \dfrac{\mathrm{A}_\rho}{\Delta t} \, \Delta\dot{\tilde{\mathbf{u}}} + \mathbf{I}'_\alpha \, \tilde{\mathbf{\Lambda}}_{n+\frac{1}{2}} \, \tilde{\mathbf{\Lambda}}_0 \, \tilde{\mathbf{N}}_{n+\frac{1}{2}} - \mathbf{I}_\alpha \left(\mathrm{A}_\rho \, \mathbf{b} + \bar{\mathbf{T}} \right) \\ \mathbf{I}_\alpha \, \dfrac{\mathrm{I}_\rho}{\Delta t} \, \Delta\dot{\theta} - \mathbf{I}_\alpha \left[\tilde{\mathbf{r}}'_{n+\frac{1}{2}} \right]_\times \cdot \tilde{\mathbf{\Lambda}}_{n+\frac{1}{2}} \, \tilde{\mathbf{\Lambda}}_0 \, \tilde{\mathbf{N}}_{n+\frac{1}{2}} + \mathbf{I}'_\alpha \, \mathrm{s}(\underline{\omega}) \, \mathrm{M}_{n+\frac{1}{2}} \end{Bmatrix} \mathrm{d}X \, ,$$

where we can use the shape functions completeness conditions - see (2.14) - to sum the contribution of (D.5) over the n nodes and derive that

$$\frac{1}{\Delta t} \int_{\mathrm{L}} \begin{Bmatrix} \Delta\mathbf{l}_f \\ \Delta\mathrm{l}_m \end{Bmatrix} \mathrm{d}X = \int_{\mathrm{L}} \begin{Bmatrix} \mathrm{A}_\rho \, \mathbf{b} + \bar{\mathbf{T}} \\ \left[\tilde{\mathbf{r}}'_{n+\frac{1}{2}} \right]_\times \cdot \tilde{\mathbf{\Lambda}}_{n+\frac{1}{2}} \, \tilde{\mathbf{\Lambda}}_0 \, \tilde{\mathbf{N}}_{n+\frac{1}{2}} \end{Bmatrix} \mathrm{d}X \, . \tag{D.6}$$

On the other hand, the increment of momenta over a time step reads

$$\Delta\mathbf{\Xi} = \int_{\mathrm{L}} \begin{Bmatrix} \Delta\mathbf{l}_f \\ \Delta\mathrm{l}_m + \mathrm{A}_\rho \, \Delta \left(\tilde{\mathbf{r}} \times \dot{\tilde{\mathbf{u}}} \right) \end{Bmatrix} \mathrm{d}X$$
$$= \int_{\mathrm{L}} \begin{Bmatrix} \Delta\mathbf{l}_f \\ \Delta\mathrm{l}_m + \mathrm{A}_\rho \left(\left[\tilde{\mathbf{r}}_{n+\frac{1}{2}} \right]_\times \cdot \Delta\dot{\tilde{\mathbf{u}}} + [\Delta\tilde{\mathbf{u}}]_\times \cdot \dot{\tilde{\mathbf{u}}}_{n+\frac{1}{2}} \right) \end{Bmatrix} \mathrm{d}X \, . \tag{D.7}$$

It is first observed from (D.6) that if non external loads occur, the linear momentum is conserved: $\Delta\mathbf{\Xi}_f = \mathbf{0}$. Regarding the increment of angular momemtum $\Delta\Xi_m$, we observe that recalling the mid-point rule in (3.34), the last term of (D.7) vanishes due to the collinearity between $\Delta\tilde{\mathbf{u}}$ and $\dot{\tilde{\mathbf{u}}}_{n+\frac{1}{2}}$. We finally rewritte the increment of Ξ_m using the rotational equilibrium from (D.6):

$$\Delta\Xi_m = \int_{\mathrm{L}} \left(\Delta t \left[\tilde{\mathbf{r}}'_{n+\frac{1}{2}} \right]_\times \cdot \tilde{\mathbf{\Lambda}}_{n+\frac{1}{2}} \, \tilde{\mathbf{\Lambda}}_0 \, \tilde{\mathbf{N}}_{n+\frac{1}{2}} + \mathrm{A}_\rho \left[\tilde{\mathbf{r}}_{n+\frac{1}{2}} \right]_\times \cdot \Delta\dot{\tilde{\mathbf{u}}} \right) \mathrm{d}X \, . \tag{D.8}$$

By inserting into the previous the dot product: $\Delta t \left[\tilde{\mathbf{r}}^{\alpha}_{n+\frac{1}{2}} \right]_\times \cdot \underline{\mathbf{g}}^{\Delta,\, f}_{\alpha_{n+\frac{1}{2}}}$ from equation (D.5), it follows that

$$\Delta\Xi_m = \Delta t \int_{\mathrm{L}} \left[\tilde{\mathbf{r}}_{n+\frac{1}{2}}\right]_{\times} \cdot \left(\mathrm{A}_\rho\, \mathbf{b} + \bar{\mathbf{T}}\right) \mathrm{d}X\,, \tag{D.9}$$

which clearly vanishes if non external forces exist.

Increment of angular momentum for *unscaled* rotations

We will use similar arguments to the ones exposed in the previous Section, to show that even in absence of external loads the interpolation of *unscaled* incremental rotations ω will lead to a non-angular conserving algorithm. In the present case, the nodal residuals conform the following set of non-linear equations:

$$\mathbf{g}^{\Delta}_{\alpha\,n+\frac{1}{2}} = \mathbf{g}^{\Delta,\,d}_{\alpha\,n+\frac{1}{2}} + \mathbf{g}^{\Delta,\,e}_{\alpha\,n+\frac{1}{2}} - \mathbf{f}_\alpha = \mathbf{0}\,;\; \alpha = 1, \ldots, n\;, \tag{D.10}$$

together with the following expressions (see Subsection 3.2.2):

$$\mathbf{g}^{\Delta,\,d}_{\alpha\,n+\frac{1}{2}} = \frac{1}{\Delta t} \int_{\mathrm{L}} \mathbf{I}_\alpha\, \Delta\mathbf{l}\, \mathrm{d}X\,, \tag{D.11a}$$

$$\mathbf{g}^{\Delta,\,e}_{\alpha\,n+\frac{1}{2}} = \int_{\mathrm{L}} \begin{bmatrix} \mathbf{I}'_\alpha\, \tilde{\mathbb{1}} & 0 \\ -\mathbf{I}_\alpha\, \frac{\tan(\omega/2)}{\omega/2} \left[\tilde{\mathbf{r}}'_{n+\frac{1}{2}}\right]^{\mathrm{T}}_{\times} & \mathbf{I}'_\alpha \end{bmatrix} \begin{Bmatrix} \tilde{\mathbf{\Lambda}}_{n+\frac{1}{2}}\, \tilde{\mathbf{\Lambda}}_0\, \tilde{\mathbf{N}}_{n+\frac{1}{2}} \\ \mathrm{M}_{n+\frac{1}{2}} \end{Bmatrix} \mathrm{d}X\,, \tag{D.11b}$$

$$\mathbf{f}_\alpha = \int_{\mathrm{L}} \begin{Bmatrix} \mathbf{I}_\alpha \left(\mathrm{A}_\rho\, \mathbf{b} + \bar{\mathbf{T}}\right) \\ 0 \end{Bmatrix} \mathrm{d}X\,. \tag{D.11c}$$

The n nodal equilibrium equations yield

$$\mathbf{g}^{\Delta}_{\alpha\,n+\frac{1}{2}} = \begin{Bmatrix} \mathbf{g}^{\Delta,\,f}_{\alpha\,n+\frac{1}{2}} \\ g^{\Delta,\,m}_{\alpha\,n+\frac{1}{2}} \end{Bmatrix} = \mathbf{0} \tag{D.12}$$

$$= \int_{\mathrm{L}} \begin{Bmatrix} \mathbf{I}_\alpha\, \frac{\mathrm{A}_\rho}{\Delta t}\, \Delta\dot{\tilde{\mathbf{u}}} + \mathbf{I}'_\alpha\, \tilde{\mathbf{\Lambda}}_{n+\frac{1}{2}}\, \tilde{\mathbf{\Lambda}}_0\, \tilde{\mathbf{N}}_{n+\frac{1}{2}} - \mathbf{I}_\alpha \left(\mathrm{A}_\rho\, \mathbf{b} + \bar{\mathbf{T}}\right) \\ \mathbf{I}_\alpha\, \frac{\mathrm{I}_\rho}{\Delta t}\, \Delta\dot{\theta} - \mathbf{I}_\alpha\, \frac{\tan(\omega/2)}{\omega/2} \left[\tilde{\mathbf{r}}'_{n+\frac{1}{2}}\right]_{\times} \cdot \tilde{\mathbf{\Lambda}}_{n+\frac{1}{2}}\, \tilde{\mathbf{\Lambda}}_0\, \tilde{\mathbf{N}}_{n+\frac{1}{2}} + \mathbf{I}'_\alpha\, \mathrm{M}_{n+\frac{1}{2}} \end{Bmatrix} \mathrm{d}X\,,$$

and again applying the shape functions completeness properties for the sum of (D.12) over all the nodes gives rise to

$$\frac{1}{\Delta t} \int_{\mathrm{L}} \begin{Bmatrix} \Delta\mathbf{l}_f \\ \Delta\mathrm{l}_m \end{Bmatrix} \mathrm{d}X = \int_{\mathrm{L}} \begin{Bmatrix} \mathrm{A}_\rho\, \mathbf{b} + \bar{\mathbf{T}} \\ \frac{\tan(\omega/2)}{\omega/2} \left[\tilde{\mathbf{r}}'_{n+\frac{1}{2}}\right]_{\times} \cdot \tilde{\mathbf{\Lambda}}_{n+\frac{1}{2}}\, \tilde{\mathbf{\Lambda}}_0\, \tilde{\mathbf{N}}_{n+\frac{1}{2}} \end{Bmatrix} \mathrm{d}X\,. \tag{D.13}$$

Since there are non changes in the time integration rule for the translations - compare (3.15) and (3.34) -, we will write the same increment of momenta over a time step from (D.7) using the collinearity condition between $\Delta\tilde{\mathbf{u}}$ and $\dot{\tilde{\mathbf{u}}}_{n+\frac{1}{2}}$:

$$\Delta\boldsymbol{\Xi} = \int_{\mathrm{L}} \begin{Bmatrix} \Delta\mathbf{l}_f \\ \Delta\mathrm{l}_m + \mathrm{A}_\rho \left[\tilde{\mathbf{r}}_{n+\frac{1}{2}}\right]_\times \cdot \Delta\dot{\tilde{\mathbf{u}}} \end{Bmatrix} \mathrm{d}X \,. \tag{D.14}$$

The first equations in (D.14) and (D.13) lead to conservation of linear momentum if non external forces occur. On the other hand, by recalling the rotational part of (D.13), we can express the increment of Ξ_m as

$$\Delta\Xi_m = \left[\tilde{\mathbf{r}}^{\alpha}_{n+\frac{1}{2}}\right]_\times \cdot \int_{\mathrm{L}} \mathrm{A}_\rho \mathbf{I}_\alpha \Delta\dot{\tilde{\mathbf{u}}}\, \mathrm{d}X + \int_{\mathrm{L}} \Delta t \frac{\tan(\omega/2)}{\omega/2} \left[\tilde{\mathbf{r}}'_{n+\frac{1}{2}}\right]_\times \cdot \tilde{\boldsymbol{\Lambda}}_{n+\frac{1}{2}} \tilde{\boldsymbol{\Lambda}}_0 \tilde{\mathbf{N}}_{n+\frac{1}{2}}\, \mathrm{d}X \,. \tag{D.15}$$

From the nodal equilibrium equations in (D.12) it follows that $\mathrm{A}_\rho \mathbf{I}_\alpha \Delta\dot{\tilde{\mathbf{u}}}$ can be replaced in (D.15) using $\Delta t \left(\mathbf{I}_\alpha \left(\mathrm{A}_\rho \mathbf{b} + \bar{\mathbf{T}}\right) - \mathbf{I}'_\alpha \tilde{\boldsymbol{\Lambda}}_{n+\frac{1}{2}} \tilde{\boldsymbol{\Lambda}}_0 \tilde{\mathbf{N}}_{n+\frac{1}{2}}\right)$ instead, and by considering a system with non external loads we arrive to the following result:

$$\Delta\Xi_m = \Delta t \int_{\mathrm{L}} \left(\frac{\tan(\omega/2)}{\omega/2} - 1\right) \left[\tilde{\mathbf{r}}'_{n+\frac{1}{2}}\right]_\times \cdot \tilde{\boldsymbol{\Lambda}}_{n+\frac{1}{2}}\, \tilde{\boldsymbol{\Lambda}}_0\, \tilde{\mathbf{N}}_{n+\frac{1}{2}}\, \mathrm{d}X \,. \tag{D.16}$$

Bibliography

[AP98] F. Armero and E. Petőcz. Formulation and analysis of conserving algorithms for frictionless dynamic contact/impact problems. *Comput. Methods Appl. Mech. Engng*, 158:269–300, 1998.

[AR01] F. Armero and I. Romero. On the formulation of high-frequency dissipative time-stepping algorithms for nonlinear dynamics. Part I: Low order methods for two model problems and nonlinear elastodynamics. *Comput. Methods Appl. Mech. Engng*, 190:2603–2649, 2001.

[Bau00] O.A. Bauchau. On the modeling of prismatic joints in flexible multybody systems. *Comput. Methods Appl. Mech. Engng*, 181:87–105, 2000.

[BB99] O.A. Bauchau and C.L. Bottasso. On the Design of Energy Preserving and Decaying Schemes for Flexible, Nonlinear Multi-Body Systems. *Comput. Methods Appl. Mech. Engng*, 169:61–79, 1999.

[BB01] O.A. Bauchau and C.L. Bottasso. Contact Conditions for Cylindrical, Prismatic, and Screw Joints in Flexible Multibody Systems. *Multibody System Dyn.*, 5:251–278, 2001.

[CJ96] M.A. Crisfield and G. Jelenić. Non-linear masterslave relationships for joints in 3D beams with large rotations. *Comput. Methods Appl. Mech. Engng*, 135:211–228, 1996.

[CPF07] O. Chaudhuri, S. Parekhand, and D. Fletcher. Reversible stress softening of actin networks. *Nature*, 445:295–298, 2007.

[Cri97] M.A. Crisfield. *Non-linear finite element analysis of solids and structures*, volume 2: Advanced topics. John Wiley & Sons, Chichester, 1997.

[HCB05] T.J.R. Hughes, J.A. Cottrell, and Y. Bazilevs. Isogeometric analysis: CAD, finite elements, NURBS, exact geometry and mesh refinement. *Comput. Methods Appl. Mech. Engng*, 194:41354195, 2005.

[HCL78] T.J.R. Hughes, T.K. Caughey, and W.K. Liu. Finite-element methods for nonlinear elastodynamics which conserve energy. *J. of Appl. Mech.*, 45:336–370, 1978.

[Ibr95] A. Ibrahimbegović. On finite element implementation of geometrically non-linear Reissner's beam theory: three-dimensional curved beams elements. *Comput. Methods Appl. Mech. Engng*, 122:11–26, 1995.

[KC99] D. Kuhl and M.A. Crisfield. Energy-conserving and decaying algorithms in non-linear structural dynamics. *Int. J. Num. Meth. Engng.*, 45:569–599, 1999.

[MJ04] J. Muñoz and G. Jelenić. Sliding contact conditions using the master-slave approach with applications on the geometrically non-linear beams. *Int. J. Solids Struct.*, 41:6963–6992, 2004.

[MJ06] J. Muñoz and G. Jelenić. Sliding joints in 3D beams: Conserving algorithms using the master-slave approach. *Multibody Syst. Dyn.*, 16:237–261, 2006.

[Muñ04] J. Muñoz. *Finite-element analysis of flexible mechanisms using the master-slave approach with emphasis on the modelling of joints*. PhD thesis, Imperial College London, 2004.

[Muñ08] J. Muñoz. Modelling unilateral frictionless contact using the null-space method and cubic B-Spline interpolation. *Comput. Methods Appl. Mech. Engng*, 197:979–993, 2008.

[New59] N.M. Newmark. A method of computation for structural dynamics. *J. Engin. Mech. Div.*, 85(3):67–94, 1959.

[PT97] L. Piegl and W. Tiller. *The Nurbs Book*. Springer, Germany, second edition, 1997.

[Rei72] E. Reissner. On one-dimensional finite-strain beam theory: the plane problem. *J. Appl. Math. Phys. (ZAMP)*, 23:795–804, 1972.

[Rei73] E. Reissner. On one-dimensional large-displacement finite-strain beam theory. *Studies in Applied Mathem.*, 52:87–95, 1973.

[Rei81] E. Reissner. On finite deformations of space-curved beams. *J. Appl. Math. Phys. (ZAMP)*, 32:734–744, 1981.

[Sim85] J.C. Simo. A finite strain beam formulation. The three dimensional dynamic problem. Part I. *Comput. Methods Appl. Mech. Engng*, 49:55–70, 1985.

[SM11] A. Sibileau and J. Muñoz. Conservative time integration on beams under contact constrains using B-Spline interpolation. In *MULTIBODY DYNAMICS ECCOMAS Thematic Conference*, Brussels, July 2011. Paper submitted.

[SS96] N. Stander and E. Stein. An energy-conserving planar finite beam element for dynamics of flexible mechanisms. *Engng. Comput.*, 16:60–85, 1996.

[ST92] J.C. Simo and N. Tarnow. The discrete energy-momentum method. Conserving algorithms for nonlinear elastodynamics. *J. Appl. Math. Phys. (ZAMP)*, 43:757–792, 1992.

[STD95] J.C. Simo, N. Tarnow, and M. Doblare. Non-linear dynamics of three-dimensional rods: exact energy and momentum conserving algorithms. *Int. J. Num. Meth. Engng*, 38:1431–1473, 1995.

[SVQ86a] J.C. Simo and L. Vu-Quoc. A three-dimensional finite-strain rod model. Part II: computational aspects. *Comput. Methods Appl. Mech. Engng*, 58:79–116, 1986.

[SVQ86b] J.C. Simo and L. Vu-Quoc. On the Dynamics of Flexible Beams Under Large Overall Motions - The Plane Case: Part I. *ASME J. of Appl. Mech.*, 53:849–854, 1986.

[SVQ86c] J.C. Simo and L. Vu-Quoc. On the Dynamics of Flexible Beams Under Large Overall Motions - The Plane Case: Part II. *ASME J. of Appl. Mech.*, 53:855–863, 1986.

[SVQ88] J.C. Simo and L. Vu-Quoc. On the dynamics in space of rods undergoing large motions -a geometrically exact approach. *Comput. Methods Appl. Mech. Engng*, 53:125–161,, 1988.

[SW91] J.C. Simo and K.K. Wong. Unconditionally stable algorithms for rigid body dynamics that exactly preserve energy and momentum. *Int. J. Num. Meth. Engng*, 31(1):19–52, 1991.

[TWH11] I. Temizer, P. Wriggers, and T.J.R. Hughes. Contact treatment in isogeometric analysis with NURBS. *Comput. Methods Appl. Mech. Engng*, 200:1100–1112, 2011.

[ZT00] O.C. Zienkiewicz and R.L. Taylor. *The Finite Element Method*, volume 2: Solid Mechanics, chapter 11: Non-linear structural problems -large displacement and instability. Butterworth-Heinemann, Oxford, fifth edition, 2000.